ISSN 1913-1844 (Print)
ISSN 1913-1852 (Online)

MODERN APPLIED SCIENCE

Vol. 3, No. 8
August 2009

Canadian Center of Science and Education

Editorial Board

CCSE

Modern Applied Science

www.ccsenet.org/journal.html

Vol. 3, No. 8
August 2009

Contents

Modern Applied Science

www.ccsenet.org/journal.html

Vol. 3, No. 8

August 2009

Physical and Mechanical Properties of Flame Retardant-Treated *Hibiscus Cannabinus* Particleboard

Izran Kamal (Corresponding author), Abdul Rashid Abdul Malek

Mohd. Nor Mohd Yusof & Khairul Masseat

Forest Research Institute Malaysia (FRIM)

52109, Kepong, Malaysia

Tel: 60-3-6279-7285 E-mail: izran_kamal@yahoo.com

Zaidon Ashaari & Faizah Abood

Faculty of Forestry, Universiti Putra Malaysia

43400, Serdang, Selangor, Malaysia

Tel: 60-3-8946-7161 E-mail: zaidon@putra.upm.edu.my

The research is financed by Forest Research Institute Malaysia. TGP-KL-1107-004/40310403005

Abstract

Physical and mechanical properties of flame retardant-treated kenaf particleboards were studied using physical tests such as water absorption, thickness swelling and mechanical tests such as modulus of rupture (MOR), modulus of elasticity (MOE) and internal bond (IB). The kenaf core particles were treated with 10% concentrations of three types of flame retardants namely diammonium phosphate ($(NH_4)_2HPO_4$), monoammnium phosphate ($(NH_4)HPO_4$) and BP® [mixture of 27-33 % boric acid, 67-73 % guanylurea phosphate and 0.0-4.2 % phosphoric acid]. The study showed that DAP-treated particleboards complied with the thickness swelling and water absorption of British-European standard [BS EN 317:1993] requirements. BP®-treated particleboards were found to have performance values superior than the British-European standard requirement values for MOR [BS EN 310:1993] and MOE [BS EN 310:1996]. MAP-treated particleboards surpassed the standard requirement value for IB [BS EN 319:1993]. However, all treated particleboards complied with the standard requirement value of MOE except DAP-treated particleboards**.** The untreated particleboards complied with all the standard requirements of the physical and mechanical tests. Overall, the flame retardants affected the physical and mechanical properties of the kenaf core particleboard

Keywords: Kenaf, Fire retardants, Hot and cold, Water absorption, Thickness swelling, Modulus of rupture, Modulus of elasticity, Internal bond

1. Introduction

There are many studies have been done around the world to prove that kenaf can be used to produce kenaf-based composites with acceptable physical and mechanical properties. It has been reported by Paridah et al (2004) and (2009) that kenaf core-based particle boards were able to give better MOR, MOE, internal bond, thickness swelling and water absorption performances than that of rubberwood-based particleboards. Muehl et al (1999) studied the strength of kenaf-based particleboard with the influences of different amount of resin and wax used to the strength of the particleboards. He found out that the mechanical performance of kenaf-based particleboards could be improved with the reduction of wax and increase of resin loading. However, the increase of the resin loading caused the particleboards to have poor water absorption and thickness swelling performance. Kenaf also has been used as a raw material to produce kenaf-based plastic polymer composite which have superb strength performances. Based on the research done by Mohamad Zharif (2008), where he tested the kenaf-based polymer composite with seven different mechanical tests such as fractural modulus, fractural strength, impact strength, tensile strength, yield strength, elongation at break and tensile

modulus. He recorded in his report that the kenaf-based polymer composite had superb performance for all the tests and surpassed the ASTM standard requirements for those mechanical tests. The results were in a good agreement with Jalaludin (2001). With the evidences shown above, kenaf is no doubt can be utilized in many ways for composite industries. Particleboard is a structural material made of wood fragments, such as chips or shavings, which are mechanically pressed into sheet form and bonded together with resin (Anon, 2000). Other definition of particleboard is panel from dry wood particles that have been sprayed or dusted with a binder resin, and are bonded together with resin and heat (Charles, 1986). Particles for the particleboards can be made from almost any type of wood, whether whole logs or log residues such as trimmings and shavings from lumber or plywood manufacturing (Charles, 1986) .This panel is available in large panel sizes which are suitable for many uses such as furniture components and partitioning. This engineered panel is often modified to many high-value products for different situations of usages such as fire-retardant treated particle board (for fire protection purposes), moisture resistant particle board (for outdoor use), thin particle board (for furniture industry), high density particle board (for flooring). The fire resistance of the composite is very important nowadays, especially when the composite is used as structural components. The primary objective of a fire-resistant structural design is to maintain the structural intergrity during a fire for a sufficient period so that all the occupants may safely evacuate, firemen may extinguish the fire, and the loss of property may be minimized (Park *et al.,*2004). According to Abdul Rashid et al (1990), particleboard is a combustible material. Previous studies revealed that treating particleboards with flame retardants were effective to reduce the combustibility and heat release of the panel (Abdul Rashid *et al.,*1990; Izran *et al.,*2008a, 2009a and 2009b). Most of the strength and physical properties of the treated particleboards however, were sharply reduced. Improper curing of the adhesive was identified as the cause for the poor performance of boards. This was attributed to the interference caused by the dry salt retention during manufacture of the boards (Izran *et al,* 2009b and Zaidon *et al.,* 2007). Other than the dry salt retention, the buffering capacity of the material used was also proved to cause the improper curing of the resin (Izran *et al.,* 2008b). This paper reports the mechanical and physical properties of flame retardant-treated *Hibiscus cannabinus* core particleboards.

2. Materials and Method

2.1 Particle preparation and treatment

Kenaf core was used as raw material for the research. The kenaf core is light and porous, having a bulk density of 0.10 – 0.20 g/cm^3. It can be crushed easily into light-weight particles. Kenaf core has cellulose and lignin content as same as wood [31-33% cellulose and 23-27% lignin] and it has higher content of hemicellulose than wood (Paridah et al, 2009). The raw material was supplied in chip form by Lembaga Tembakau Negara (LTN), Malaysia. The chips then were flaked and screened into 1–2 mm. The particles were dried at 105±2ºC to reduce the moisture content to 5% before the particles were treated with the fire retardants through hot and cold bath soaking process. Flame retardants used to treat the particles were commercialized ammonia-formulated-phosphorous-based fire retardants namely diammonium phosphate (DAP), monoammonium phosphate (MAP) and boron-formulated-phosphorous-based fire retardant, BP® [mixture of 27-33 % boric acid, 67-73 % guanylurea phosphate and 0.0-4.2 % phosphoric acid]. Adhesive used in this study was urea formaldehyde (UF) supplied by Malaysian Adhesive Company Sdn. Bhd., Shah Alam. For the treatment, dried kenaf core particles firstly, were hot soaked in the flame retardant solutions (dissolved with water to 10% concentration) for 10 minutes at the temperature of 70ºC and were left to ambient temperature.Then the particles were cold soaked for 15 minutes in MAP solution, 36 minutes in BP® solution and 14 minutes DAP solution to achieve 7.19 % dry salt retention (dry salt retention for 1029 g dried particles to produced a particleboard with 700 kg/m^3 as targeted density) to meet the standard requirement.. Standard chemical loading for a board (50mm and thinner board and a minimum penetration of 12mm) recommended by American Wood Preservers Association (AWPA) Standard C 20-6 is 50kg/m^3(Anon, 1968). The flame retardant concentration, dry salt retention and cold soaking time were determined through preliminary studies (Izran *et al.,* 2008c).

2.2 Particleboard fabrication

The targeted board density was 700 kg/m^3. Amount of dried kenaf core particles to produce a board with that density was 1029 g. The parameters used for manufacture of the particleboards are exhibit in Table. 1. Firstly, the dried treated kenaf core particles were taken out from the oven and were weighed to get the desired weight. Then, the particles were directly placed into the particleboard mixer. Urea formaldehyde resin mixed with wax and hardener was sprayed to the kenaf core particles in the particleboard mixer, which was equipped with airless spray gun. The moisture content of the furnish was 20%, which was higher than the targeted moisture content, therefore the furnish was re-dried for three hours to 12% MC. The re-dried furnish was then formed in a former, pre-pressed and subsequently pressed in a hot press at 160ºC. The pressing time for each treatment varied from 6 to 9 minutes. Variations in pressing time for different flame retardant treatments were occupied based on the effect of flame retardant to the gelation time of the resin reported by (Izran *et al.,*2008b and Izran *et al.,* 2009c). The DAP-treated furnish was hot pressed for 9 minutes, the BP®-treated furnish and untreated furnish were pressed for 7 minutes and MAP-treated furnish was pressed for 6 minutes. Prior to

cutting into testing blocks, all boards were conditioned at 20ºC and 65% relative humidity until equilibrium, i.e 12%. Total of three boards for each treatment were trimmed according to the standard requirement size and were distributed for the strength tests.

2.3 Mechanical and physical property evaluation

The tests were conducted in accordance with British Standard EN. The physical and mechanical testing conducted were static bending (BS EN 310:1993), thickness swelling and water absorption (BS EN 317:1993), internal bond (BS EN 319:1993) and density (BS EN 323:1993).

2.4 Data adjustment using ANOCOV

The densities of the particleboards were found to be in the range of 590 kg/m^3 to 780 kg/m^3. Due to that, an adjustment using analysis of covariance (ANOCOV) was performed to correct for expected differences in physical and mechanical properties due to the difference of density value (Zaidon *et al.,*2008) .Density was chosen as a covariate variable and adjusted means were separated using Least Significance Different (LSD) method.

3. Results and Discussions

3.1 Mechanical and Physical Properties of treated and untreated particleboards

The adjusted data for physical and mechanical properties of treated and untreated particleboards are demonstrated in Table 2. For modulus of rupture (MOR) and modulus of elasticity (MOE) values, the negative signs indicate a reduction in the value of properties, while for thickness swelling and water absorption, the negative sign reflects an improvement in dimensional stability.

3.1.1 Mechanical Property Evaluation

The MOR values for particleboards treated with DAP; BP® and MAP were reduced by 54.61%, 38.95% and 52.86% respectively, which are significantly lower compared to the untreated particleboards. The MOR value of the untreated particleboards was 15.74 N/mm^2. The MOR values for the MAP and DAP-treated particleboards were found to be lower than the BP®-treated particleboards. However for MOE, treatment using BP® did not affect the MOE of the particleboards as the stiffness value of the particleboards was 3.72% higher than the untreated particleboards. The MOE value for the untreated particleboards was 2066 N/mm^2. The treatments using DAP and MAP, both caused reduction of the MOE of the particleboard by 19.96% and 10.34% from the original stiffness. The longer and shorter pressing time occupied for the treated furnishes was expected to be a factor that influencing the MOR, MOE and IB of the treated particleboards. Different pressing time was applied due to the effect of fire retardants to the curing of the resin (Izran *et al.,* 2008b and 2009c). It was also suspected that strength loss occurred during chemical treatment and subsequent redrying of the panel (White and Sweet, 1992). The percent relative change in MOR and MOE is exhibit in Figure 1. More than 50% reductions were recorded for IB values of all treated particleboards. The reductions were 63.29% for the DAP-treated particleboards, 64.59% for the BP®-treated particleboards and 84.39% for the MAP-treated particleboards from the IB value of the untreated particleboards, which was 0.69N/mm^2. The percentage of reduction for each treatment is present in Figure 2. The reductions of the IB values for the treated particleboards may be attributed to insufficient or over sufficient curing of the resin. It was indicated that, flame retardants affected the pH glueline which slows down or aggravates up the polymerization reaction rate (Izran *et al.,* 2008b and 2009c). Thus, modifications on the hot pressing time and temperature were required to fully cure the resin.

3.1.2 Physical Properties Evaluation

With regards to physical properties, all flame retardant-treated particleboards exhibit higher thickness swelling (15.43%-21.64%), compared to the untreated boards (13.87%). Thickness swelling is to measure the dimensional stability of the particleboards. Lower thickness swelling value indicates a more stable board. The results show the flame-retardant treatments reduced the dimensional stability of the particleboards. In general, all flame retardant treatments increased the water absorption of these particleboards except for particleboards treated with DAP. Flame retardants are hygroscopic in nature and with that characteristic; they increased the water absorption of the treated particleboards. The percent relative change of thickness swelling and water absorption against the untreated particleboard is presented in Figure 3. Muehl et al (1999) treated boards made from waste paper with flame retardants with retention range from 10 %, 15 %, 20% and 25 %. The results of the research were the moisture content of the boards increased as the concentration of the fire retardants increased, even though the boards were not exposed to water. The water absorption of MAP-treated particle boards can be reduced by increasing the concentration to 20 %. However, for boron-based flame retardant, the water absorption rate increased together with the increment of the concentration (Abdul Rashid *et al.,* 1990).

4. Conclusions

The findings from this study revealed that flame retardant treatments significantly affect the physical and mechanical properties of the kenaf core particleboards. The flame retardants were found to affect the curing of the resin and

modification on the hot pressing time was occupied to be sure that the resin is fully cured and compact particleboards could be produced. The BP®-treated particleboards performed the best in the mechanical tests even though the IB value for the particleboards was slightly 1.31% lower than the DAP-treated particleboards. In fact the MOE performances of the BP® particleboards were better than the untreated particleboards. The reductions of the mechanical properties were expected caused by the hot pressing temperature, time and subsequent re-drying of the particleboards. Physical properties were dominated by the DAP-treated particleboards. The DAP-treated particleboards were having the lowest thickness swelling value compared to the other treated particleboards. It is interesting to note here that the water absorption of the DAP-treated particleboards was lower than the untreated particleboards. As a whole, the treatment system used in this study may be suitable for the manufacturing of flame retardant-treated particleboard from kenaf core. Further study on improving the mechanical and physical performances of the treated particleboards should be conducted to expand the usage of the particleboards. Besides, the increase in resistivity against thermal degradation will further expand the usage of the panels.

5. Acknowledgements

A special thank to FRIM for securing grant for this project and to members of FRIM and Faculty of Forestry, Universiti Putra Malaysia, for their supervision in this research work.

References

Abdul Rashid, A.M., and Chew, L.T., Fire retardant treated chipboards*,* In. *Conference on Forestry and Forest Product Resource. CFFPR-90*, Malaysia, (1990). pp.37.

Anonymous, (2000). Definition of particle board, In. *American Heritage ® Dictionary of the English Language*, Fourth Edition*,*Houghton Miffilin Company.

Anonymous. (1963). Structural lumber, fire retardant treatment by pressure processes,*Standard C 20-60.AWPA.*

Anonymous. (2003). Toyota to use ecofriendly plastic, [Online] Available: http://www.climateark.org/shared/reader/welcome.aspx?linki=19060 (February 12, 2008).

Charles, C. (1986). Wood particle and flakeboard: Types, grades, and uses. In *General Technology Report FPL-GTR-53*, Madison, WI: US Department of Agriculture., Forest Service. Forest Products Laboratory.

Izran, K, Zaidon, A, Abdul Rashid, A.M, F, Abood, Mohamad jani, S., Nor Yuziah,M.Y, Suffian, M. and Zaihan, J. (2008b). Buffering capacity and gelation time of fire retardant treated kenaf particles and urea formaldehyde resin admixture, *Poster presented at National Symposium. of Polymeric Materials*, Universiti Sains Malaysia.

Izran, K., Zaidon, A., Abdul Rashid, A.M, F., Abood, Mohamad Jani, S., Zaihan, J. and Faezah, M., (2009c), A preliminary study in Determining the Curing Time of Urea Formaldehyde resin mixed with different concentrations of fire retardants and assessments of its properties**,**In. *Proceedings of National Postgraduate Conference on Engineering, Science and Technology*, Malaysia, pp.89.

Izran, K., Zaidon, A., Abdul Rashid, A.M, F., Abood, U.M.K., Anwar, Mohamad Jani, S., Hashim, W.S.,and Suffian, M., (2008c), Optimizing treatment system of kenaf core particleboard with fire retardants, *poster presented at Naiona. Conference on Forest Proucts. 2008,"Towards competitiveness and sustainability",* Kuala Lumpur, Malaysia.

Izran, K., Zaidon, A., Abdul Rashid, A.M., F., Abood, Mohamad Jani, S., T., Ahmad Zharif, and M., Khairul, (2009b). Fire propagation and strength performance of fire retardant-treated *Hibiscus cannabinus* particleboard, In. *Properties evaluation of particleboard made from kenaf core treated with fire retardants, Unpublished report.*

Izran, K., Zaidon, A., Abdul Rashid, A.M., F., Abood, Zaihan, J., and Beyer,.G, (2009a). Fire Resistance and early burning performance of kenaf (*Hibiscus cannabinus*) particleboard treated with phosphorous based fire retardants, in Proceedings of National Postgraduate Conference on Engineering, Science and Technology, Universiti Teknologi Petronas: Malaysia*,* pp. 83.

Jalaludin, H. (2005). Emerging source of raw material for bio composites and pulp and paper industries in Malaysia, In. *Seminar on kenaf: A New Source of Growth*, Malaysia: MTIB and MARDI, pp.21-25.

M.Z., Ahmad Thirmizir. Mechanical properties, In. *Study on mechanical and performance of kenaf bast fibre filled biodegradable poly butylenes succiante,* (2009). M sc. thesis, USM.

Mohamad Jani, S., Rahim, S., Koh, M.P., Saimin, B., Nordin,P. & Jalali, S. (2004). The Technical Feasibility of Producing Kenaf Particleboard and Fibreboard, In. Mohd Nor,M.Y, Koh, M.P, Suffian, M, Wan Asma, W.I and Rahim, S (Eds.), *Proceedings of the Fourth National Seminar on Wood Based Panel Products, "Towards Meeting Global Challenges"*, 28-30 September 2004, Kuala Lumpur.

Muehl,H.J.,Kryzsik, M.A., Youngquist, A.J., Chow, P, & Bao, Z. (1999). Performance of hardboard from kenaf, In. Terry Sellers, J.R., Nancy A. Reichert, Eugene P. Columbus. Marty J. Fuller, and Karen Williams (Eds.), *Kenaf*

properties:processing and products. Mississippi State University.

Paridah, M.T., Nor Hafizah, A., Zaidon, A. Azmi, I., Mohd Nor, M.Y and Nor Yuziah, M.Y. (2009). Bonding properties and performance of multi-layered kenaf board, *Journal of Tropical Science* 21(2):113-122.

Paridah, M.T., Norhafizah, A.W., Jalaluddin, H., Azmi, I., and Nor Yuziah, M.Y. (2007). Properties of kenaf board bonded with formaldehyde based adhesives, paper presented at *2007 IUFRO Forest Products and Environment: A Productive Symbiosis,* Taipei: Taiwan.

Park,S.J. and Lee. J.J. (2004). Fire resistance of light-framed wood floors exposed to real and standard fire, Journal of Fire Sciences, 22, 449-471.

White, H.R., Sweet, M.S. (1992). Flame Retardancy of Wood: Present Status, Recent Problems, And Future Fields In. *Recent Advances in Flame Retardancy of Polymeric Materials: Proceedings of 3rd annual BCC Conference. on Flame Retardance*, Stamford CT. Norwalk, CT: Business Communications Company, Inc, pp. 250-257.

Zaidon, A., Abood, F., Norhairul Nizam, A.W., Mohd Nor, M.Y., Paridah, M.T., Nor Yuziah, M.Y. and Jalaludin, H. (2008). Properties of pyrethoids-treated particleboards manufactured from rubberwood and oil palm empty fruit bunches (EFB), *Pertanika Journal Tropical Agricultural Science*, 21:171-178.

Zaidon, A., Norhairul Nizam, A.M., Mohd. Nor, M.Y., F., Abood, Paridah, M.T., Nor Yuziah M.Y. and Jalaludin,. H., (2007). Properties of particleboard made from pretreated particles of rubberwood, EFB and rubberwood-EFB blend, *Journal of Applied Science,* 8: 1145-1151.

Table 1. Parameters used for manufacture of the particleboards

Raw Material	kenaf (1-2 mm particle size)
Targeted board density	700 kg/m^3
Targeted board MC	12%
Board Size	(350 x 350 x 12) mm^3
Adhesive	
UF resin	12% (w/w of dried particles)
Hardener (NH_4Cl)	3% (based on resin)
Wax	1% (based on dried particles)
Flame retardants	
1.diammonium phosphate (DAP)	10% (w/w of particles) decided after preliminary test of hot and cold bath Treatment
2.monoammonium phosphate (MAP)	
3.Mixture of BP®:	
i) guanylurea phosphate (67-73%)	
ii) phosphoric acid (0.0-4.2%)	
iii) boric acid (27-33%)	

Table 2. Adjusted mean mechanical and physical values and percent change in properties for flame retardant-treated particleboards compared to untreated

Peformance	Standard requirements	Board density (kg/m^{-3})	Flame retardant treatments			
			Control ± S.D	DAP ± S.D	BP® ± S.D	MAP ± S.D
MOR (N/mm^2) Change (%)	≥ 14N/mm^2	701.68	15.74^{a} ± 1.70	7.14^{b} ± 1.06 (-54.61)	9.61^{c} ± 2.39 (-38.95)	7.42^{bd} ± 0.86 (-52.86)
IB (N/mm^2) Change (%)	≥ 0.4N/mm^2	678.28	0.69^{a} ± 0.50	0.26^{b} ± 0.51 (-63.29)	0.25^{ba} ± 0.41 (-64.59)	0.11^{c} ± 0.41 (-84.39)
MOE(N/mm^2) Change (%)	≥1800N/mm^2	701.68	2066^{ac} ± 297.69	1670.06^{b} ± 378.31 (-19.96)	2145.79^{a} ± 565.34 (3.72)	1852.37^{bc} ± 229.93 (-10.34)
TS (%) Change (%)	≤ 16 %	NA	13.87 ± 0.91	15.43 ± 4.96 (10.11)	21.64 ± 3.06 (35.91)	18.62 ± 5.62 (25.51)
WA Change (%)	NA	NA	37.23 ± 2.63	35.82 ± 14.19 (-3.79)	58.09 ± 8.08 (35.91)	48.16 ± 8.14 (29.36)

[1]Means within a row followed by the same alphabets are not significantly different at p≤0.05,

[2]Percent change over untreated and ± are standard deviations, [3]Values are adjusted mean of ten samples

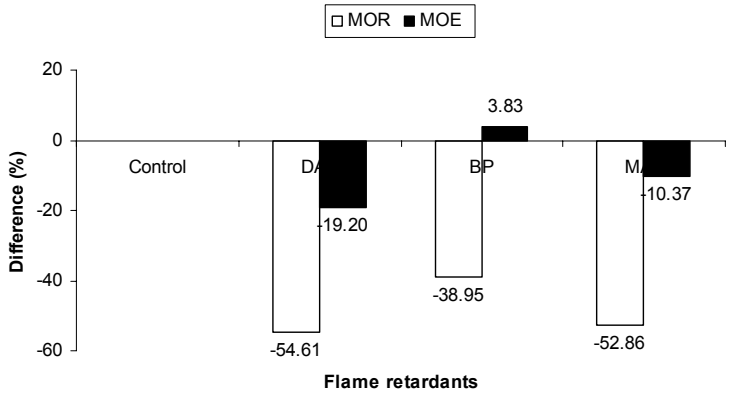

Figure 1. Percent relative change in MOR and MOE against the untreated

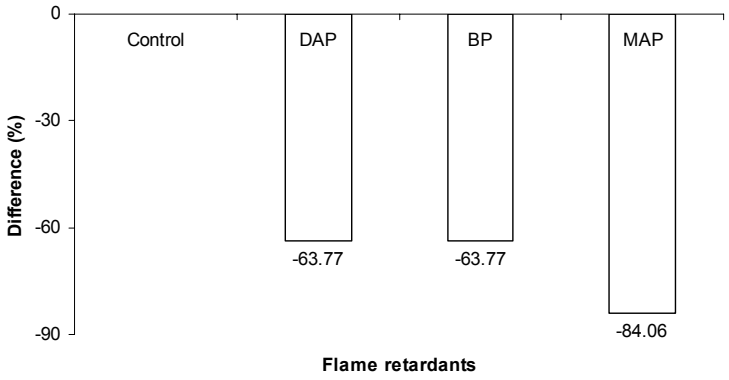

Figure 2. Percent relative change in internal bond against untreated

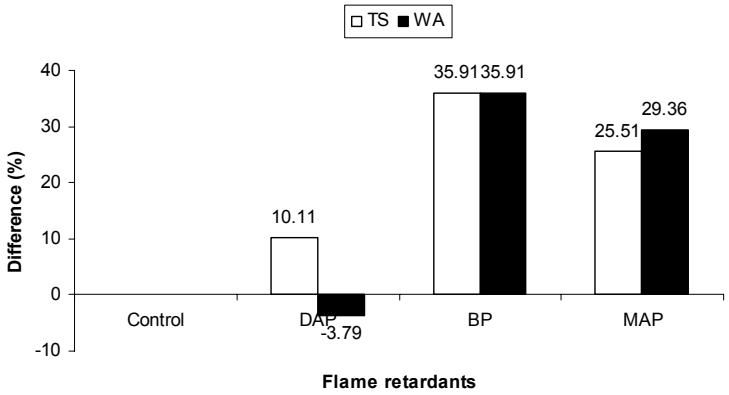

Figure 3. Percent relative change in thickness swelling and water absorption against untreated

Modern Applied Science

www.ccsenet.org/journal.html

Vol. 3, No. 8

August 2009

Study on the Material Requisition System Based on Data Mining

Xuyun Hong

Business School, University of Shanghai for Science and Technology, Shanghai 200093, China

Tel: 86-21-5527-6487 E-mail: XUYUNH@usst.edu.cn

Liangwei Zhong (Corresponding author)

CAD Center, University of Shanghai for Science and Technology, Shanghai 200093, China

Tel: 86-21-5527-6487 E-mail: zlv@usst.edu.cn

Jing Ni

Business School, University of Shanghai for Science and Technology, Shanghai 200093, China

Tel: 86-21-5527-1343 E-mail: nijing501@126.com

The research is financed by the Shanghai Leading Academic Discipline Project (No. S30504, J50503).

Abstract

The material requisition flow in the warehousing management was studied in the article, and combining the mining algorithm of causal rules, the material requisition based on data mining was developed. The system could fulfill the management requirements of the material requisition process for the enterprise, mine the data of material return and deeply analyze reasons, which can help the enterprise to enhance the production quality and reduce the production cost.

Keywords: Material requisition, Material return, Data mining, Causal rules

1. Introduction

The warehousing management information system has been used by many enterprises at present, and one important part in the system is the problems about how to require materials and distribute the material requisition for the manufacture enterprise. But the system can only simplify operators' operations to some extent, and it can not control the material requisition, and analyze the data of the material wastes.

To solve above problems, the material requisition system based on data mining is developed by J2EE. It can realize data sharing with PDM, avoid the data failure because of manual input, realize the material requisition control and data query and statistic analysis, and liberate operators from multifarious operation flows and large numerous of product information. The new system uses the data mining technology to analyze the data of material requisition and help decision-making, which can reduce the manufacturing cost.

2. Function design

The material consumption norm is the amount of various raw materials which must be consumed to make unit product (or part) according to many regulations such as product design structure, technical requirement, technical method and production technical condition under certain production, technology and organization conditions. It can standardize the management of the material distribution and use process, and it is the important system to realize the real-time control of the material cost. Its target is to strictly implement the material management system, strengthen saving, reduce waste, realize the real-time control of material cost in the workshop, strengthen the dynamic management of the material consumption norm, reduce the material consumption cost and enhance the economic benefits. Based on product design, production technology and arts, it can realize the cost control by systematic and refined management.

The material requisition is the process that the manufacturing department draws the materials from the warehouse according to BOM and implements manufacturing or assembling, so it uses the ODBC technology to link the material data in the PDM system and realize the real-time updating of data.

Except for the basic material data, the type and quantity of requisition materials are the direct problem faced by the manufacture enterprises, so before the concrete contents of the material requisition are confirmed, the product type, material sort and material norm should be first confirmed. Generally, these contents are contained in the work order, and one work order can confirm the product name, the product chart No., product type and specs, sub-factory and product quantity. It comes from two departments. First, according to the yearly performance, the enterprise management department establishes the product manufacture plan of the next year, and the plan is turned into the work order according to the corresponding rules, and the work order is issued to the workshop, and these products are the pre-investing products, i.e. the standard type specs, and the production quantity of each product and each work order is a fixed value. Second, the work order comes from the sales department, if the products signed in the contract are non-pre-investing products (the product type and specs are non-standard), the non-pre-investing work order is generated, and the demand quantity is the production quantity, and the order is transferred to the workshop. If the sales quantity of the pre-investing product exceeds the planning quantity, so the new work order is generated. The storage personnel confirm the part material and material norm according to the work order, and fill in the material requisition according to the demand quantity of the workshop.

The requisition materials in the workshop are divided into the general requisition materials, odd lot (shortage) requisition materials and return materials. The material return is the operation that after the material requisition is filled in, the quality problem in the roughcast or disqualified manufacturing is found in the material requisition or production process, and the materials need to be returned. The reasons of material return include the material scrap and the working scrap. The material scarp occurs because of the problems existing in the raw materials, such as the material crack, and illegal roughcast size. The working scrap means the wasters induced in the manufacturing process, and except for the manufacture personnel are not familiar with the operation or perform incorrect manipulation, most working scarps come down to the quality of the product design and technological method. However, many records of material return are accumulated in the database, and they can not be utilized to embody their values, so much information is wasted. In addition, the increase of wasted materials will increase the material consumption, and enhance the production cost of the product, and reduce the profit of enterprise, so the occurrence of scrap should be reduced from the economic angle. The enterprise should effectively utilize the data of material return, deeply analyze and mine the biggest factor influencing the production in the workshop, discover the concrete reasons and possible problems to form the information for the decision-making, and accordingly standardize the material return and the material utilization, and reduce the manufacturing cost.

Figure 1 is the system functional diagram.

User management: the operations such as adding, freezing, deleting and modifying user information, and the setting of right.

Material requisition print: the material requisition is divided into the general material requisition, shortage, working scrap and material scrap, and the operations when the printer breaks down or jams papers. To simplify the operation, the check box is set up for users to select the appointed parts, and the users can also appoint printing one or multiple parts, and the operation is more convenient.

Data query: users can inquire the requisition record of certain part according to the requisition number, work order, production and part information, and inquire the requisition of various parts under appointed work order for the surplus of the corresponding work order.

Data analysis: according to the time input by the users, the system can calculate the happening probability of various reasons for each product, mine the main reason to induce the working scrap, and generate the important information to enhance the quality of product design and productivity, and save resources. The outputs of various statistical analysis values under this module include the product quantity, proportion, total happening probability of various reasons, and happening probability of various products, main influencing factor and heavy weight in the periodic production.

3. Key technology

The key technology of the system is the data analysis module, and one associated rule miner is developed, and it takes various reasons to induce the working scrap in the production as the analysis variables, discovers the concealed rules in large numerous material return data, finds out the concealed association in data, i.e. the association between variables and working scrap, so the information which can help the enterprise to make decision will be formed.

The mining of associated rules is one important part of data mining. If certain rule exists in two or multiple variables, it is called the association, and it can be divided into simple association, time association and causal association. The target of association analysis is to discover the interesting association or correlative relation in larger numerous information or information items. Sometimes, the associated function of data in the database is not known, even can not be confirmed, so the rules to generate the association analysis have certain creditability.

Supposed that D is the appointed database, and minsupp, minconf, γ, α, λ and η are appointed threshold values and $M_{Y|X}$

is the conditional probability matrix, so the mining algorithm of the associated rules in the data base D can be described as follows.

Algorithm1 Causality DB

Input: D: database, minsupp, minconf, α, λ, η: threshold values;

Output: X→Y: causal rule, $M_{Y|X}$: the conditional probability matrix of Y given X;

(1) call procedure partitionData;

(2) for X, Y∈OIV do

for each element a in R(X) and b in R(Y) do

let p(Y = b |X= a) =p(Y = b∧X = a)/p(X = a);

let CRSET←the rule X→Y as a candidate rule;

with conditional probability matrix of Y given X:$M_{Y|X}$;

end for

end for

(3) for each extracted rule R with $M_{Y|X}$ in CRSET do

let $S_{support}\leftarrow\{(x_j,y_i)\ |p(y_i\cup x_j)\geq minsupp\wedge(1\leq i\leq m)\wedge(1\leq j\leq n)\}$;

let $S_{conf}\leftarrow\{(xj,y_i)\ |p(Y=y_i|\ X=x_j)\geq minconf\wedge(1\leq i\leq m)\wedge(1\leq j\leq n)\}$;

let $S_{depend}\leftarrow\{(x_j,y_i)\ |p(Y=y_i|\ X=x_j)\text{-}p(Y=y_i)\geq\lambda\wedge(1\leq i\leq m)\wedge(1\leq j\leq n)$

if $|\ S_{support}|<\min\{n,m,\gamma\}$ then

generate item-based rules or quantative rules for $S_{support}$;

else if $|\ S_{conf}|<\min\{n,m,\eta\}$then

generate item-based rules or quantitave rules for S_{conf};

else if $|\ S_{depend}|<\min\{n,m,\alpha\}$ then

generate item-based rules or quantitative rules for S_{depend};

else let RSET←the rule X→Y as an interest rule;

with conditional probability matrix of Y given X:$M_{Y|X}$; end do;

The statistical results of the working scarp requisition in the database denotes the conditional probability, and 19.5% denotes the happening probability of the coarse jaw breaking scrap by the workers' incorrect manipulation.

The scraps are divided into eleven sorts including coarse jaw breaking, fined jaw breaking, counterattack breaking, taper breaking, hammer breaking, roller breaking and so on, and the reasons of working scrap are divided into the workers' incorrect manipulation, damaged tools, improper manufacturing technology, inexact clamp, improper structure design and sufficient material performance (seen in Table 1).

The causal relations reflected in Table 1 are denoted as the conditional probability matrix, and various breaking factors are the state variable X.

The matrix formed from Table 1 is

$$A_{11\times 6}=\begin{pmatrix} 0.235 & 0.088 & 0.118 & 0.294 & 0.118 & 0.147 \\ 0.195 & 0.049 & 0.122 & 0.293 & 0.146 & 0.195 \\ 0.172 & 0.034 & 0.103 & 0.172 & 0.172 & 0.345 \\ 0.24 & 0.04 & 0.08 & 0.28 & 0.16 & 0.02 \\ 0.176 & 0.294 & 0.059 & 0.235 & 0.176 & 0.235 \\ 0.190 & 0.143 & 0.048 & 0.286 & 0.095 & 0.238 \\ 0.1 & 0.1 & 0.1 & 0.15 & 0.25 & 0.3 \\ 0.052 & 0.052 & 0.158 & 0.105 & 0.368 & 0.263 \\ 0.125 & 0.041 & 0.083 & 0.208 & 0.25 & 0.292 \\ 0.08 & 0.12 & 0.16 & 0.32 & 0.08 & 0.24 \\ 0.2 & 0.1 & 0.15 & 0.2 & 0.15 & 0.15 \end{pmatrix} \quad (1)$$

In the statistical time, the production quantities of various products respectively are 40, 3, 9, 101, 1, 9, 61, 2, 23, 3 and 3, and the production proportion of various products is Z= (0.157, 0.012, 0.035, 0.396, 0.004, 0.035, 0.239, 0.008, 0.090, 0.012, 0.012), so according to $Z \times A_{11 \times 6}$=Y, Y= (0.186575, 0.068261, 0.093545, 0.239174, 0.181641, 0.159448), and Y is the weight value of various reasons combining the production proportion. From the information in Y, the improper structure design will impact the total production most, the technical improvement needs to be done by the technical department, and though the improper manufacturing technology has same impact on the scrap records with the improper structure design, but the improper manufacturing technology mainly impact the products with small production quantity, so its impacts are far less than the improper structure design. The system can deduct concrete rule expression aiming at concrete certain product, for example, the material return of drying breaking is mainly induced by the incorrect clamp. Therefore, the enterprise can adopt corresponding measures to modify the deficiencies according to the analysis results.

4. System implementation

The system adopts the B/S frame which is composed by server, networking computer and printer. The background database is the SQL Server 2000 relation database.

The user can click the tag page on the interface to operate. The materials are divided into the main machine and the structured part first, and then they are further sorted, which can help users to realize the print of various types of materials under the work order.

User can click “query of printing record”, and inquire the total happening amount of scrap by inputting the checking conditions, and click the tag of “analyzing data”, and input the time period, so the system can display the part sort and quantity of working scrap in this period, the working scrap happening amount of various products, the happening probability of various reasons, and the input reasoning rules.

5. Conclusions

Based on BOM data, the material requisition control system is designed and developed by adopting the B/S data interview mode, and it can simplify users’ operations, realize the control of material requisition sort and quantity, implement data mining for the records of working scrap, analyze the main potential influencing factors, help the management layer to make relative decisions, and reduce the production cost. At present, the reason analysis is still deficient, and the system can only calculate the data according to the production amount proportion, and if the system can refer to the profits of various products to calculate the proportion of various products, the result will be more close to the benefits of the enterprise.

References

Lu, Juemin & Zheng, Yu. (2007). Application of the Data Mining Technology Based on Matrix in Digital Library. *Modern Information.* No.12. P.92-98.

Lu, Jun, Zhong, Liangwei & Ni, Jing. (2008). Application of Data Mining in Material Withdrawing and Returning Management System. *Manufacturing Technology & Machine Tool.* No.7. P.138-141.

Shahbaz M., Srinivas, Harding, J.A. & Turner, M. (2006). Product design and manufacturing process improvement using association rules. *Proceedings of the Institution of Mechanical Engineers, Part B: Journal of Engineering Manufacture.* No.220(2). P.243-254.

Siradeghyan Y., Zakarian A. & Mohanty P. (2008). Entropy-based associative classification algorithm for mining manufacturing data. *International Journal of Computer Integrated Manufacturing.* No.21(7). P.825-838.

Zhang, Deqiang, Wang, Yansong, & Geng, Aili. (2002). Development of the Material Information System. *Journal of Liaoning Institute of Technology (Natural Science Edition).* No.22(5). P.23-24.

Zhong, Zhi, Su, Yijuan & Zhang, Shichao. (2002). Mining Causal Rules in Databases. *Journal of Guangxi Teachers College (Natural Science Edition).* No.19(4). P.77-80.

Table 1. Data statistics

Reason / *Product type*	*Failure of workers to operate*	*Damage of tools*	*Deficient material performance*	*Improper structure design*	*Inexact clamp*	*Improper manufacturing techniques*
Coarse jaw breaking	8 (23.5%)	3 (8.8%)	4 (11.8%)	10 (29.4%)	4 (11.8%)	5 (14.7%)
Fined jaw breaking	8 (19.5%)	2 (4.9%)	5 (12.2%)	12 (29.3%)	6 (14.6%)	8 (19.5%)
Counterattack breaking	5 (17.2%)	1 (3.4%)	3 (10.3%)	5 (17.2%)	5 (17.2%)	10 (34.5%)
Taper breaking	6 (24%)	1 (4%)	2 (8%)	7 (28%)	4 (16%)	5 (2%)
New taper	3 (17.6%)	2 (29.4%)	1 (5.9%)	4 (23.5%)	3 (17.6%)	4 (23.5%)
Roller breaking	4 (19.0%)	3 (14.3%)	1 (4.8%)	6 (28.6%)	2 (9.5%)	5 (23.8%)
Hammer breaking	2 (10%)	2 (10%)	2 (10%)	3 (15%)	5 (25%)	6 (30%)
Drying breaking	1 (5.2%)	1 (5.2%)	3 (15.8%)	2 (10.5%)	7 (36.8%)	5 (26.3%)
Vibration feeding machine	3 (12.5)	1 (4.1%)	2 (8.3%)	5 (20.8%)	6 (25%)	7 (29.2%)
vibration sieve	2 (8%)	3 (12%)	4 (16%)	8 (32%)	2 (8%)	6 (24%)
Plate feeding machine	4 (20%)	2 (10%)	3 (15%)	4 (20%)	3 (15%)	4 (15%)
	46	21	30	66	47	65

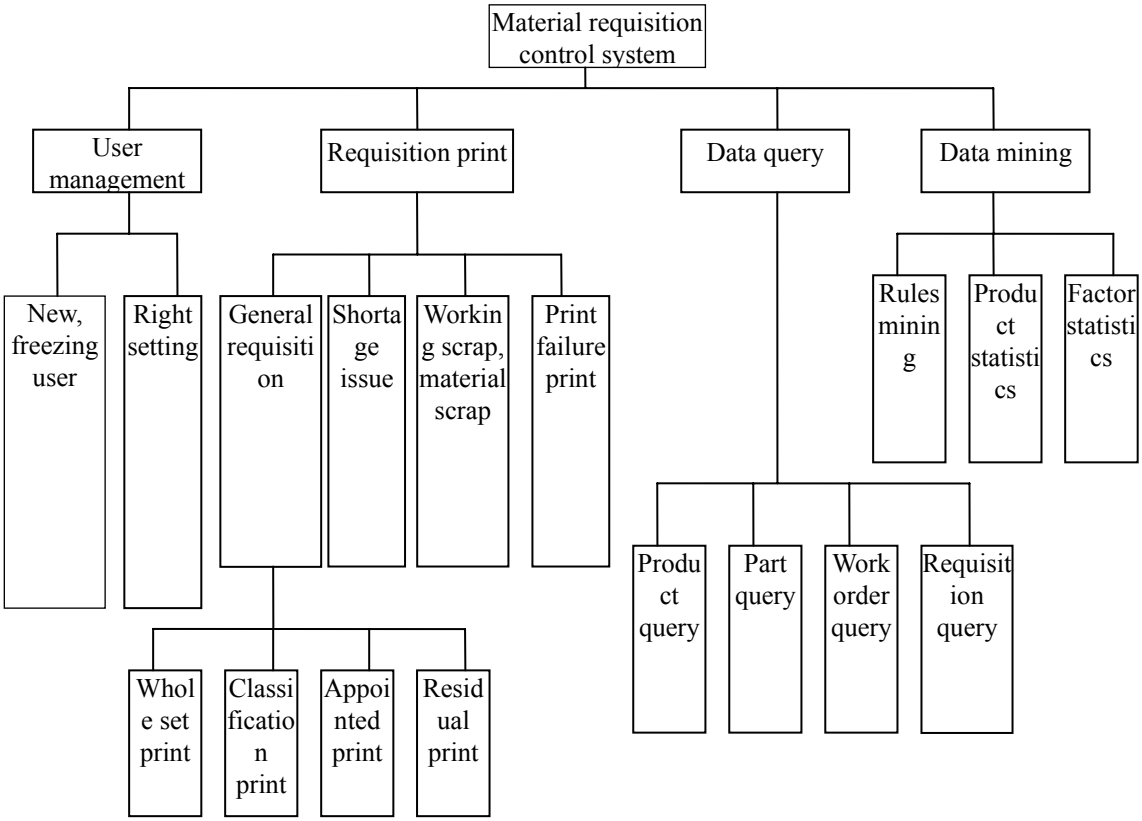

Figure 1. System Functional Diagram

Modern Applied Science

www.ccsenet.org/journal.html

Vol. 3, No. 8

August 2009

Decolorization and COD Removal of Reactive Yellow 16 by Fenton Oxidation and Comparison of Dye Removal with Photo Fenton and Sono Fenton Process

T.R.Sundararaman (Corresponding author)

Department of Chemical Engineering

Adhiparasakthi Engineering College

Melmaruvathur – 603 319, India

Tel: 91-44-23774493 E-mail: sundararamantr@yahoo.co.in

Dr. V. Ramamurthi

Department of Chemical Engineering

Anna University, Chennai – 600 025, India

Tel: 91-44-2235-2642 E-mail: ramamur1951@yahoo.co.in

Dr. N.Partha

Department of Chemical Engineering

Anna University, Chennai – 600 025, India

Tel: 91-44-22203534 E-mail: npartha62@yahoo.co.in

Abstract

Wastewaters from textile industry contain various pollutants including a high content of organic matter, surfactants, additives and dyes. Dyes have obtained notoriety as hazardous substances, because most of them are toxic and considered to be resistant to biodegradation. Recently, advanced oxidation processes (AOP) have received considerable attention because it is possible to degrade organic compounds and color from wastewaters. This study was performed to investigate the removal of COD and color for Reactive yellow 16 using Fenton oxidation. The comparisons of removal efficiencies were made among Fenton, Photo Fenton and Sono Fenton process. Removal of COD and color of 80% & 90%, 90% & 98%, and 82% & 95% can be achieved by Fenton, Photo Fenton and Sono Fenton process. The results showed that H_2O_2/Fe^{2+}/UV process was more effective in COD and color removal.

Keywords: Ultraviolet, Sono, Advanced oxidation processes (AOPs), Reactive dye, Decolorization Hydrogen peroxide, COD

1. Introduction

The problem of colored effluent has been a major challenge and an integral part of textile effluent treatment as a result of stricter environmental regulations. The presence of dyes in receiving media is easily detectable even when released in small concentrations (Little et al., 1974; Nigam et al., 2000). This is not only unsightly but dyes in the effluent may have a serious inhibitory effect on aquatic ecosystems as mentioned above. Commonly applied treatment methods for color removal from dye contaminated effluents consist of integrated processes involving various combinations of biological, physical and chemical decolorization methods (Galindo et al., 2001; Robinson et al., 2001). These integrated treatment methods are efficient but not cost effective. Traditional physical–chemical techniques such as ultra filtration, reverse osmosis, ion exchange and adsorption on various adsorbents (activated carbon, peat, flyash and coal, wood

chips, silica gel, corncob, barley etc.) have efficiently been used for the purpose of color removal from textile effluents. Activated carbon is the most commonly applied method for color removal

especially for cationic, mordant, and acid dyes and a slightly lesser extent, dispersed, direct, vat, pigment and reactive dyes (Raghavacharya, 1997). Carbon adsorption of dyes is only successful in some classes of dye (ionic type and hydrophobicity) for a given type of carbon in a certain pH range (Hao et al., 2000). Nevertheless, these techniques are non-destructive, since they just transfer the pollutant from water to solid matrix. Consequently, expensive operations such as regeneration of the adsorbent materials and post-treatment of solid wastes are needed.

Coagulation may not remove highly soluble dyes and it may be good for disperse dyes, but it produces a large quantity of sludge. Some processes are effective within a narrow pH range, for example pH<3.5 for Fenton's reagent. Ozonation alone is not effective for disperse dyes (Solozhenko et al., 1995). A combination of these processes is necessary to achieve the desirable goal. For example, the degree of the inhibition for a synthetic dye in a biological-activated sludge system has been reduced from 47% to 10% after a pretreatment with O3/UV or O_3/H_2O_2/UV (Ledakowicz and Gonera, 1999). Advanced oxidation processes (O_3, O_3/H_2O_2, O_3/UV, H_2O_2/UV, O_3/H_2O_2/UV, Fe^{2+}/ H_2O_2 for the degradation of non-biodegradable organic contaminants in industrial effluents are attractive alternatives to conventional treatment methods. AOPs based on the generation of very reactive and oxidizing free radicals have been used with an increasing interest due to the their high oxidant power. Production of those radicals is achieved either using single oxidants or combinations of ozone, hydrogen peroxide and UV radiation (Glaze and Kang, 1989) and also, with the combination of hydrogen peroxide with ferrous ions in the so-called Fenton's reagent (Walling, 1975). Although AOPs have a significant advantages over conventional treatment methods since chemical oxidation do not result in high amount of either chemical or biological sludge and almost complete demineralization of organics is possible, the main handicap with AOPs lies in the high cost of reagents or energy sources like ultraviolet light (Galindo et al., 2001).

Decolorization of textile effluents is of major environmental concern that remains to be solved. AOPs have been thoroughly and comparatively evaluated for a variety of organic compounds and wastewaters in the past but with several limitations. Also many investigations have demonstrated that AOPs are effectively removing color and partially organic content of dyestuffs (Legrini et al., 1983; Marechal et al., 1997).

1.1 Principles of AOPs

AOPs have common principles in terms of the participation of hydroxyl radicals that are assumed to be operative during the reaction. Although it is claimed that there are other species involved, the active species responsible for the destruction of contaminants in most cases seems to be the hydroxyl radical (OH.) which is unstable and quite reactive. Due to the instability of OH. radical, it must be generated continuously ''in situ'' through chemical or photochemical reactions described in the literature (Oliver et al., 2000).Hydroxyl radicals produced in either way of described above may attack organic molecules by abstracting a hydrogen atom from the molecule (Clarke and Knowles, 1982). Carey (1990) described a common pathway for the degradation of organics by the hydroxyl radicals as follows:

$OH^{\cdot} + RH \rightarrow H2O + R^{\cdot}$

$R^{\cdot} + H_2O_2 \rightarrow ROH + OH^{\cdot}$

$R^{\cdot} + O_2 \rightarrow ROO^{\cdot}$

$ROO^{\cdot} + RH \rightarrow ROOH + R^{\cdot}$

2. Materials and methods

2.1 Experimental setups

Reactive yellow 16 of commercial grade was used. HCl and NaOH analytical grade was used for this study. All the experiments were carried out at room temperature. Fenton oxidation studies were conducted in a one litre beaker. Sample volume for dye solution used was 500 ml. After settlement of the sludge, the supernatant was collected for the absorbance measurement and the % color removal calculated.

Dye Concentration used was 50 mg/L. Concentration of the dye samples were measured at the wavelength of the maximum absorbance (λ_{max}), which was determined using a UV-Vis spectrophotometer. The percentage removal of a dye was calculated from the absorbance of the supernatant to the standard curve of each dye obtained from its concentration.

Fenton's reagent experiments were carried out at room temperature in a 1 litre reactor using varying hydrogen peroxide and $FeSO_4$ dosages at varying pH values in order to determine the optimum conditions for best COD and color removal. Optimum P_H determination was carried out for chemical dosages of H_2O_2 = 900 mg/lit and $FeSO_4$ = 1000 mg/lit. In order to find optimum chemical dosages at a predetermined optimum pH, H_2O_2 and $FeSO_4$ dosages varied between 100 and 1000 mg/lit. The solutions were mixed by means of magnetic stirrer.

A photoreactor was set up for the experiments with UV in batch mode operation. A Phillips 250 W mercury lamp (wavelength of 420 nm) was used. After addition of predetermined amount of Hydrogen peroxide and Ferrous sulphate in to the dye sample, the solution within the UV irradiated reactor was mixed by the help of a magnetic stirrer to ensure homogeneous mixture. In addition, both sodium hydroxide and sulphuric acid were used to adjust the $P_{H.}$

Sonolysis experiments were performed in a Sono reactor (DU-MINI-120), at an ultrasound frequency of 34 KHz in a continuous wave mode. The power output was 120 W. The volume of solutions sonicated was 500 ml. Experiments were carried out under atmospheric conditions and at room temperature.

3. Results and Discussions

3.1 Fenton oxidation of dye solutions

It is known that the dye removal efficiency by Fenton oxidation is not affected by pH changes in the range of 2–7.However, the Fenton oxidation is not applicable to alkaline solutions, when pH > 8, Fe^{2+} ion begins to form floc and precipitates and H_2O_2 is also unstable and may decompose to give oxygen and water, and finally loses its oxidation ability. Most studies show that pH between 2 and 3 is the most effective in the degradation reactions.

The effects of Fe^{2+}, H_2O_2 dose were investigated and the molar ratios of Fe^{2+} and H_2O_2 were optimized. Firstly, in order to investigate the effect of Fe^{2+} concentration on the dye degradation, experiments were conducted at different Fe^{2+} concentration and at fixed H_2O_2 concentrations of 900 mg/lit for reactive yellow 16. Fig.3 shows the COD and dye removal as a function of the concentration of Fe^{2+}. The trends of COD removal according to Fe^{2+} dose were similar with those of dye removal as shown in Fig.4. The highest COD and dye removals were showed at 1 g/lit of Fe^{2+} concentration for reactive yellow 16.The COD and dye removal efficiencies of reactive dyes are 80 –90 %, respectively. After the optimal Fe^{2+} addition the higher addition of Fe^{2+} resulted in a brown turbidity that causes the

recombination of hydroxyl radicals and Fe^{2+} reacts with hydroxyl radicals as a scavenger. Therefore, the COD removal could decrease .The main cost of Fenton reaction process is the cost of H_2O_2. So, it is important to optimize the amount of H_2O_2 in the Fenton oxidation. The COD and dye removals as a function of $[H_2O_2]$ were presented in Fig. 5 and 6. The results indicate that the removals of COD and dye increase with the increase in the $[Fe^{2+}]$ and $[H_2O_2]$ concentrations. Then, it shows that the fractional degradations of the COD were maximum at 900 mg of $[H_2O_2]$ for reactive yellow 16. The optimum $[H_2O_2]$ doses for dye removals are also found to be around1.15mM of $[H_2O_2]$. These values are in agreement with the dose values of $[H_2O_2]$ for COD removals. The highest removal efficiencies of the COD at a fixed $[Fe^{2+}]$:$[H_2O_2]$ molar ratio for reactive yellow 16 was 80 %, at the optimal $[H_2O_2]$ doses as aforementioned. The maximum dye removal efficiency was 92.0%. However, further increase in $[H_2O_2]$ has negligible effects. At higher H_2O_2 concentration, there is a competition between the substrate and H_2O_2. H_2O_2 in high concentration acts as a scavenger of the hydroxyl radical (HO•) to produce per hydroxyl radical (HO2•) which has much lower oxidation capacities than hydroxyl radical. These results indicate that the efficiencies of Fenton oxidation of reactive dye solutions are higher. In addition, the dye removals by Fenton oxidation were noticeably higher than the COD removal. This can be attributable to fact that the organics, which were decomposed to the smaller organics, still have COD, although the dye solutions were decolorized by the cleavage of critical dye bonds, for example azo double bonds or aromatic ring linkages, as a result of Fenton oxidation.

3.2 Comparison of Fenton oxidation with photo fenton and sono fenton

In order to evaluate the characteristics of Fenton oxidation, Photo fenton and Sono fenton, of Reactive dye, the COD and dye amounts removed were determined and compared. With regard to fentons oxidation 80 % COD and 90 % dye were removed at pH 3.Experiments were conducted in photochemical reactor and Sono chemical reactor at this optimum pH 3. With regard to Photo fenton, 90 % COD and 98 % dye were removed. With regard to Sono fenton, 82 % COD and 95 % dye were removed. Photo fenton and Sono fenton process, showed higher COD and color removal efficiency compared to fentons oxidation.

4. Conclusions

A comparative color and COD removal study combining Fentons oxidation and AOPs, which reveal the merits of green chemistry, was carried out for treating Reactive yellow 16. The following conclusions can be drawn from this study:

(i) AOPs have a superior performance compared to the Fentons oxidation process for the removal of COD and color of Reactive yellow 16. Fenton's oxidation resulted in 80 % COD and 90 % color removal.

(ii) AOPs resulted over 85 % removal for both COD and color. Among the AOPs (H_2O_2/Fe^{2+}/UV, H_2O_2/Fe^{2+}/Sono) studied, the combination of H_2O_2/Fe^{2+}/UV appeared to be the most efficient in terms of COD and color removal with 90% and 98%, respectively. Cost evaluation from the operating cost point of view suggested that Fenton's reagent showed a satisfactory COD and color removal performance and to be economically more viable choice for Reactive yellow 16 on the basis of 90% removal. Among the AOPs processes used in this study, photo fenton process appeared to be the most efficient in terms of COD and color removal with 95% and 98%, respectively.

References

Alaton.I.A, Balcioglu.I.A, Bahnemann.D.W. (2002). Advanced oxidation of a reactive dye bath effluent: comparison of O3, H2O2/UV-C and TiO2/UV-A processes, *Water Res.*, 36, 1143-1154.

Aleboyed.A, Aleboyeh.H, Moussa.Y.”a”. (2003). Decolorisation of Acid Blue 74 by ultraviolet/H2O2, Environ. *Chem.Lett*., 1161-164.

Aleboyed.A, Moussa.Y, Aleboyed.H.”b”. (2005). The effect of operational parameters on UV/H2O2 decolorisation of Acid Blue 74, *Dyes Pigments*, 66, 129-134.

Al-Momani.F, Touraud.E, Degource-Dumas.J.R, Roussy.J,Thomas.O. (2002). Biodegradability enhancement of textile dyes and textile wastewater by UV photolysis, *J. Photochem. Photobiol. A:Chem*. 153, 191-197.

Alnaizy.R, Akgerman.A. (2000). Advanced oxidation of phenolic compounds, Adv. Environ. Res., 4, 233-244.

Azbar.N, Yonar.T, Kestioglu.K. (2004). Comparison of various Advanced Oxidation processes and Chemical treatment methods for COD and Color removal of Polyester and acetate fiber dyeing effluent, Chemosphere, 55, 35-43.

Behnajady.M.A, Modirshahla.N, Shokri.M. (2004). Photodestruction of Acid Orange 7(AO7) in aqueous solutions by UV/H2O2: influence of operational parameters, Chemosphere, 55, 129-134.

Galindo, C., Jacques, P., Kalt, A., (2001). Photochemical and photocatalytic degradation of an indigolid dye: a case study of acid blue 74(AB74). *J. Photochem. Photobiol.A: Chem.*[4], 47-56.

Glaze, W.H., Kang, J.W., (1989). Advanced oxidation processes. Description of kinetic model for the oxidation of hazardous materials in aqueous media with ozone and hydrogen peroxide in a semibatch reactor. *Ind. Eng. Chem. Res.* 28, 1573 – 1587.

Hao, O.J., Ki, H., Chiang, P.C., 2000. Decolorization of wastewater. Crit.Rev.Environ.Sci.Technol.30 (4), 449-505.

Kang.S.F, Chang.H.M. (1997). Coagulation of textile secondary effluents with Fenton’s reagent, *Water Sci.Technol.*, 36,(12) 215-222.

Kuo.W.G. (1992). Decolorizing Dye waste water with Fenton’s Reagent, *water Res.*, Vol 26, No.7, 881- 886.

Kang.S.F, Liao.C.H, HungH.P. (1999). Peroxidation treatment of dye manufacturing waste water in the presence of ultraviolet light and ferrous ions, *Journal of Hazardous Materials*, 317-333.

Ledakowics.S, Gonera, M., (1999). Optimization of oxidant dose for combined chemical and biological treatment of textile wastewater. *Water Res.* 33(1), 2511-2516.

Legrini. O., Oliveros.E. Braun, A.M., (1983). Photochemical processes for water treatment. *Chem. Rev.* 93, 671-698.

Muruganandham.M, Swamination.M. (2004). Decolorisation of Reactive Orange 4 by Fenton and Photo-Fenton oxidation technology, *Dyes Pigments,* 63, 315-321.

Nigam, P., Armour, G., Banat, I.M., Singh, D., Marchant, R., (2000). Physical removal of textile dyes and solid state fermentation of dye-adsorbed agricultural residues. *Bioresour. Technol.* 72, 219-226.

Oliver, J.H., Hyunook, K., Pen-Chi, C., (2000). Decolorization of wastewater. Crit. Rev. Environ. Sci. Technol. 30 (4), 499-505.

Raghavacharya, C., (1997). Colour removal from industrial effluents-a comparative review of available technologies. *Chem. Eng. World*. 32, 53-54.

Robinson, T., McMullan, G., Marchant, R., Nigam, P., (2001). Remediation of dyes in textile effluents; a critical review on current treatment technologies with a proposed alternative. *Bioresour. Technol.*77, 247-255.

Schrank.S.G, Jean Nonato Ribeiro Clos Santos, Danillo San to S Souza, Elayne Ernilia Santos Souza. (2007). Decolorization of Vat Green 01 textile dye and textile waste water using H_2O_2/UV process, *Journal of Photo Chemistry and Photobiology*, 125-129.

Solozhenko, E.G., Soboleva, N.M., Goncharuk, V.V., (1995). Decolourization azodye solutions by Fenton’s oxidation. *Water Res.* 29 (9), 2206-2210.

Shu.H.Y, Chang.M.C. (2005). ”a”. Pre-ozonation coupled with UV/H2O2 process for the decolorization and mineralization of cotton dyeing effluent and synthesized C.I. Direct Black 22 wastewater, *J. Hazard. Mater.,* B 121, 127-133.

Shu.H.Y, Chang.M.C. (2005).”b”. Decolorization and mineralization of phthalocyanine dye C.I. Direct Blue 199 using UV/H2O2 process, *J. Hazard. Mater., B* 125, 96-101.

Shu.H.Y, Chang.M.C.”c”. (2005). Decolorization effects of Siz azo dyes by O3, UV/O3 and UV/H2O2 processes, *dyes and pigments,* 25-31.

ShuH.Y."d". (2006). Degradation of dye house effluent containing C.I. Direct Blue 199 by processes of ozonation, UV/H2O2 and in sequence of ozonation with UV/H2O2 , *J. Hazard. Mater.*, 13, 392-98.

Walling, C., (1975). Fenton's reagent revisited. *Acc. Chem. Res.* 8, 125-131.

GRAPHS

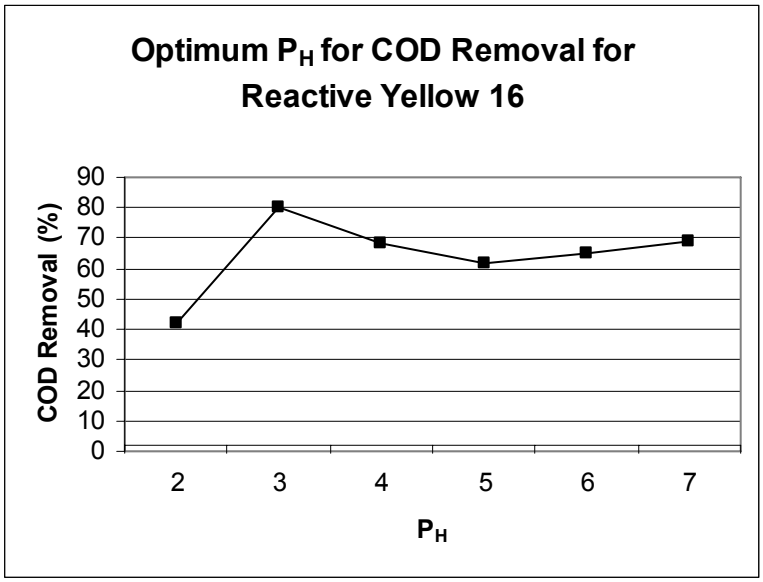

Figure 1. Effect of pH (C_{H2O2} = 0.9 g/lit and C_{FeSo4} = 1 g/lit) on COD removal in Fenton's process

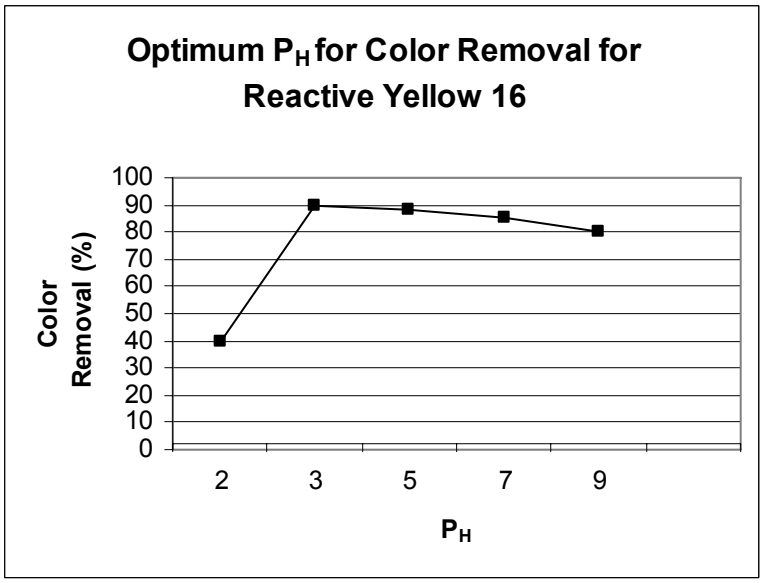

Figure 2. Effect of pH (C_{H2O2} = 0.9 g/lit and C_{FeSo4} = 1 g/lit) on Color removal in Fenton's process

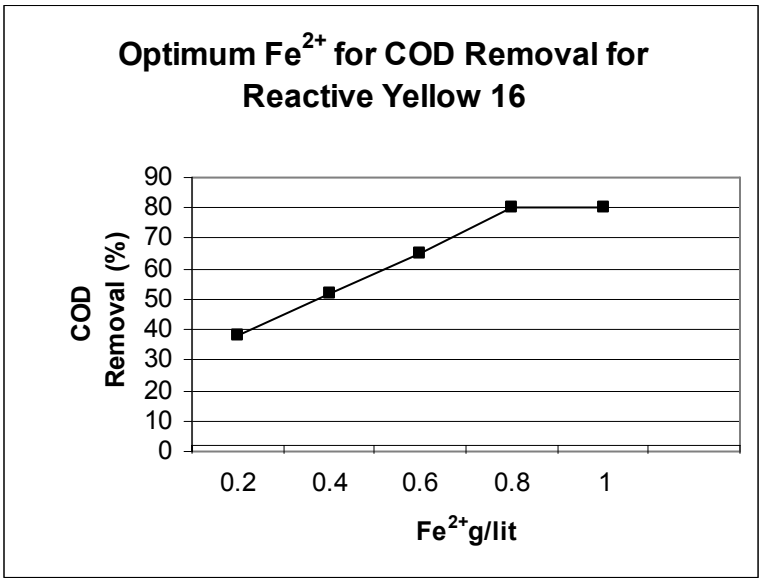

Figure 3. Effect of varying $FeSo_4$ dosages (pH = 3 and C_{H2O2} = 0.9 g/lit) on COD removal in Fenton's process

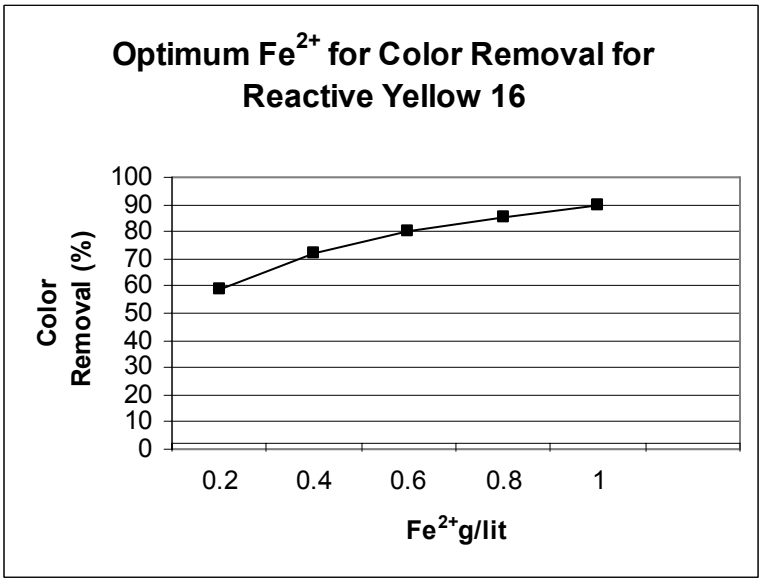

Figure 4. Effect of varying $FeSo_4$ dosages (pH = 3 and C_{H2O2} = 0.9 g/lit) on Color removal in Fenton's process

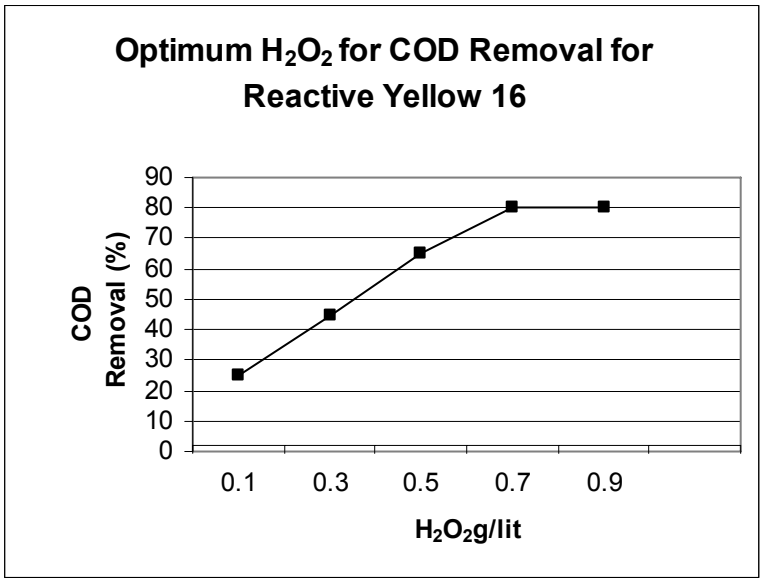

Figure 5. Effect of varying H_2O_2 dosages (pH = 3 and C_{FeSo4} = g/lit) on COD removal in Fenton's process

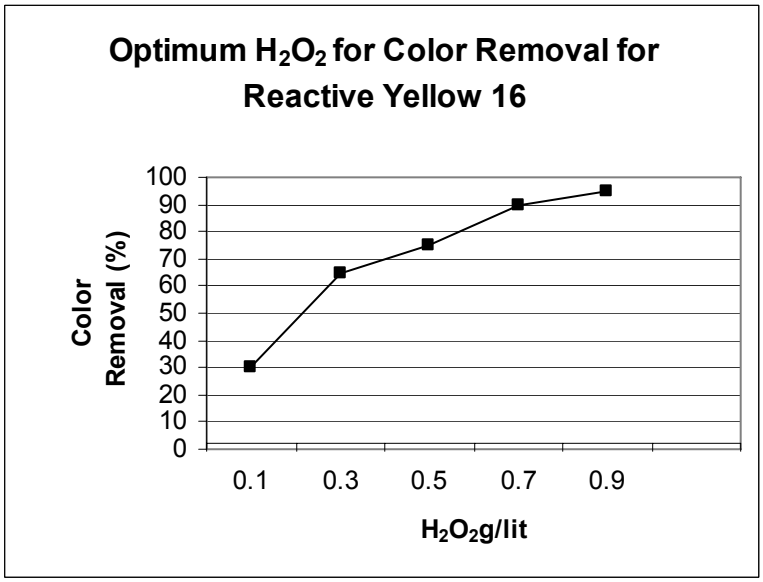

Figure 6. Effect of varying H_2O_2 dosages (pH = 3 and C_{FeSo4} = 1 g/lit) on Color removal in Fenton's process

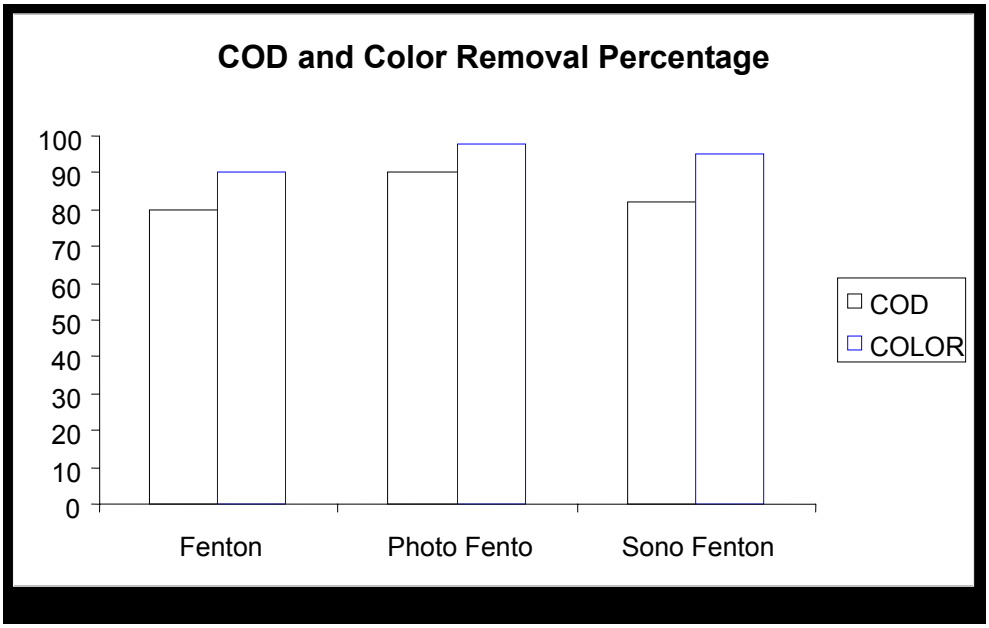

Figure 7. Comparison of Fenton, Photo Fenton, and Sono Fenton process on COD and Color removal

Modern Applied Science

www.ccsenet.org/journal.html

Vol. 3, No. 8

August 2009

Study on the Vehicle Increase Prediction Model on Chinese Highways

Wei Fu

Department of Basic Course, Southwest Jiaotong University, Emei 614202, China

E-mail: wei_f730@163.com

Abstract

The vehicle increase prediction was discussed in the article. Starting from the actual situation and the characters of vehicle increase on the highways, various factors such as the large base of vehicle amount, the increase of average income, rural vehicle amount, the enhancement of comprehensive vehicle amount and the increase phenomena of vehicle purchase by young people to impact the vehicle increase on highways were considered comprehensively, and the statistical analysis were made aiming at these factors one by one, and the impacts of these factors on the vehicle increase on highways and the concrete impacting modes were discussed, and the vehicle increase model were established and improved. By the statistical software SPSS, the regression analysis of the curve parameter estimation was made to confirm the function form of the concrete curve, and the Mathematica and Matlab were used to confirm the parameters and influences of various factors in the model by a series of data fitting, and the final model were established.

Keywords: Statistical analysis, Curve fitting, Grey prediction, Differential equation

1. Description of the problem

Some new characters have occurred in the development of the vehicle on highways in recent years, and the increase of amount, the continual rise of the ratio of different vehicles, the average income and other factors all influence the increase of vehicle on highways. The “Report of National Vehicle Development Strategic Research” issued in the beginning of 2007 also further analyzed these characters.

There are many researches about the amount of vehicle, and abundant data materials have been accumulated.

In the article, starting from above characters about the actual situation of highway and the increase of vehicle, and using relative data (including searching relative literatures and supplementing new data) in the Appendix 2 for references, the mathematical model of the vehicle increase on highways is established, and the model is used to predict the middle and short-term trend and the long-term trend of the vehicle increase on highways.

2. Hypotheses of the problem

(1) Under normal situation, there are not large numerous of vehicles to enter and quit.

(2) The influence degrees of all discussed factors on the vehicles on highways can be denoted by the function about the time t, and they all change with the changes of t according to certain rule.

(3) The ideal vehicle entering and quitting proportion is about 1:1, and this proportion will not influence the settlement of the problem.

(4) The ideal vehicle structure is the time structure in the stable vehicle model.

(5) Entering and quitting are independent each other.

(6) The speed of vehicle increase v is proportional to the base amount of vehicle.

(7) The vehicle increase is limited by the total amount.

(8) The level of vehicle is higher, and the increase speed of vehicle amount is slower.

(9) It is generally to think that the unreasonable structure of vehicle increases the increase of vehicle on highways.

3. Denotation of symbols

N is the total amount of vehicle at the time of t.

v is the vehicle increase speed at the time of t.

r is the vehicle increase rate at the time of t.

η is the measurement value of vehicle quality at the time of t.

N_m denotes the most total amount of vehicle which can be accepted by the highway.

S denotes the difference between the vehicle structure and the expectation structure at the time of t.

W is the proportion of urban vehicle at the time of t.

b is the vehicle increase rate at the time of t.

d is the vehicle scarp rate at the time of t.

δ is the proportion of vehicle transfer at the time of t.

4. Analysis of the problem

According to the statistical data of the traffic office, the core indexes influencing the vehicle increase on highway include the amount of vehicle possessed by the city along the highway, the vehicle structure (including truck and car), the vehicle speed, the speeds of vehicles with different structures, the work efficiency of the highway toll station, and the vehicle fault rate.

In recent years, the vehicle development of highway continually rise with the development of the society, the increase of vehicle speed, the continual increase of vehicle amount, the increase of rural vehicle, and the speed-raising of highway, and these factors all impact the amount of vehicle on highways.

Concretely speaking, the increase rate of highway vehicle amount is impacted by many factors, and the vehicle structure decides different speeds of vehicles, and the vehicle increase speed will be impacted to slow down, and the increase of vehicle speed will decrease the natural increase of vehicle amount, and the increase of vehicle fault rate will decrease the increase speed of the highway vehicle amount, and the increase of vehicle will accelerate the increase of the highway vehicle amount, and the vehicle structure will influence the increase rate of vehicle amount, i.e. the level of vehicle is higher and the fault rate is lower, which will make the natural increase rate of vehicle amount decrease, and the uncertain vehicle amount will accelerate the vehicle change, and the speed of vehicle increase is related with the base amount of highway vehicle, and the base amount of vehicle is larger, and the speed of vehicle increase is higher.

The classic model to describe the highway vehicle increase (Yang, 2003) is

$$\begin{cases} v = \dfrac{dN}{dt} = \mathrm{r}(1 - \dfrac{N}{N_m})N \\ N(t_0) = N_0 \end{cases}$$

Where, N_m denotes the most total amount of vehicle which can be accepted by the highway and r is the natural increase rate.

This model only considers the base amount of vehicle and the influence of limited resource to the vehicle increase, but doesn't consider the influences of vehicle speed, the continual increase of vehicle amount and the increase of urban vehicle on the highway vehicle increase, so we need improving this model to comprehensively consider these factors.

(1) Considering the influence of the base amount of vehicle, the speed of vehicle increase v is proportional to the base amount of vehicle, i.e.

$v \propto N$

(2) Considering the factor of limited resource, the increase of vehicle is limited by the total amount of highway vehicle, and the mathematical description is

$v \propto (1 - N/N_{\mathrm{m}})$

(3) Considering the running speed of vehicle, i.e. the influence of the vehicle speed on the amount increase speed, the speed is higher and the vehicle increase speed is lower, i.e.

$$v \propto 1/\eta$$

$$\eta = \sum_i W_i \eta_i$$

Where, W_i denote the proportions of various types of vehicle. η_i denotes the vehicle speed, and for the yearly value of η_i, $\eta_i \in \{0.25, 0.50, 0.75, 1.0\}$, and for the type C vehicle speed, $\eta_1 = 0.25$, and for the type B vehicle speed, $\eta_1 = 0.50$, and for the type A vehicle speed, $\eta_1 = 0.75$, and for the vehicle speed with higher types, $\eta_1 = 1.0$.

(4) Considering the influence of amount structure on the vehicle increase speed, the reasonless vehicle structure will accelerate the increase of vehicle amount, i.e.

$v \propto S$

The so-called vehicle expectation structure means the stably increasing vehicle model in the vehicle increase model, and it can be denoted by the vehicle rate of each type.

$$S = \sum_i (b_i - a_i)^2$$

Where, a_i denotes the proportion of various vehicle amounts in the expectation time structure, b_i denotes the rate of the i'th vehicle at the time of t.

Concretely, according to the mathematical knowledge of social vehicle, the static vehicle increase model, i.e. the age structure of stable model, is seen in Table 1.

(5) Considering the influence of village and town distribution on the vehicle increase speed, the town living condition is better than the condition of village, so the town vehicle will accelerate the increase of highway vehicle increase, i.e.

$v \propto W$

(6) Considering the influence of the vehicle type rate on the vehicle increase speed, the vehicle type rate is higher, and the increase of vehicle amount will be limited, so

$v \propto 1/(1+S)$

(7) Considering the influence of entering rate and quitting rate of vehicle amount on the vehicle increase, the natural increase rate of vehicle amount equals to the different of the entering rate and the quitting rate, i.e.

r=b-d

Where, the vehicle entering rate is

$$b = \frac{enteringam\ ount}{totalamoun\ t(highway)}$$

And it is influenced by the vehicle increase rate, and the entering rate from the city to the highway = entering amount/ the total amount of vehicle in the city. So,

$$b = \frac{enteringam\ ount}{totalcitya\ mount * totalamoun\ t(highway)}$$

At the same time, the vehicle increase speed is proportional to the natural increase rate of vehicle amount r, so

$$v \propto r = b - d$$

(8) Considering the influence of the proportion of fault vehicle amount in the vehicle amount on the vehicle increase, the fault proportion is higher, and the increase of vehicle amount is more limited, i.e. the increase speed is lower, $v \propto 1/\delta$.

(9) The influence of flow vehicle amount on the vehicle increase speed, i.e. the increase of flow vehicle amount will add pressure to the highway, will accelerate the vehicle increase speed, and this factor and its influences are not considered in the article.

(10) Considering the influence of vehicle life on the vehicle increase, the enhancement of average vehicle life will increase the vehicle amount, and the vehicle increase will be impacted, and the vehicle increase speed will be accelerated.

So based on above factors influencing vehicle increase, the vehicle increase speed model can be established. Through data fitting by corresponding data, corresponding parameters can be solved, so the development trend of future vehicle amount can be predicted.

5. Establishment of the model

For the long-term prediction of highway vehicle increase, the model is established to predict this trend.

First, nine factors influencing the vehicle increase speed in the problem are changeable, i.e. these factors are the functions about the time t, and they can be denoted by

$$f_i = f_i(t); i = 1, 2, .., 9$$

So, the model equation about the vehicle increase speed can be denoted by

*Model*1:

$$\begin{cases} v = \dfrac{dN}{dt} = K_1 \prod_{i=1}^{9} f_i(t) \\ N(t_0) = N_0 \end{cases}$$

Where, K_1 is a constant number.

Because the data can not allow us to quantitatively discuss the eighth and ninth factors (i.e. the proportion of fault vehicle amount in the total vehicle amount and the amount of flow vehicle), so the factors from the first factor to the seventh factor are used to establish the model.

Concretely, replace Model 1 by the concrete expressions of 7 factors, and the following model expression can be obtained.

$Model2$:

$$\begin{cases} v = \dfrac{dN}{dt} = \dfrac{K_2 NWSr(1 - N/N_m)}{\eta(1+\delta)(1+\varphi)} \\ N(t_0) = N_0 \end{cases}$$

Where, K_2 is a constant number, and

$N = N(t); S = S(t); \varphi = \varphi(t);$

$r = r(t); W = W(t); \eta = \eta(t)$

$$\eta(t) = \sum_i W_i \eta_i$$

$$S(t) = \sum_i (b_i - a_i)^2$$

According to relative data, the mathematical software is used to perform the data fitting to all functions about the time t, and the mathematical expressions about the time t with good fitting effect are

$N = N(t); S = S(t); \varphi = \varphi(t); r = r(t); W = W(t); \delta = \delta(t); \eta = \eta(t)$

Put them into the original model equation, so

$Model3$:

$$\begin{cases} v = \dfrac{dN(t)}{dt} = \dfrac{K_3 N(t) W(t) S(t) r(t)[1 - N(t)/N_m]}{\eta(t)[1+\delta(t)][1+\varphi(t)]} \\ N(t_0) = N_0 \end{cases}$$

Where, K_3 is a constant number.

But, because the actual data are limited, the influences of the vehicle fault rate, the vehicle level and the flow vehicle amount on the vehicle increase speed are not analyzed, so these factors are not considered in the concrete problem. Modify the model 3 and eliminate δ, η and the flow vehicle amount, and the model 4 can be obtained.

$Model4$:

$$\begin{cases} v = \dfrac{dN(t)}{dt} = \dfrac{KN(t) W(t) S(t) r(t)[1 - N(t)/N_m]}{[1+\varphi(t)]} \\ N(t_0) = N_0 \end{cases}$$

Where, K is a constant number.

According to above formula, the mathematical software *Mathematica* is used to solve the vehicle amount function about the time t (year) (concrete program is seen in Appendix 3).

$Model5$:

$N = N(t)$

The expression is denoted by *t, K and N*.

Replace the actual vehicle amount data (t_1, N_1) and (t_2, N_2) in $N = N(t)$, we can obtain the values of K and N, so the expression of vehicle amount can be obtained.

$N = N(t)$

The problem is to predict the vehicle amount in future certain year, and to obtain the highway vehicle amount in future period, replace the time t_i in the vehicle amount expression, so the predicted vehicle amount of that year can be obtained.

$N_i = N(t_i)$

By this way, we can obtain long-term prediction result.

For the middle-term and short-term prediction of highway vehicle increase, the $GM(1,1)$ model is used to perform the grey prediction.

(1) Associated coefficients.

Supposed that

$$\hat{N}^{(0)}(k)=\left\{\hat{N}^{(0)}(1),\hat{N}^{(0)}(2),...,\hat{N}^{(0)}(n)\right\} \quad N^{(0)}(k)=\left\{N^{(0)}(1),N^{(0)}(2),...,N^{(0)}(n)\right\}[0,1]$$

So the associated coefficient is defined as

$$\eta(k)=\frac{\min\min\left|\hat{N}^{(0)}(k)-N^{(0)}(k)\right|+\rho\max\max\left|\hat{N}^{(0)}(k)-N^{(0)}(k)\right|}{\left|\hat{N}^{(0)}(k)-N^{(0)}(k)\right|+\rho\max\max\left|\hat{N}^{(0)}(k)-N^{(0)}(k)\right|}$$

Where, $\left|\hat{N}^{(0)}(k)-N^{(0)}(k)\right|$ is the absolute error between the k'th point $X^{(0)}$ and $\hat{X}^{(0)}$.

$\min\min\left|\hat{N}^{(0)}(k)-N^{(0)}(k)\right|$ is the minimum error between two classes.

$\max\max\left|\hat{N}^{(0)}(k)-N^{(0)}(k)\right|$ is the maximum error between two classes.

p is the distinguish-ability, 0<ρ<1, generally, ρ=0.5.

For the sequences with different units and different initial values, they should be initialized before computing relative coefficients, i.e. eliminate the first value in all data in this sequence.

(2) Degree of association.

$r=\frac{1}{n}\sum_{k=1}^{n}\eta(k)$ is the association degree between $N^{(0)}(k)$ and $\hat{N}^{(0)}(k)$.

For the establishment of the $GM(1,1)$ model,

First, the time sequence $X^{(0)}$ has n observation values, $N^{(0)}=\left\{N^{(0)}(1),N^{(0)}(2),...,N^{(0)}(n)\right\}$, and through accumulation, the new sequence $N^{(1)}=\left\{N^{(1)}(1),N^{(1)}(2),...,N^{(1)}(n)\right\}$ generates, so the corresponding differential equation of the model $GM(1,1)$ is

$$\frac{dN^{(1)}}{dt}+aN^{(1)}=\mu$$

Where, α is the grey number of development, and μ is the endogenetic grey number.

Second, supposed $\hat{\alpha}$ is the solve-for parameter vector, $\hat{\alpha}=\left(\frac{a}{\mu}\right)$, it can be solved by the least square method.

$$\hat{\alpha}=\left(B^{T}B\right)^{-1}B^{T}Y_{n}$$

Solve the differential equation, and the prediction model can be obtained.

*Model*6:

$$\hat{N}^{(1)}(k+1)=\left[N^{(0)}(1)-\frac{\mu}{a}\right]e^{-ak}+\frac{\mu}{a},\quad k=0,1,2...,n$$

Third, the test of grey prediction is the residual error test.

For the short-term and middle-term predictions of vehicle increase, the Model 5 can be used to solve these predictions.

6. Solution of the problem

(1) The grey prediction to the future short-term and middle-term vehicle amounts

According to the data, the statistics of the highway vehicle amount in recent years is seen in Table 2.

The corresponding scatter diagram is showed as follows.

FIGURE (simulation)

The grey prediction model of Model 6 is utilized to obtain the short-term vehicle amount by the *Mathematica* software, and the concrete situation is seen in Table 3 (concrete program is seen in Appendix).

(2) The model prediction to the long-term vehicle amount

First, solve the concrete expression of the model. To solve the function expressions of various factors about the time t, the data fitting should be implemented for corresponding data.

The least square method is used to perform the curve fitting of data.

Supposed the curve expression is $y=y(x)$.

Solve the objective function $\min z=\sum_i[y(x_i)-y_i]^2$, i.e. minimize z.

(1) The relationship fitting between the difference S of the age structure and the expectation age structure of vehicle amount at the time of t and the time of t

By the software of EXCEL, the data in the appendix (including data from Internet) are processed to table the corresponding values of s and t (seen in Table 4).

From the data in the table, (supposed) on abnormal point (11, 0.0027) is found, the data fitting at this point should not be performed. Perform the relationship fitting of S and t by the data. First, the future vehicle amount fault rate will be reduced gradually according to the prediction information (seen in Figure 1), and the reasonless speed of vehicle structure will be reduced also, so one function curve corresponding with the curve in the following figure is tried to find to perform the data fitting.

Figure 1. Prediction Diagram

For the data analysis, the software SPSS is used to perform the multiple regression analysis about the curve parameter estimation, and the information obtained is seen in Table 5.

From the information in Table 5, through repetitive fitting and analysis of curve, the function form with good fitting curve with the original data, i.e. the power function form can be found.

For the parameter estimation, perform the power function curve fitting to the data, so

$$S(t)=0.0000039666\,t^3-0.023714\,t^2+47.259\,t-31393$$

(2) The relationship fitting between the difference φ of the vehicle type rate and normal value in the year t and the time of t

In the same way of (1), the corresponding values of φ and t are seen in Table 6.

According to the prediction information in appendix (seen in Figure 2), the general development trend of the future vehicle type rate can be obtained, so one curve basically corresponding with the curve in the following figure can be found to perform the data fitting.

Figure 2. Variance of New-added Vehicle Type Rate Period

In the same ways of (1), the SPSS is used to perform the regression analysis to the data, the fitting function form of the optimal fitting curve, i.e. trigonometric function, can be obtained, and then use the Matlab to perform the curve fitting of data. By the data fitting, the following formula can be obtained.

$$\varphi(t)=0.0152104\ \mathrm{Sin}(81.5969+0.960176\ x)$$

(3) The relationship fitting of the natural increase rate r of the vehicle amount and the time of t in the t'th month

As seen in Table 7, the quitting rate can be computed according to the relative data.

Part result of data processing is seen in Table 8.

So the data about the corresponding natural increase rate r can be obtained.

In the same way of (1), combining with the entering rate and the quitting rate, the corresponding values of r and t are seen in Table 9.

In the same way of (1), the SPSS is used to perform the regression analysis for the data, and the fitting function form of the optimal fitting curve can be obtained, and then the Matlab is used to perform the curve fitting for data.

Through data fitting, the following formula can be obtained.

$r(t) = 0.00048983\,t^3$-$2.9258\,t^2$+$5824.8t$-3864900

(4) The relationship fitting between the urban vehicle amount proportion and the time of t in the year of t

In the same way of (1), combining with the entering rate and the quitting rate, the corresponding values of W and t are seen in Table 10.

In the same way of (1), the SPSS is used to perform the regression analysis for the data, and the fitting function form of the optimal fitting curve can be obtained, and then the Matlab is used to perform the curve fitting for data.

Through the data fitting, the following formula can be obtained.

$W(t) = -0.000060889t^3 + 0.36533\,t^2 - 730.66\ t + 487090$

The relationships between four factors including the vehicle amount age structure, the natural increase rate, the type property, and the urban vehicle amount proportion with the time t are found through above analysis and computations, i.e.

$S = S(t); \qquad \varphi = \varphi(t);$

$r = r(t); \qquad W = W(t)$

According to the model 4, replace the concrete expressions of $s = s(t); \varphi = \varphi(t); r = r(t); W = W(t)$, and $N(t_0 = 2005) = 1308$ (supposed that the total vehicle amount is 13.08 million in January of certain year) in the model 4, the differential equation about the time t can be obtained.

$$\begin{cases} \dfrac{dN(t)}{dt} = \dfrac{KN(t)W(t)S(t)r(t)[1 - N(t)/N_m]}{[1+\varphi(t)]} \\ N(t_0 = 2005) = 1308 \\ S(t) = 0.0000039666\,t^3 - 0.023714\,t^2 + 47.259\,t - 31393 \\ r(t) = 0.00048983\,t^3 - 2.9258\,t^2 + 5824.8\ t - 3864900 \\ W(t) = -0.000060889t^3 + 0.36533\,t^2 - 730.66\ t + 487090 \\ \varphi(t) = 0.0152104\ \mathrm{Sin}(81.5969 + 0.960176\ \mathrm{t}) \end{cases}$$

Utilize the software *Mathematica* to solve the differential equation, and the expression about t, K and N_m of the vehicle amount can be obtained (program and result are seen in appendix 4). Replace any two groups of actual vehicle amount data (t_1, N_1) and (t_2, N_2) in $N = N(t)$, and use the software of *Matlab* to solve the equation group with two unknowns, and $K = -1.1e^{-6}$, N_m=81. So the expression of vehicle amount can be obtained.

$$N(t) = \frac{810000}{1 + \dfrac{1}{130756} e^{(-1.2\times10^{-11}t^7 - 1.6228\times10^{-7}t^6 - 0.00097t^5 + 3.23082t^4 - 6446.693t^3 + 7717896t^2 - 5133023692t)}}$$

Next, this model is used to predict the development of vehicle amount in future 50 years in China.

Replace the time (year) in the expression, and obtain the predicted vehicle amount.

$N_i = N(i); i = 2006, 2007, .., 2055$

N_i denotes the total amount of vehicle in the years of i, and the total vehicle amount in china from 2006 to 2055 can be predicted.

The software *Matlab* can be used to seek the total amount of vehicle in China from 2006 to 2055.

The mathematical software is used to draw the long-term vehicle increase line chare on highways.

7. Evaluation and extension of the model

This model comprehensively considers the influences of numerous factors on the vehicle increase speed in China, and a comprehensively general mathematical model about the vehicle increase is established. The character of this model is to take the function model of vehicle amount about the time of t as the base, and respectively establish function relationships about the time of t under the influences of many factors such as vehicle type proportion, vehicle amount age structure, vehicle amount comprehensive quality, and the village and city vehicle amount distribution. These factors were comprehensively considered to establish the vehicle amount prediction model to perform the prediction. By this way, the analysis of single variable will reduce the complexity of the problem and make the establishment of the model become more easily. At the same time, in the settlement of the model, the fitting precision is considered fully, so the final model is more reasonable, and the prediction result of the vehicle amount is more reasonable.

There are deficiencies in the model. For the short-term and middle-term vehicle amount prediction, only the classic grey prediction method was used, but the grey prediction can only predict the short-term vehicle increase, and it will produce large prediction error for the long-term vehicle amount. So we attempted to use the prediction result of the first time to predict the result of the second time, but the prediction effect was not good, so for the middle-term vehicle amount prediction, the method is not efficient enough. At the same time, the rationality and the validity of the model will depend on the fitting precision and quality of a series of data, which would bring difficulties to establish the reasonable model and prediction.

In addition, for part problems in the vehicle amount model, the probability statistics knowledge can be used to establish the model, and the normal distribution can be used to establish and solve the model.

This model is the vehicle amount prediction model, and this model can predict the vehicle amount on highways in future, which can help the traffic office to control the vehicle amount and eliminate the burst fuse of the vehicle amount on highways.

References

Jiang, Qiyuan et al. (2003). *Mathematical Model (3rd edition).* Beijing: Higher Education Press. Aug of 2003.

Tan, Yongji et al. (2004). *Mathematical Model.* Shanghai: Fudan University Press. Aug of 2004.

Xiao, Wei et al. (2005). *Matlab Program Design and Application.* Beijing: Tsinghua University Press & Beijing Jiaotong University Press. July of 2003.

Yang, Mingsheng et al. (2003). *Mathematica Base and Mathematical Software.* Dalian: Dalian University of Technology Press. Aug of 2003.

Table 1. Age structure of the quiet vehicle increase mode

Vehicle type	A	B	C	Senior vehicle
Proportion	0.25	0.5	0.2	0.05

Table 2. Data statistics of vehicle amount (unit: million)

Month	1	2	3	4	5	6	7	8	9	10
Amount of vehicle	1224	1236	1248	1258	1267	1276	1285	1292	1300	1308

Table 3. Short-term prediction of vehicle amount (unit: million)

Year	11	12	13	14	15	16	17	18	19	20
Amount of vehicle	1319	1328	1337	1346	1356	1365	1375	1384	1394	1403

Table 4. Corresponding values of S and t

t (month)	16	15	14	13	12	11	10	9
S (t)	0.0638	0.0624	0.0607	0.0592	0.0577	0.0027	0.0553	0.0551
T (month)	8	7	6	5	4	3	2	1
S (t)	0.0548	0.0545	0.0543	0.0541	0.0538	0.0536	0.0535	0.0534

Table 5. Model summary and parameter estimates

Dependent Variable: VAR00002

	Model Summary					Parameter Estimates			
Equation	R Square	F	df1	df2	Sig.	Constant	b1	b2	b3
Linear	.154	1.090	1	6	.337	-6.424	.003		
Logarithmi	.154	1.089	1	6	.337	-49.168	6.475		
Quadratic	.154	1.090	1	6	.337	-3.187	.000	08E-007	
Cubic	.154	1.091	1	6	.336	-2.108	.000	.000	69E-010
Compound	.086	.566	1	6	.480	35E-115	1.139		
Power	.086	.565	1	6	.481	.000	261.173		
S	.086	.565	1	6	.481	257.849	-522776		
Growth	.086	.566	1	6	.480	-264.497	.130		
Exponentia	.086	.566	1	6	.480	35E-115	.130		

The independent variable is VAR00001.

Table 6. Corresponding values of the vehicle type rate warp and the time t

t (month)	15	14	13	12	11	10	9	8
φ (t)	0.0630	0.0629	0.0620	0.0606	0.0600	0.0674	0.0589	0.0513
t (year)	7	6	5	4	3	2	1	0
φ (t)	0.0436	0.033411	0.042065	0.045082	0.041812	0.04273	0.055166	0.062693

Table 7. Fitting of the relationship between the natural increase rate of vehicle amount in the t'th month with the time t

Unit: %	8	9	10	11	12	13	14	15
Entering rate b	15.64	14.64	14.03	13.38	12.86	12.41	12.29	12.4

Table 8. Part result of data processing

Unit: ‰	8	9	10	11	12	13	4	15
Quitting rate b	6.5	6.46	6.45	6.43	6.41	6.4	6.42	6.51

Table 9. Corresponding values of r and t

t (month)	15	14	13	12	11	10	9	8
r (t)	5.89	5.87	6.01	6.45	6.95	7.58	8.18	9.14
t (month)	7	6	5	4	3	2	1	0
r (t)	10.06	10.42	10.55	11.21	11.45	11.6	12.98	14.39

Table 10. Corresponding values of W and t

t (month)	1	2	3	4	5	6	7	8
W (t)	26.94%	27.46%	27.99%	28.51%	29.04%	30.48%	31.91%	33.35%
t (month)	9	10	11	12	13	14	15	
W (t)	34.78%	36.22%	37.66%	39.09%	40.53%	41.76%	42.99%	

Modern Applied Science

www.ccsenet.org/journal.html

Vol. 3, No. 8

August 2009

Production of Bio-ethanol from Sugar Molasses Using *Saccharomyces Cerevisiae*

Shanmugam Periyasamy

Department of Mechatronics Engineering, K. S. R College of Technology

Tiruchengodu, TN, India

Tel: 91-4288-274741 E-mail: shanmugam2002@gmail.com

Sivakumar Venkatachalam (Corresponding author)

Department of Food Technology, Kongu Engineering College

Perundurai, Erode - 638052, TN, India

Tel: 91-4294-226-602 E-mail: drvsivakumar@yahoo.com

Sridhar Ramasamy

Department of Chemical Engineering, Kongu Engineering College

Perundurai, Erode - 638052, TN, India

Tel: 91-4294-226-602 E-mail: sridhar36k@yahoo.co.in

Venkatesan Srinivasan

Department of Chemical Engineering, Kongu Engineering College

Perundurai, Erode - 638052, TN, India

Tel: 91-4294-226-602 E-mail: venkatesan79@gmail.com

Abstract

Saccharomyces cerevisiae is the cheapest strain available for the conversion of biomass substrate. In the present study, it is used for bio-ethanol production from sugar molasses. The influencing parameters that affect the production of bio-ethanol from sugar molasses are optimized. The optimal values of the parameters such as temperature, pH, substrate concentration, enzyme concentration and fermentation period are found to be 35°C, 4.0, 300 gm/l, 2 gm/l and 72 h respectively. Under this optimum operating condition the maximum of 53% bio-ethanol yield is achieved. The rate of formation of bio-ethanol is found to be well fitted with Michael-Menten equation and the rate constants such as V_{max} and K_m are found to be 0.71 mol/l sec and 81.63 mol/l respectively.

Keywords: Bio-ethanol, Sugar molasses, Fermentation, Saccharomyces cerevisiae

1. Introduction

Nowadays the petroleum products are running out of race due to unbalanced relation between supply and demand besides air pollution of sources. The hike in petrol cost is mainly due to shortage of resources which leads to search for alternate fuel to replace fossil fuels. An eco-friendly bio-ethanol is one such alternate fuel that can be used in unmodified petrol engines with current fueling infrastructure and it is easily applicable in present day combustion engine, as mixing with gasoline (Hansen et al., 2005). Combustion of ethanol results in relatively low emission of volatile organic compounds, carbon monoxide and nitrogen oxides. The emission and toxicity of ethanol are lower than those of fossil fuels such as petroleum, diesel etc., (Wyman & Hinman, 1990). More than a few decades, though there have been several reviews of literature (Beatriz Palmarola et al., 2005, Dale, 1987, Ferrari et al., 1992, Martin et al.,

2006, Nigam, 1992, Olsson & Hahn-Hagerdal, 1996) available for the production of bio-ethanol from various sources, only a very few authors (De Vasconcelos et al., 1998; Doelle and Greenfield, 1985; Huertaz-Díaz et al., 1991) have studied kinetics for the production of ethanol from sugar cane using yeast cells (*Saccharomyces cerevisiae*). Hence in this present research an attempt has been made to optimize the variables which affect the bio-ethanol production from sugar molasses and the experimental results are compared with the available reaction kinetics.

2. Material and Methods

2.1 Experimental methods

A known quantity of sugar molasses and Baker's Yeast (*saccharomyces cerevisiae*) were taken in fermentation flask and kept in a constant temperature shaker. An anaerobic condition was maintained for four days and during this period, the strain converts sugar into bio-ethanol with the evolution of CO_2. A known fermented sample was collected for every 12 h interval. The same procedure was repeated to optimize the parameters such as pH, Temperature, substrate concentration and yeast concentration.

2.2 Identification of bio-ethanol

About 5 to 10 ml fermented sample was taken and pinch a of potassium dichromate and a few drop of H_2SO_4 were added. The colour of the sample turns from pink to green which indicates the presence of bio-ethanol.

2.3 Determination of sugar concentration

The sugar concentration was determined by Rapid method. The 5 ml of fermented sample was taken and dissolved in 100 ml of distilled water and mixed with 5 ml of conc. HCL acid and is heated at 70^{o}C for a period of 10 min. The obtained sample was neutralized by adding NaOH and it was prepared to 1000 ml and taken into burette solution. The 5 ml of Fehling A and 5 ml of Fehling B were taken and mixed with 10 to 15 ml of distilled water in a conical flask and Methylene blue indicator was added. The conical flask solution was titrated with burette solution in boiling conditions until disappearance of blue colour. The sugar concentration was calculated by using the formula given below:

Sugar Concentration (gm/l) = [(Dilution factor x Fehling factor) / Titrate value] x 100

2.4 Determination of ethanol concentration and pH

Ethanol concentrations were determined by gas chromatography, using a CG-3537D gas chromatograph manufactured by Instruments Scientifics CG LTDA with a flame ionization detector and a CG-300 integrator. The pH was determined with a B272 pH digital meter, manufactured by MICRONAL.

3. Result and Discussion

3.1 Optimization of pH

The sample was fermented to different pH values between 1.0 and 8.0 to obtain maximum yield of bio-ethanol by adding lime or sulphuric acid. The samples were kept in anaerobic condition for a period of four days and the fermented solution was analyzed for every 12 h intervals. Figure 1 show that the bio-ethanol concentration gradually increases along with the increase in pH and reaches a maximum percentage of bio-ethanol production when pH is equal to 4 and later it starts declining due to the lesser activity of yeast. De Vasconcelos et al., (1998) and Nigam, (1999) are also observed the maximum ethanol productivity at pH of 4.2 to 4.5.

3.2 Optimization of Fermentation temperature

The sample maintained at an optimum pH (4pH) was fermented to different temperatures like 25^{o}C, 30^{o}C, 35^{o}C, 40^{o}C and 45^{o}C. The samples were kept for fermentation period of four days and the fermented solution was analyzed for every 12 h intervals. Bio-ethanol production increases with the increase in temperature and reaches maximum value at 35^{0}C (Figure 2). Further the increasing temperature reduces the percentage of ethanol production and it is mainly due to the denature of the yeast cells.

3.3 Optimization of sugar molasses concentration

The sample was fermented with different quantity of sugar molasses concentration such as 50 gm/l, 100 gm/l, 200 gm/l, 300 gm/l and 400 gm/l at an optimum operating condition. Figure 3 shows that the concentration of bio-ethanol increases along with the increase in sugar concentration and reaches maximum ethanol production at sugar concentration of 300 gm/l and further increasing sugar molasses concentration inhibit the ethanol productivity. Bai et al., (2004) and Vasconcelos et al., (1998) are also observed the maximum ethanol productivity.

3.4 Optimization of yeast concentration

The optimum quantity of sugar molasses solution was taken in fermentation flask and the pH and temperature were maintained at 4.0 and 35^{o}C. The various quantities of yeast like 1.0 gm, 2.0 gm, 4.0 gm and 8.0 gm were added and kept for a period of four days and the fermented solution was analyzed at every 12 h intervals. Figure 4 shows that as the concentration of yeast increases, the yield of bio-ethanol increase up to 2 gm and then it starts to decrease.

3.5 Productivity of ethanol from sugar molasses

Figure 5 shows the productivity of bio-ethanol increases along with the increase in fermentation period and the maximum yield was obtained at 72 h. The maximum concentration of bio-ethanol was found to be 53% at the temperature of 35^{o}C, pH of 4 and yeast concentration of 2 gm.

The rate of formation of bio-ethanol is compared with Michael and Mentan equation and was found to be good fit and the rate constants such as V_{max} and K_m are found to be 0.71 mol/l sec and 81.63 mol/l respectively (Figure 6).

4. Conclusion

The optimized conditions were found by analyzing the sugar molasses in the process of fermentation under various parameters like temperature, pH, and time, to obtain maximum yield of bio-ethanol. The optimized conditions of sugar molasses are of temperature 35^{0}C, pH 4.0 and the time 72 h which gives maximum bio-ethanol yield of 53%. The fermentation was carried out under anaerobic condition and the results were compared with Michaelis- Menten equation and the obtained values of V_{max} and K_m are 0.71 mol/l sec and 81.63 mol/l respectively.

5. Nomenclature

l	liter
h	hour
gm	gram
gm/l	gram/liter
K_m	Michaelis- Menten constant
V_{max}	maximum forward velocity of the reaction

References

Bai, F.W., Chen, L.J., Zhang, Z., Anderson, W.A., & Moo-Young, (2004). Continuous ethanol production and evaluation of yeast cell lysis and viability loss under very high gravity medium conditions. *J. of Biotechnology,* 110, 287-293.

Beatriz Palmarola-Adrados, Mats galbe, & Guido Zacchi. (2005). Pretreatment of barley husk for bio-ethanol production. *J. of Chemical Technology and Biotechnology*, 80, 85-91.

Bulock, J.D., Combarbach, D.M., & Ghommidh, C. (1984). Fermentation of biomass for ethanol production. *J. of Chem. Engg,* 29, B9-B24.

Dale BE, (1987). Lignocellulose conversion and the future of fermentation biotechnology. *TIBTECH,* 5, 287-291.

De Vasconcelos, J.N., Lopes, C.E., & de França, F.P. (1998). Yeast immobilization on cane stalks for fermentation. *International Sugar J,* 100(1190), 73-75.

Diez, J.C., & Yokoya, F. (1996). Effect of temperature and p^{H} on ethanol and levan production during sucrose fermentation by zymomonas mobilis. *Arq. Biol. Technol*, 39, 129-137.

Doelle, H.W., & Greenfield, P.F. (1985). The production of ethanol from sucrose using zymomonas mobilis. *Appl. Microbial. Biotecnol,* 22, 405-410.

Favela Torres, E., & Baratti, J. (1987). The effect of p^{H}, temperature and sucrose concentration on high productivity continuous ethanol fermentation using zymomonas mobilis. *Appl. Microbial. Biotechnol,* 27, 121-128.

Ferrari, M.D., Neirotti, E., Albornoz, C., & Saucedo, E. (1992). Ethanol production from eucalyptus wood hemicellulose hydrolysis by Pichia stipitis. *Biotechnol. Bioeng,* 40, 753-759.

Hansen, Alan C., Qin Zhang, Peter, W.L. Lyne. (2005). Ethanol diesel fuel blends – a review. *Bioresource Technol,* 96, 277-285.

Hridayabhiranjan Shukla, Lakshmikanthrao Viswanathan, & Niranjan Prasad Shukla, (1984). Reaction kinetics of D-glucose fermentation by Saccharomyces Cerevisiae. *Enzyme Microb. Technol*, 6, 560-564.

Huertaz-Díaz, H., Cacho, C.L., & Bernard, L. (1991). Fermentation of sugarcane juice and blackstrap molasses by zymomonas mobilis. *J. Agric. Univ.P.R,* 75(1), 43-50.

Kotter, P., & Ciriacy, M. (1993). Xylose fermentation by saccharomyces cerevisiae. *Appl. Microbial. Biotechnol*, 38 (6), 776–783.

Marcia Sadae Tano, & Joao Batista Buzato. (2003). Effect of the presence of initial ethanol on ethanol production in sugar cane juice fermented by zymomonas mobilis. *Brazilian J. of Micro*, 34, 242-244.

Martin, C., Lopez, Y., Plasencia, Y., & Hernandez. (2006). Characterization of agricultural and agro-industrial residues as raw materials for ethanol production. *Chem.Biochem.Eng,* 20 (4), 443-447.

Nigam, J.N. (1999). Continuous ethanol production from pineapple cannery waste. *J. of Biotechnol*, 72, 197-202.

Olsson, L., & Hahn-Hägerdal, B. (1996). Fermentation of lignocellulosic hydrolysis's for ethanol production. *Enzyme Microb. Technol*, 18, 312-331.

Peres, M.F.S., & Laluce, C. (1998). Ethanol tolerance of thermo tolerant yeasts cultivated on mixtures of sucrose and ethanol. *J. Ferment. Bioengin*, 85(4), 388-397.

Wyman, C.E., & Hinman, N.D. (1990). Ethanol: Fundamentals of ethanol production from renewable feedstocks and use as a transportation fuel. *Appl. Biochem. Biotechnol*, 24:25, 735–753.

Table 1. Properties of baker's yeast

Baker's Yeast	**Property**
Dry material	30 - 33%
Nitrogen	6.5 - 9.3%
Proteins	40.6 - 58%
Carbohydrates	35 - 45%
Lipids	5.0 - 7.5%

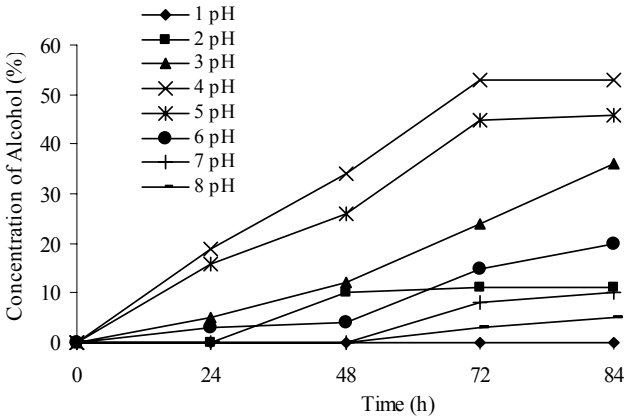

Figure 1. Optimization of pH

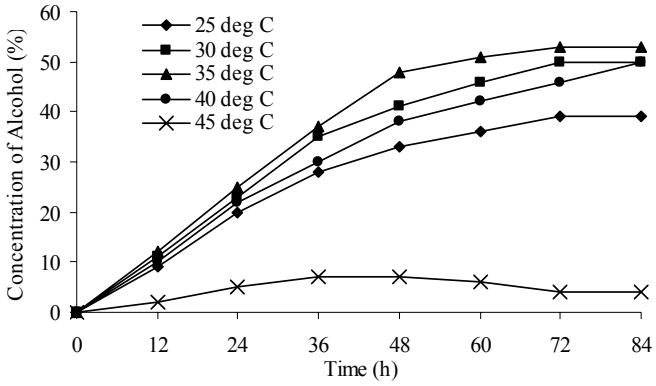

Figure 2. Optimization of temperature

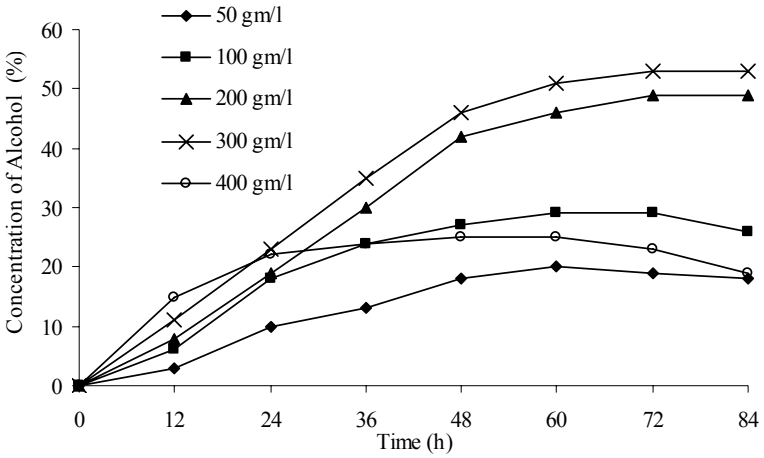

Figure 3. Optimization of sugar molasses concentration

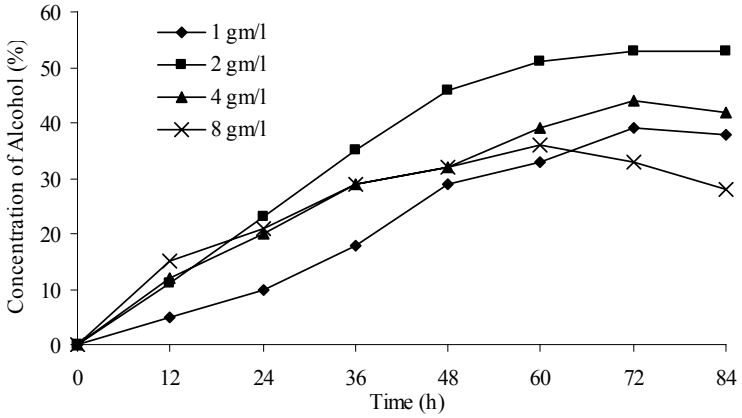

Figure 4. Optimization of yeast concentration

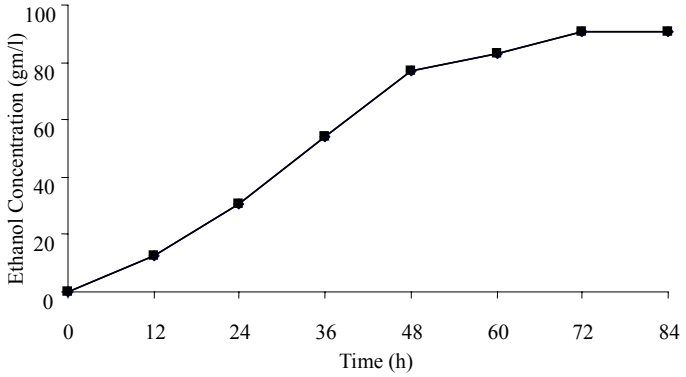

Figure 5. Productivity of bio-ethanol

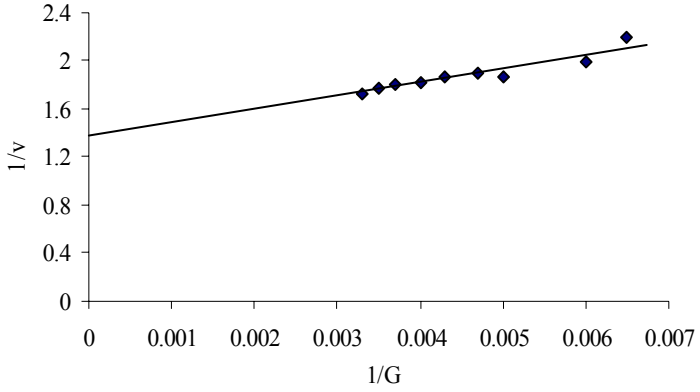

Figure 6. Plot of 1/G vs. 1/v

Modern Applied Science

www.ccsenet.org/journal.html

Vol. 3, No. 8

August 2009

Study on Error Measurement Method for Actuator Frequency Characteristic Test System

Rufei Zhang (Corresponding author)

Institute of Precision Guidance and Control, Northwestern Polytechnical University

PO box 250, Xi'an 710072, China

Tel: 86-029-8207-3095 E-mail: zrf_lucky@sina.com

Jun Zhou

Institute of Precision Guidance and Control, Northwestern Polytechnical University

Xi'an 710072, China

Xiaozhou Yu

Institute of Precision Guidance and Control, Northwestern Polytechnical University

Xi'an 710072, China

Abstract

System error measurement is key step in actuator frequency characteristic test and practical system error measurement methods must be studied to provide qualified results for system error compensation. Two error measurement methods (swept sine and FFT: fast Fourier transform) are explored, a strong anti-jamming frequency characteristic algorithm is perfected for swept sine and digital smoothing is introduced for improving accuracy of FFT. Numerical examples verified accuracy and robustness of swept sine and validity of FFT. These methods were applied to measure system error in missile actuator test system, the experiments showed that swept sine method could gain smooth and stable results and FFT method could achieve rather close results with swept sine. This study is part of general test system of some missile and provides valid technology analysis and reliable measurement results of system error for its actuator test.

Keywords: Frequency characteristic, System error, Swept sine, Curve fitting, Modulated frequency, Fast Fourier transform

1. Introduction

Actuator frequency characteristic test is an important part of general missile test system, and used for missile production, maintenance and launching test. In order to raise test accuracy and save precious hardware resources, for example, some PXI DAQ (data acquisition) card only has four channels for A/D, so it must be avoided to analyze and compensate all existent system error in test system under synchronous sampling on input and output; meanwhile, to reduce heat wastage of actuator and the effect on measurement, test efficiency must be raised. Therefore, the choice of measurement method directly decides the results of actuator frequency characteristic test, test accuracy and efficiency must be synthetically considered and how to measure system error with high accuracy and high efficiency becomes necessary step and important part of actuator frequency characteristic test.

In test system, system error mainly comes from A/D, D/A converter, input preprocessing, output processing, disturbance, noise and system nonlinearity(WANG Shou-kun, WANG Jun-zheng, 2007) . The paper emphasizes two methods for system error measurement; one is swept sine method which works according to swept sine principle, the other is FFT method (fast Fourier transform) which calculates spectrum of input and output according to fast Fourier transformation, figures out system error according to frequency characteristic definition, and then use digital smoothing to raise test accuracy.

The paper executes theoretical analysis and numerical simulation on the two methods, and then applies them to the measurement of system error in actuator frequency characteristic test system. Swept sine method grows maturely, and it has higher test accuracy but low efficiency. Taking the measurement of swept sine as criterion, swept sine method and FFT method are compared from the viewpoints of accuracy and efficiency, which demonstrates that, FFT method has rather high efficiency and completes measurement in ten seconds or a little more; furthermore, its accuracy is close to that of swept sine, it realizes high efficiency and high accuracy and can solve the problems of low efficiency and heat wastage from swept sine based frequency characteristic test.

2. System Error Analysis

2.1 System Error Distribution

Practical systems always have system error which can be divided into two types: analytic error and non-analytic error. The former expresses error analytically according to known test parameters and it comes from A/D, D/A, signal preprocessing and filtering; the latter includes noise, disturbance and nonlinearity which can not be described through analytic formula.

Based on system input and output, swept sine method and FFT method could raise accuracy of system error measurement because their results contain varieties of system error, even the error introduced by swept sine method and FFT method themselves. Because noise is random, there are always differences among multiple measurements from the two methods, but noise has low power and it will not influence measurements extraordinarily; electromagnetic disturbance is the principal disturbance factor in actuator test system, and it takes great effect on actuator frequency characteristic test.

According to the position relative to test plant, system error can be classified as prepositive error and postpositive error, which are described in Figure 1, where $H_1(\omega)$ is prepositive error, $H_2(\omega)$ is postpositive error and $H(\omega)$ is test plant.

Suppose frequency characteristic between input and output shown in Figure 1

$$H_c(\omega) = Y(\omega) / X(\omega) = H_2(\omega)H(\omega)H_1(\omega) \tag{1}$$

Therefore, the real characteristic $H(\omega)$ for plant

$$H(\omega) = \frac{H_c(\omega)}{H_2(\omega)H_1(\omega)} = H_c(\omega) / H_e(\omega) \tag{2}$$

where $H_e(\omega) = H_1(\omega)H_2(\omega)$ is just system error. Seen from (2), system error measurement is the necessary step for frequency characteristic test. Simulation and experiment show that, A/D and D/A will cause phase delay of 20^o at least at $100Hz$ frequency point, and if signal processing loop exists, system error will grow increasingly.

2.2 Low-Pass Filter

As an electro-mechanic system, actuator are often disturbed by high frequency vibration and electromagnetic signal under test circumstances, therefore actuator output must be filtered through low pass filter so as to eliminate the effect from high frequency disturbance. In order to accommodate more types of actuator or plant and ensure high accuracy of frequency characteristic test in the range of actuator band width, it is required that the band width of low pass filter $H_F(\omega)$ is three times wider or more than that of test plant.

In some actuator frequency characteristic test system, both D/A and A/D in the applied DAQ card are realized as zero-order holder and their frequency characteristic are expressed as $H_{DA}(\omega)$ and $H_{AD}(\omega)$ which are referred to classical control theory. Contrasted with the distribution model shown in Figure 1, system error can be analytically described as

$$H_e(\omega) = H_{AD}(\omega)H_F(\omega)H_{DA}(\omega) \tag{3}$$

where postpositive error $H_2(\omega) = H_{AD}(\omega)H_F(\omega)$, and prepositive error $H_1(\omega) = H_{DA}(\omega)$. In later experiment, the expression is call analytic method.

3. System Error Measurement

3.1 Swept Sine Method

Swept sine method is mature and reliable for frequency characteristic test, but measurement noise existent in test system will make output apparently malformed and cause the test accuracy very low. Curve fitting (LIU Qiang, LIU De-peng, 2005) can overcome the above problems and it can be deduced from contradictory equations theory. Since curve fitting is a digital processing loop, it will introduce new system error inevitably.

Suppose system input at frequency f_i

$$u_i(t) = A_a \sin(2\pi f_i t + \phi_i) \tag{4}$$

where A_m is amplitude, ϕ_i is initial phase, often making ϕ_i=0.

According to swept sine principle, the response can be supposed as

$$y_o(t) = A_r \sin(2\pi f_i t + \phi_i + \Delta\phi) \tag{5}$$

where A_r is amplitude, $\Delta\phi$ is phase difference, namely the phase characteristic of test plant as frequency f_i.

Further decompose $y_0(t)$ as

$$\begin{aligned} y_0(t) &= \sin(2\pi f_i t + \phi_i) A_r \cos(\Delta\phi) + \cos(2\pi f_i t + \phi_i) A_r \sin(\Delta\phi) \\ &= \left[\sin(2\pi f_i t + \phi_i) \quad \cos(2\pi f_i t + \phi_i)\right] \begin{bmatrix} A_r \cos(\Delta\phi) \\ A_r \sin(\Delta\phi) \end{bmatrix} \end{aligned} \tag{6}$$

Suppose sampling period T, sampling time $t=0,T,2T,\ldots,nT$, the contradictory equations from (6) is

$$\begin{bmatrix} \sin(\phi_i) & \cos(\phi_i) \\ \sin(2\pi f_i T + \phi_i) & \cos(2\pi f_i T + \phi_i) \\ \cdots & \cdots \\ \sin(2\pi f_i nT + \phi_i) & \cos(2\pi f_i nT + \phi_i) \end{bmatrix} \begin{bmatrix} A_r \cos(\Delta\phi) \\ A_r \sin(\Delta\phi) \end{bmatrix} = \begin{bmatrix} y_0(0) \\ y_0(T) \\ \cdots \\ y_0(nT) \end{bmatrix} \tag{7}$$

According to contradictory equations theory, for contradictory equations $Ax = b$, its least squares solution is decided by

$$A^T Ax = A^T b \tag{8}$$

It is easily seen that, the coefficient matrix rank $rank(A)$=2 in equations (7), so $A^T A$ is nonsingular, and the least squares solution is

$$x = (A^T A)^{-1} A^T b \tag{9}$$

where $b = [y_0(0), y_0(T), \cdots, y_0(nT)]^T$, and the solution $x = [A_r \cos(\Delta\phi), A_r \sin(\Delta\phi)]^T$, further get the magnitude ($= A_r / A_a$) and the phase $\Delta\phi$ at frequency point f_i.

3.2 Fast Fourier Transformation Method

3.2.1 Modulated Frequency Signal Analysis

Proper selection of input signal is crucial to raise test accuracy, and when hardware permits, the signal which has strong power and wide band should be adopted as input. Modulated frequency signal $x(t) = A\cos(2\pi ft)$ has rather stable power spectrum in wider frequency range and choosing $f = \beta t + f_0$ will produce linear modulated frequency signal, where A is magnitude, β is frequency change rate, and f_0 is initial frequency.

Frequency change rate β indicates the spectrum distribution of modulated frequency signal, shown as Figure 2, and the power are equably centralized in the frequency range of 0.5 β *Hz*. To adopt modulated frequency signal as input for frequency characteristic test can not only get higher accuracy in swept band, but also figure out frequency characteristic in this band through sweeping once, which avoids sweeping point by point in given frequency range and therefore accelerate test speed. But if the swept band is too wide and β is rather big, the power of modulated frequency signal will distribute dispersedly. In this case, the amplitude of modulated frequency signal should be amplified so as to get stronger spectrum, but the amplitude will be limited by hardware specification. So, modulated frequency signal is mainly used for frequency characteristic test of the plants whose band width is under 200*Hz*; for actuator with band with 30*Hz* or so, modulated frequency signal is adequate to provide satisfactory accuracy.

3.2.2 Key Procedures

Fast Fourier transformation (FFT) is a fast algorithm for discrete Fourier transformation and widely used to fault diagnosis(Z. Hameed, Y.S. Hong, Y.M. Cho, S.H. Ahn and C.K. Song, 2007)(V.K. Rai, A.R. Mohanty, 2007), frequency characteristic calculation (WANG Shou-kun, WANG Jun-zheng, 2006). Many improved fast algorithms have raised the calculation efficiency of FFT further (John D. Markel, 1971)(Fan Chih-Peng, Su Guo-An, 2007), and if data quantity is not too much, FFT already has adequate efficiency. Choose modulated frequency signal as test input(WANG Shou-kun, WANG Jun-zheng, 2006)(G. Gloth, M. Sinapius, 2004) .

Supposing input $x(t)$, its FFT is $X(k)$; sampled signal is $y(t)$ and its FFT is $Y(k)$, so get the measured system error

$$\begin{cases} |H_e(k)| = |Y(k)| / |X(k)| \\ \angle H_e(k) = \angle Y(k) - \angle X(k) \end{cases} \tag{10}$$

where $|\cdot|$ represents magnitude, $\angle\cdot$ is phase.

The key to apply FFT method is that the sampled data can effectively overcome the effect of limited time length. In example of some frequency characteristic test system, assigning modulated frequency signal $x(t) = A_a \sin[2\pi(\beta t + f_0)t]$, the band width of test plant is *B Hz*, then the following conditions had better be satisfied:

$$\begin{cases} \beta t + f_0 > \gamma B \\ \beta t + f_0 < (5 \sim 10)\gamma B \end{cases} \tag{11}$$

The sampling time length can be decided according to (11) where $\gamma > 0$ is an adjustable parameter.

1) Digital Smoothing

FFT transforms time-series data in time domain into frequency domain signal without choice, noise and disturbance are also included in transformed signals, so the transformed signal with noise and disturbance must be smoothed by digital smoothing.

Moving average filtering can effectively reject the components which are not smooth. Practice shows that, magnitude error is reduced from 2dB to 0.4dB and phase error decreases from 10^o to 4^o after applying moving average filtering, and the measured results is accurate and smooth.

4. Measurement Accuracy and Robustness

Since there are no ways to get analytic or real characteristic of system error in physical system, in order to evaluate measurement performance of swept sine method and FFT method, taking M-I: $G(s) = 200^2/(s^2 + 280s + 200^2)$ and M-II: $G(s) = 1.0/(0.003s + 1.0)$ as test plants, simulation works out the differences between the characteristic in theory and that from swept sine and FFT methods.

The noise and disturbance are set as shown in Figure 3, and the calculated results are shown in Figure 4. In practical circumstances, the accuracy of some DAQ card is more than 0.001V (volt) and it can reach 0.0002V after calibration, so it is satisfied with 0.1V setting; real electromagnetic disturbance is not constant amplitude pulse signal, it is the most serious disturbance in actuator frequency characteristic test system and takes great effect on the measurement.

It can be seen from Figure 4 that, the calculated difference range from swept sine and FFT methods on different models (M-I and M-II) is stable; the results from swept sine method is smooth and that from FFT method is apparently fluctuating. Only considering the difference range, the two methods have close accuracy and even FFT method is better than swept sine method at high frequencies.

Furthermore, swept sine method is more robust to noise and disturbance than FFT method and it is a good way for frequency characteristic test. Besides, simulation also demonstrates that, the two methods have close performance in case that noise and disturbance both are small, and the magnitude difference is under 0.2dB while the phase difference is under 1.5^o.

5. Experiments

In some actuator frequency characteristic test system, adopt DAQ-2006 multifunction DAQ card in ADLINK which has sample rate up to 250*k/s* and update rate up to 1*M/s*, and the card supports single and double buffer DMA mode which effectively alleviates the occupation of test computer resources. In experiment, A/D sample rate f_s and D/A update rate f_a both are 10*kHz*, and single buffer DMA mode is adopted. The achieved system error from the three methods (swept sine, FFT, analytic) is shown in Figure 5~Figure 7.

Figure 5 demonstrates the measurement comparison from swept sine method with different swept steps 0.5*Hz* and 1.0*Hz* respectively. We can see from the two measurements that, although least squares based curve fitting is applied, their difference is under 0.02dB on magnitude and under 0.15^o on phase and at few points, the phase difference is up to 0.5^o, which indicates that swept sine method has high accuracy on one side and noise and disturbance have taken effect on measurement on the other side.

It can be seen from Figure 6 that, FFT method has close measurement with swept sine method (S-Sine) and its magnitude difference is under 0.2dB and the phase difference at higher frequencies is under 1.8^o; but to complete the same test, swept sine method under swept step 1.0*Hz* consumes 4.3 minutes while FFT method only requires 14 seconds, and FFT method raises test efficiency remarkably. The band width of system error is 65*Hz* from swept sine method and 64.926*Hz* from FFT method, and the difference is 0.074*Hz*. So we can deem that, FFT method achieves comparative test accuracy with swept sine method, but the former works much more efficiently than the latter; furthermore, the frequency resolution of the former is 0.08*Hz* but that of the latter is 1.0*Hz* which is just swept step.

It can be seen from Figure 7 that, relative to FFT method, the difference between analytic method and swept sine method is much big, the magnitude difference reaches 1.2dB at high frequencies, and the phase difference is 1.8^o or so, which demonstrates that, the nonlinearity, noise, disturbance and the non-ideal implementation of some loops in practical system will cause the bigger difference.

6. Conclusions

System error measurement in missile actuator test system is the necessary procedure, and its test accuracy and efficiency directly affects that of actuator frequency characteristic test system. The paper focuses two system error measurement methods; swept sine method applies curve fitting to calculate the characteristic of system error according to swept output while FFT method calculates spectrum of input and output signal through fast Fourier transformation, and attains the characteristic of system error according to frequency characteristic definition and digital smoothing algorithm.

Simulation studies the produced difference from the above methods, compares and analyzes anti-noise and anti-disturbance ability, verifies the high accuracy and robustness of swept sine method and the efficacy of digital smoothing introduced in FFT method. And the two methods are applied to some missile actuator test system, the experiment indicates that, swept sine method can get smooth, stable and accurate characteristic, and FFT method can achieve high magnitude characteristic and relatively close phase characteristic. Relative to swept sine method, FFT method has rather high test efficiency and can avoid wastage of actuator performance because of heating during test.

The study is part of some general missile test system, provides reliable analysis for actuator frequency characteristic test and can be used as the principle of choosing the method for system error measurement and compensation in frequency characteristic test system.

References

Fan Chih-Peng, Su Guo-An. (2007). Pruning fast Fourier transform algorithm design using group-based method. *Signal Processing* 87 (2007) 2781–2798

G. Gloth, M. Sinapius. (2004). Analysis of swept-sine runs during modal identification. *Mechanical Systems and Signal Processing* 18 (2004) 1421–1441

John D. Markel. (1971). FFT Pruning. *IEEE Transactions on Audio and Electroacoustics*, AU-19 (4) (1971) 305-311

LIU Qiang, LIU De-peng, (2005). A Novel Precision Measuring Algorithms of Frequency Characteristic Based on Curve Fitting. *Machine Tools & Hydraulics (Chinese)* (1) (2005) 117-118

V.K. Rai, A.R. Mohanty. (2007). Bearing fault diagnosis using FFT of intrinsic mode functions in Hilbert–Huang transform. *Mechanical Systems and Signal Processing* 21 (2007) 2607–2615

WANG Shou-kun, WANG Jun-zheng, (2007). Error Analysis and Correction in the Testing of Frequency Response for Actuators. *Transactions of Beijing Institute of Technology (Chinese)* 27(1) (2007) 34-37

WANG Shou-kun, WANG Jun-zheng, (2006). Frequency Response Testing Method for Missile Actuator Based on Frequency Modulated Pulse Sweep. *Transactions of Beijing Institute of Technology (Chinese)* 26(8) (2006) 697-703

Z. Hameed, Y.S. Hong, Y.M. Cho, S.H. Ahn and C.K. Song. (2007). Condition monitoring and fault detection of wind turbines and related algorithms: A review. *Renew Sustain Energy Rev* (2007), doi:10.1016/j.rser.2007.05.008

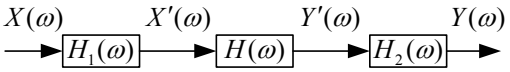

Figure 1. System error distribution model

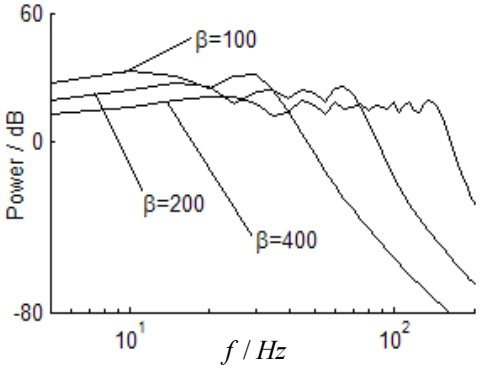

Figure 2. Influence of β on power distribution

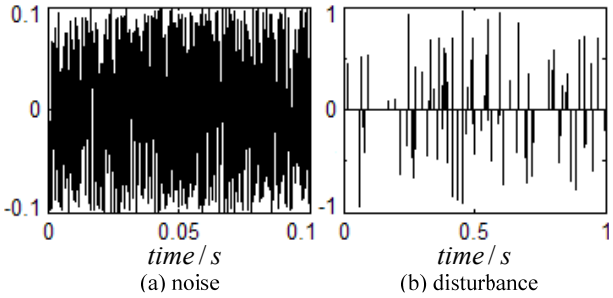

(a) noise (b) disturbance

Figure 3. Noise and electromagnetic disturbance

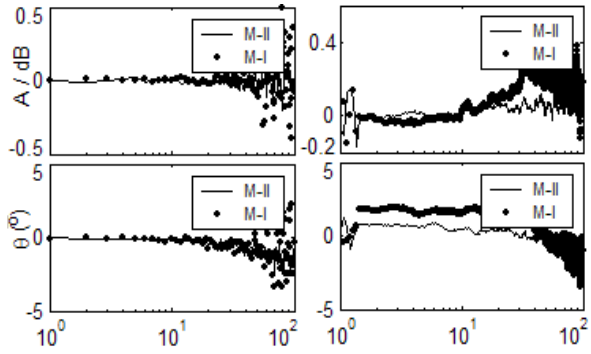

(a) swept sine method (b) FFT method

Figure 4. Measurement Error of Swept Sine and FFT

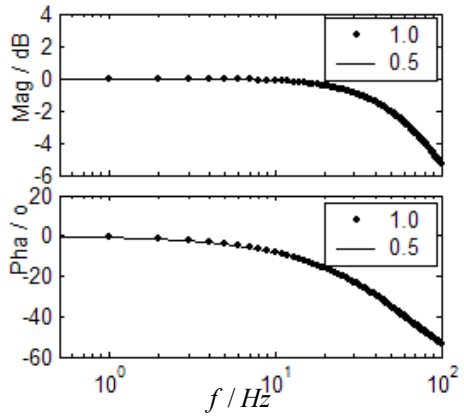

Figure 5. Swept sine under different swept steps

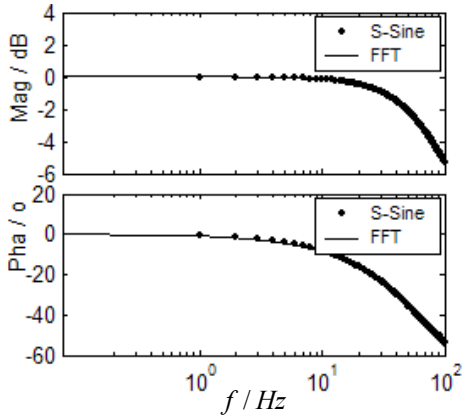

Figure 6. Comparison of FFT and swept sine methods

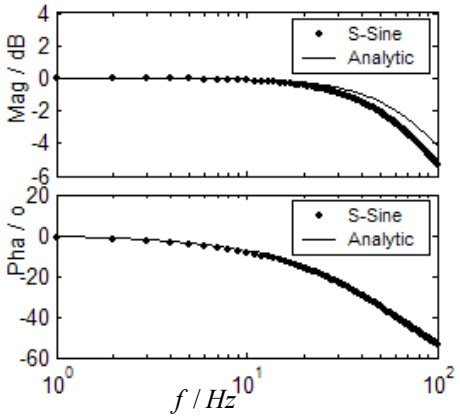

Figure 7. Comparison of analytic and swept sine methods

Modern Applied Science

www.ccsenet.org/journal.html

Vol. 3, No. 8

August 2009

Using Maximum Power Capability of Fuel Cell in Direct Methanol Fuel Cell / Battery Hybrid Power System

Mehdi Dargahi (Corresponding author)

Islamic Azad University - Jouybar Branch

Jouybar, Iran

Tel: 98-911-128-7365 E-mail: Dargahi.mehdi@gmail.com

Mohammad Rezanezhad

Faculty of Electrical Engineering, Babol University of technology

Shariati St. Babol, Iran

Tel: 98-911-314-2090 E-mail: mrezanejad@stu.nit.ac.ir

Abstract

Considering limited ability of Direct Methanol Fuel cell (DMFC) systems to produce power and importance of optimum methanol consumption, it is necessary to provide conditions, in which, the maximum power of DMFC from present fuel flow can be utilized. But, in different conditions, maximum power point (MPP) of DMFC is a unique point. So, operating point should be determined based on DMFC conditions, and load requirements are not taken into account. This means that, output voltage will not be fixed if load resistance varies. In this paper, a new control scheme for DMFC/Battery hybrid power system is proposed and analyzed. In the proposed system, a MPP tracking controller searches for MPP of DMFC in any operating conditions. Moreover, a battery charge controller is utilized to keep the battery voltage in its permissible limits. So, in the proposed scheme, MPP operation of DMFC and output voltage regulation can be achieved concurrently.

Keywords: Direct Methanol Fuel cell, Battery, Maximum Power Point Tracking

1. Introduction

DMFC is one of the newest electric power sources, which become increasingly more attractive subject for many researchers because:

- A solid polymer electrolyte is used in these kinds of fuel cells (FCs),

- Their operational temperature is relatively low, and

- Their fuel is low cost and has high energy density (Jeong et al, 2008).

A large number of internal parameters can impact on produced voltage of DMFC (Jeong et al, 2008; Guo et al, 2004; Sundmacher et al, 2001), but in any condition, there is just one unique point on V-I curve which represents MPP. In this point, DMFC can produce its maximum power. Because of the limited ability of DMFC systems to produce power from available fuel flow, it is necessary to force the system to operate in condition which matches to DMFC's MPP. This can avoid excessive fuel consumption and low efficiency operation.

A Maximum power point tracking (MPPT) controller traces the MPP of DMFC using a MPPT algorithm. The controller generates instructions for a DC-DC converter and a certain amount of current which corresponds to MPP, is extracted from DMFC.

There are several methods to search extremum value of a function (Zhi-dan et al, 2008; Wasynczuck, 1983; Hussein etal, 1995; Noguchi et al, 2002; Enslin et al.1997). Among them Perturbation and Observe (P&O) (Zhi-dan et al, 2008; Wasynczuck, 1983) is the most commonly used method because of its simple algorithm.

In this paper, DMFC MPPT, its problems and deficiencies, and proposed solution which is a hybrid Direct Methanol

Fuel cell/Battery system is presented and analyzed.

In section II, DMFC power system is reviewed. In section III, the MPPT strategy is analyzed. In next section, section IV, the proposed hybrid system and its control scheme is introduced. The results and conclusion are presented in sections V and VI respectively.

2. DMFC power system

Such as other kinds of DMFC, there are three different regions in V-I curve of DMFC. At low current densities, the voltage is dominated by the electrochemical kinetics of the anodic methanol oxidation. As current density increases, the voltage decreases further due to limitations of methanol mass transport to the anode catalyst layer and the electric resistance of the membrane. In next region, the system approaches a limiting current density ilim at which the voltage decreases rapidly. The level of the limiting current density mainly depends on the mass transport resistance of methanol in the anode diffusion layer. Methanol mass transport is based on diffusive and convective transport mechanisms. In addition, depending on the operating conditions, it is influenced by the release of CO2 bubbles from the anode surface (Sundmacher; 2001).

A multi-step reaction mechanism is used to describe reactions inside a DMFC (Sundmacher; 2001), which can be summarized as:

$$\text{Anode}: \ CH_3OH(l) + H_2O(l) \xrightarrow{Pt/Ru} CO_2(g) + 6H^+ + 6e^-$$

$$\text{Cathode}: \ \frac{3}{2}O_2(g) + 6H^+ + 6e^- \xrightarrow{Pt} 3H_2O(l)$$

$$\text{Overall}: \ CH_3OH(l) + \frac{3}{2}O_2(g) \longrightarrow CO_2(g) + 2H_2O(l)$$

Output voltage of a DMFC is function of open circuit voltage, U_{cell}^{STD}, anode overpotential, η_a, cathode overpotential, η_c and membrane ohmic overpotential, η_{ohmic}.

$$V_{cell} = U_{cell}^{STD} - \eta_a + \eta_c - \eta_{ohmic} \tag{1}$$

Using charge balance at anode and cathode sides following expressions can be achieved.

$$\frac{d\eta_a}{dt} = \frac{1}{C_a}(i_{cell} - 6Fr_a) \tag{2}$$

$$\frac{d\eta_c}{dt} = \frac{1}{C_c}(-i_{cell} - 6F(rc + n_{MeOH}^M)) \tag{3}$$

where, F is Faraday's constant, C_a and C_c are double layer capacities of anode and cathode respectively and n_{MeOH}^M is mass flux density of methanol in membrane. Rate of methanol oxidation reaction at anode catalyst layer, r_a, and oxygen reduction at cathode catalyst layer, r_c, can be expressed as:

$$r_a = k_a\left(x_{MeOH}^{CL}\exp\left(\frac{\alpha_a F}{RT}\eta_a\right) - x_{CO_2}^{CL}\exp\left(-\frac{(1-\alpha_a)F}{RT}\eta_a\right)\right) \tag{4}$$

$$r_c = k_c\left(\left(\frac{P_{O_2}}{P^{STD}}\right)^{1.5}\exp\left(-\frac{\alpha_c F}{RT}\eta_c\right) - \exp\left(\frac{(1-\alpha_c)F}{RT}\eta_c\right)\right) \tag{5}$$

where, k_c and ka are rate constant of anodic and cathodic reactions respectively, x_{MeOH}^{CL} and $x_{CO_2}^{CL}$ are mole fraction of methanol and carbon dioxide, α_a and α_c are charge transfer coefficients, P_{O_2} and P^{STD} are oxygen and standard pressures, R is universal gas constant, and T is temperature.

Extended studies about abovementioned relations and expressions can be found in (Jeong, 2008; Guo,2004; Sundmacher et al, 2001).

The output voltage of the fuel cell stack can be calculated by the following expression.

$$Vstack = NVcell \tag{6}$$

where N is the number of single cells in stack. The output power of the stack is:

$$Pstack = Vstack\ I \tag{7}$$

Choosing parameter values from (1), (2) and (3) the DMFC stack output voltage and power curves are presented in Figure1.

3. Maximum power point tracking strategy

There are various methods to find extremum value of a function (which have mostly been developed for photovoltaic arrays), such as Perturbation and Observe (P&O) (Zhi-dan et al, 2008; Wasynczuck, 1983), Incremental Conductance (Hussein etal, 1995), short-circuit current method (Noguchi et al, 2002), and the open-circuit voltage method (Enslin et al.1997 Enslin et al.1997). Considering its simple algorithm, P&O is the most commonly used method.

In P&O, as can be understood from its name, a perturbation is applied to system and its effect is observed. For DMFC system, an increment (either positive or negative) in DMFC current, ΔI, is considered as perturbation and output power variations, ΔP, will be observed. If output power is increased by a positive constant increment in DMFC current, further positive increment is needed; otherwise perturbation should be negative. In a similar way, if output power is decreased by a positive perturbation, further positive increment is needed; otherwise direction of perturbation variation should be changed. This algorithm can be summarized as flowchart shown in figure 2.

For fast tracking of maximum power point, the perturbation range should be large. This leads to more fluctuations in output power. If we want to reduce these fluctuations, the perturbation range should be small, but tracking time will be long. So, as a summary, the quick tracking time is in conflict with the suppression of fluctuations in output power. Many approaches have been proposed to improve the P&O algorithm, such as using a variable step size of perturbation instead of a constant value as following (Huynh et al, 1996):

$$I_{k+1} = I_k + M \frac{\Delta P_k}{\Delta I_k} \tag{8}$$

where M is a coefficient that modifies step size, and I_k, ΔI and ΔP are the current value, deviation of current and deviation of power at k_{th} sampling period respectively.

It should be noted that, in spite of appropriate behavior of P&O under static conditions, it will not function well if it encounters dynamic behavior of system (Zhi-dan et al, 2008). To obviate this drawback, continuous changes in DMFC operation should be avoided.

4. Hybrid system and its control scheme

A DC-DC power converter between DMFC and load can change load equivalent resistance seen by DMFC. At MPP, current gain of the converter, G, has a value which causes the load equivalent resistance to be equal to the internal resistance of the DMFC. The relationship between load equivalent resistance R_{eq} and load resistance R_{Load} is:

$$R_{eq} = G^2 R_{Load} \tag{9}$$

A MPPT controller uses DMFC voltage, current and subsequently its power, to find MPP and then generates control instructions for the power converter. The converter forces the fuel cell to work at current which is defined by MPPT controller and corresponds to MPP of DMFC. In this point, the load equivalent resistance is equal to the internal resistance of the DMFC and maximum power can be delivered to load, considering maximum power transfer principle. Figure 3 shows a generic schematic diagram of such a system.

As an example of MPPT for a DMFC system, Figure 4 shows a plot of the DMFC stack power in standard conditions. As can be seen, the MPP is found by MPPT controller and DMFC is forced to stay at this operating point.

In order to operate in MPP, DMFC output current should be constant; so, load can just receive a fixed current and power. Consequently, changes in load resistance will result in variations in output voltage. Figure 5 shows the operation of system under variable load resistance condition.

To overcome the described deficiencies, a DMFC/Battery hybrid system, which represented in Figure 6, is proposed.

In this system, battery is placed in parallel with the power converter, and is responsible to keep the output voltage constant. In order to keep the battery voltage in a predetermined limit, a battery charge controller is employed. The controller Input is the battery voltage, and its output determines the DMFC input fuel flow. This controller works in the way that, for example, if we want to keep output voltage in 100±5% of nominal voltage, when battery voltage increases to its upper limit, i.e. 100+5%, fuel flow will decrease to its minimum value, i.e. 0%. On the contrary, when battery voltage rises to its lower limit, i.e. 100-5%, battery charge controller decreases the fuel flow up to its maximum, i.e. 100%. So, with respect to load requirements, battery voltage and subsequently, DMFC input fuel flow, change in the way that, load demand is satisfied and output bus voltage is kept constant. MPPT controller traces the MPP of DMFC, in any fuel flow conditions, and sends the required instructions to the DC-DC converter, so that MPP operation of DMFC can be realized.

In order to avoid rapid and sudden changes of fuel flow, which can have serious and harmful damages for DMFC, a low pass filter should be utilized in battery charge controller output. The filter only passes slow and soft changes of fuel flow to the DMFC. To have an appropriate understanding for designing of this filter, maximum allowed rate of variations of fuel flow, which can be tolerated by DMFC, should be taken into account. Then, the filter can be tuned to

realize the desired settings. Figure 7 shows the response of a typical low pass filter with a damping factor of 1, for different cut-off frequencies, when a step change is applied as its input. Choosing such a damping factor will avoid any oscillations.

5. Simulation and results

Parameters and relationships presented in section II are used to model a DMFC stack.

A 220V lead-acid battery is used in this study. These kinds of batteries are employed in many electrical systems to store or deliver energy. There have been many proposals for lead-acid battery models. A comprehensive electrical circuit model for lead-acid batteries was proposed in (Salameh et al, 1992). This model can be simplified to the circuit shown in figure 8 (Wang and Nehrir, 2007). In this circuit model, Cb is battery capacitance, Rs is self-discharge resistance, Ri is internal resistance, Co is overvoltage capacitance, and Ro is overvoltage resistance. The battery is considered fully charged before the application of load, and permissible range for voltage is considered 100±5% of nominal voltage.

For power electronics intermediates, Buck-Boost DC-DC converters are employed. State-space averaged model can be used to analyze the converters performance (Rashid, 2001). These models can represent the average behavior of converters in steady state as well as in transients.

In order to analyze the performance of the proposed configuration, the system is tested in two stages. First, MPPT controller is tested separately, and results are shown. In the next stage, the fuel flow which determined by battery charge controller is applied to DMFC, and effects of load resistance changes on system performance are analyzed.

To investigate performance of the MPPT controller, hypothetical step changes are applied to input fuel flow of DMFC. Considering such changes, DMFC output power vs. its current is depicted in figure 9.a. Figure 9.b shows the output power of DMFC which is extracted by DC-DC converter based on MPPT controller instructions.

As can be seen, MPP of DMFC for different values of input fuel flow is traced continuously and operation of DMFC becomes fixed in this point.

Now, by adding the battery charge controller to system, the effects of load resistance changes on system performance will be analyzed. In this condition, the controller changes the input fuel flow of DMFC continuously. The filter cut-off frequency is set to 1 Hz and the damping factor is 1. Step changes of load resistance are shown in figure 10.a. The calculated fuel flow and DMFC output power are presented in figure 10.b and figure 10.c respectively. Figure 10.d represents the voltage of battery terminals.

As can be seen in above figures, in spite of the fact that changes of load resistance is in a wide range, it has no effect on the MPPT controller performance, and MPP is traced continuously. Moreover, battery voltage is regulated in the determined limits, satisfactorily.

6. Conclusion

Considering the importance of high efficiency operation and optimum fuel consumption in DMFC power systems, it is necessary to provide conditions in which DMFC can operate in its MPP, but as described in this paper, there are some problems. In order to overcome these deficiencies, a new configuration for Fuel cell / Battery hybrid power system is proposed and analyzed. This system is able to utilize DMFC maximum power and regulate output voltage simultaneously, using two sets of controller. One is a DC-DC converter in addition to a MPPT controller, which uses P&O algorithm to trace MPP. The next is a battery charge controller which regulates battery voltage by changing the input fuel flow of DMFC. So, both MPP operation of DMFC and output voltage regulation can be realized.

The proposed system is simulated and results demonstrate appropriate performance of the system and controllers.

References

Enslin, J., Wolf, M.S., Snyman, D.B. and Swiegers, W., (1997). "Integrated Photovoltaic Maximum Power Point Tracking Converter. *IEEE Trans. on Industrial Electronics*, vol. 44, pp. 769-773.

Guo, H., Ma, C., (2004). 2D analytical model of a direct methanol fuel cell. *Electrochemistry Communications* 6, pp. 306–312.

Hussein, K., Muta, I. Hoshino, T. and Osakada, M. (1995). Maximum Photovoltaic Power Tracking: An Algorithm for Rapidly Changing Atmospheric Conditions. *IEE Proc.-Generation, Transmission, Distribution,* Vol. 142, No.1, pp. 59-64.

Huynh, P., Cho, B.H., (1996). Design and Analysis of a Microprocessor-Controlled Peak-Power-Tracking System. *IEEE Trans. Aerosp. Electron. Syst*. 32 (1), pp. 182–190.

Jeong, I., Kim, J., Pak, S., Nam, S., Moon, I., (2008). Optimum operating strategies for liquid-fed direct methanol fuel cells. *Journal of Power Sources* 185, pp. 828–837.

M. H. Rashid, (2001). *Power Electronics Handbook*, New York: Academic.

Noguchi, T., Togashi, S., Nakamoto, R., (2002). Short-Current Pulse-Based Maximum-Power-Point Tracking Method for Multiple Photovoltaic and Converter Module System. *IEEE Trans. on Industrial Electronics*, vol. 49, pp. 217-223.

Salameh, Z. M., Casacca, M. A., and Lynch, W. A., (1992). A mathematical model for lead-acid batteries. *IEEE Trans. Energy Convers.*, vol. 7, no. 1, pp. 93–98.

Sundmacher, K., Schultz, T., Zhou, S., Scott, K., Ginkel, M., Gilles, E.D. (2001). Dynamics of the direct methanol fuel cell (DMFC): experiments and model-based analysis. *Chemical Engineering Science* 56, pp. 333-341.

Wang, C., Nehrir, H., (2007). Load Transient Mitigation for Stand-Alone Fuel Cell Power Generation Systems. *IEEE Trans. Energy Conversion,* 22(4), pp. 864-872.

Wasynczuck, O., (1983). Dynamic Behavior of a Class of Photovoltaic Power Systems. IEEE Trans. *Apparatus and Systems*, Vol. PAS-102, No. 9, pp. 3031-3037.

Zhi-dan, Z., Hai-bo, H., Xin-jian, H., Guang-yi, C., Yuan, R., (2008). Adaptive maximum power point tracking control of fuel cell power plants. *J. Power Sources* 176, pp. 259–269.

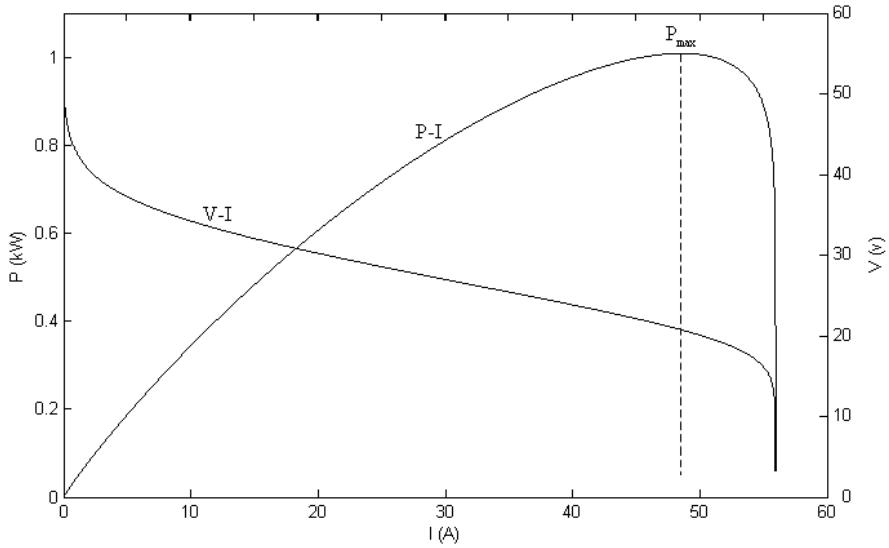

Figure 1. DMFC stack output voltage and power v.s. its current curves

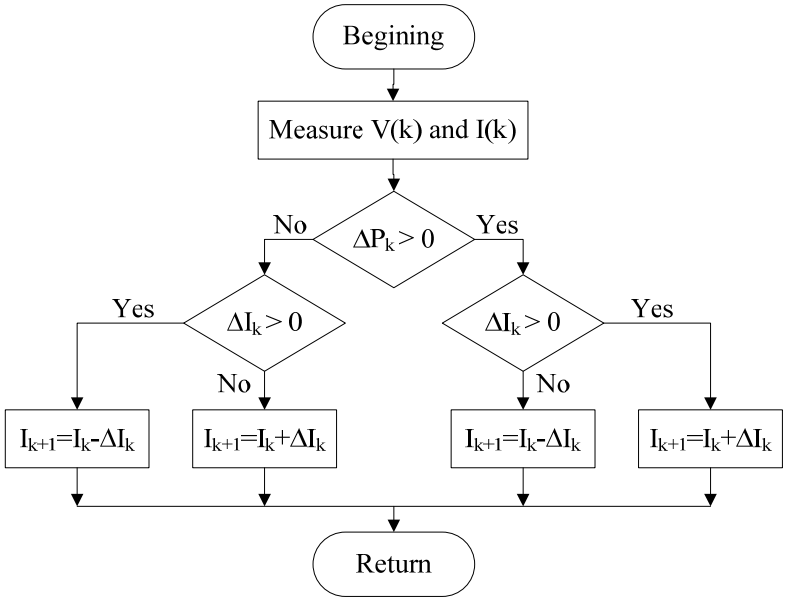

Figure 2. Flowchart of P&O algorithm

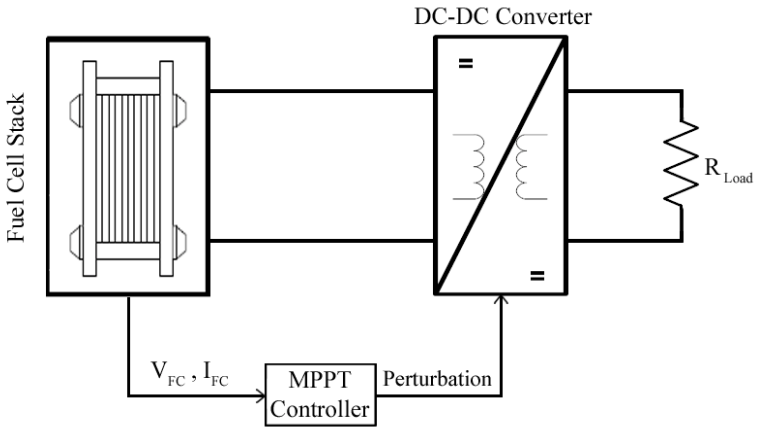

Figure 3. Schematic diagram of MPPT fot DMFC system

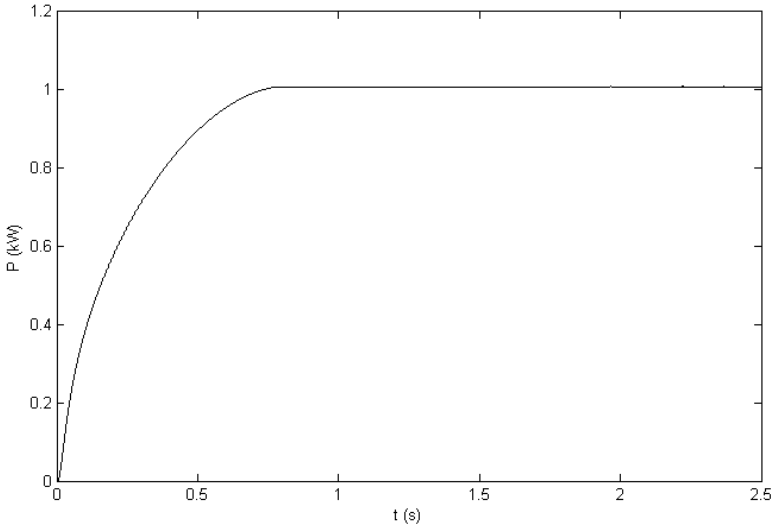

Figure 4. MPPT for a DMFC system in standard conditions

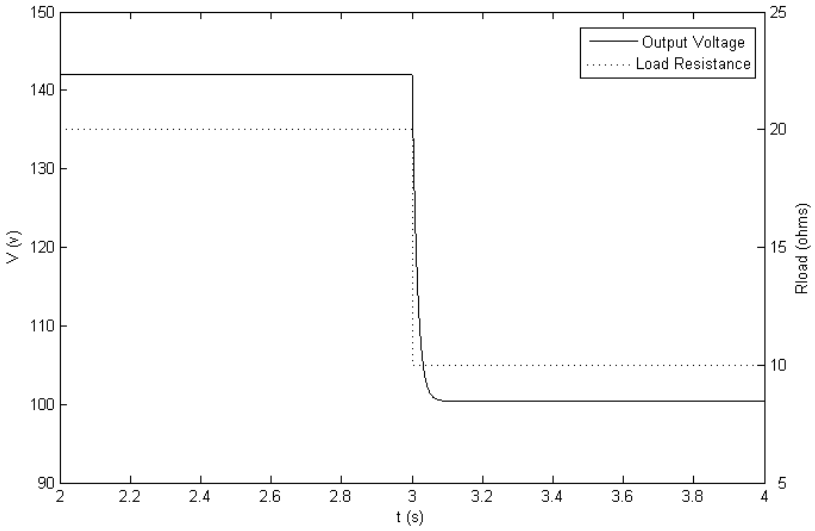

Figure 5. Output voltage variations when load resistance varies

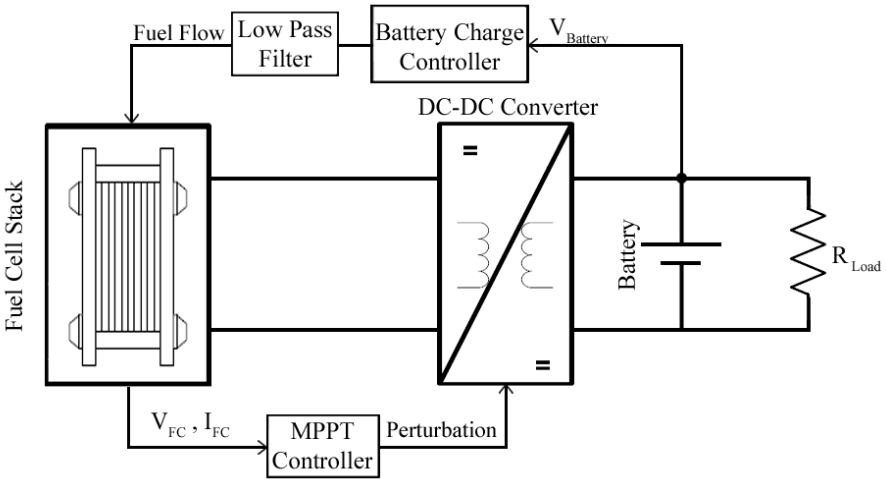

Figure 6. Complete proposed DMFC/Battery hybrid system

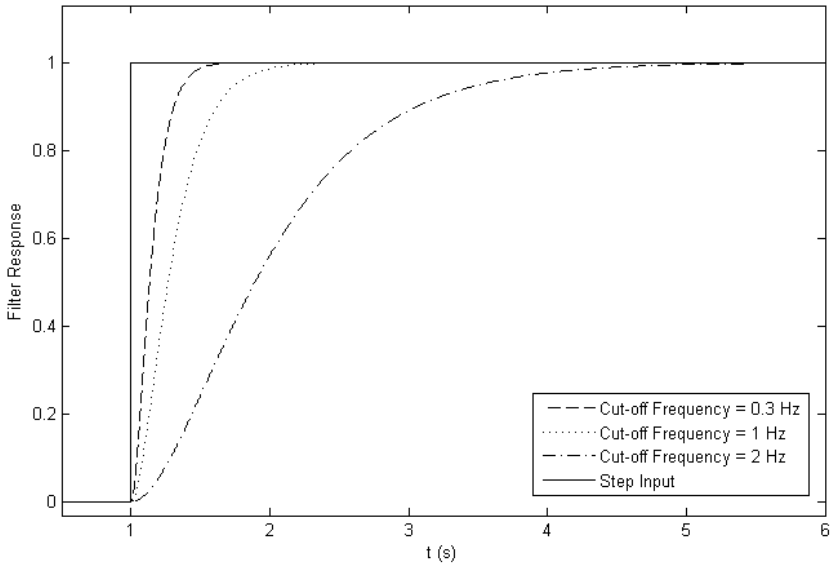

Figure 7. Response of a typical low pass filter to step input for different values of cut-off frequency

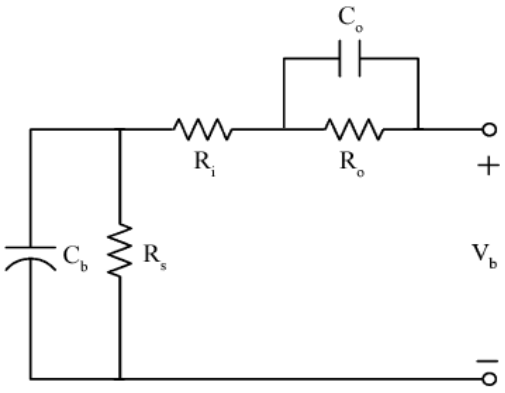

Figure 8. Simplified model for lead-acid batteries

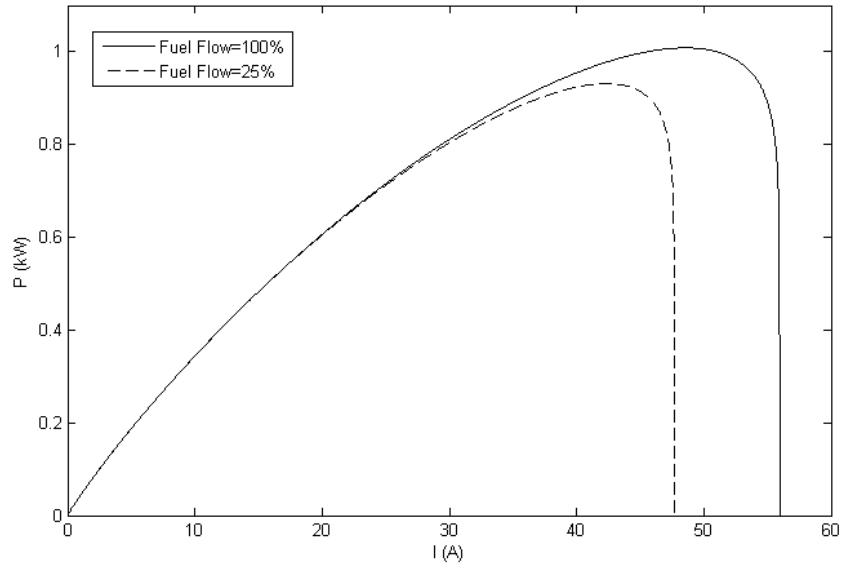

(a)

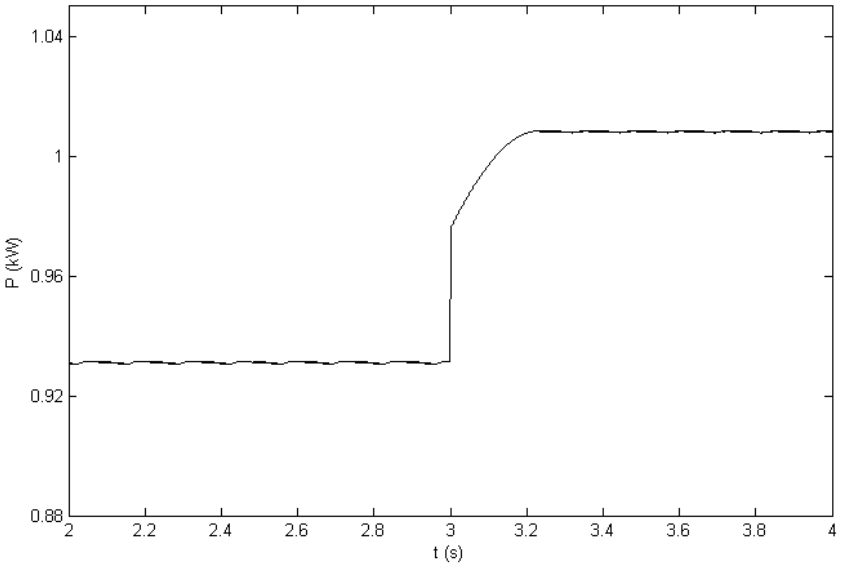

(b)

Figure 9. system performance when step changes are applied to input fuel flow.
a) DMFC output power vs. its current, b) output power of DMFC

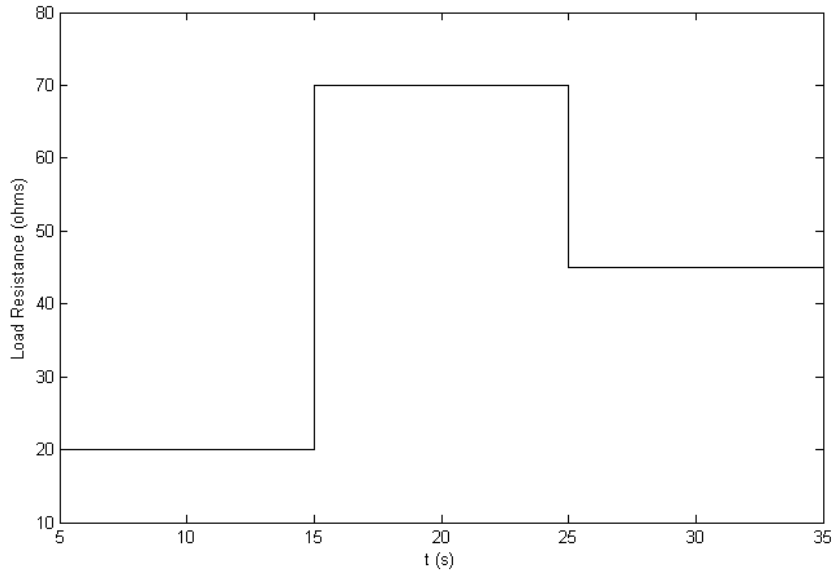
Load Resistance (ohms)
t (s)
80
70
60
50
40
30
20
10
5
10
15
20
25
30
35

(a)

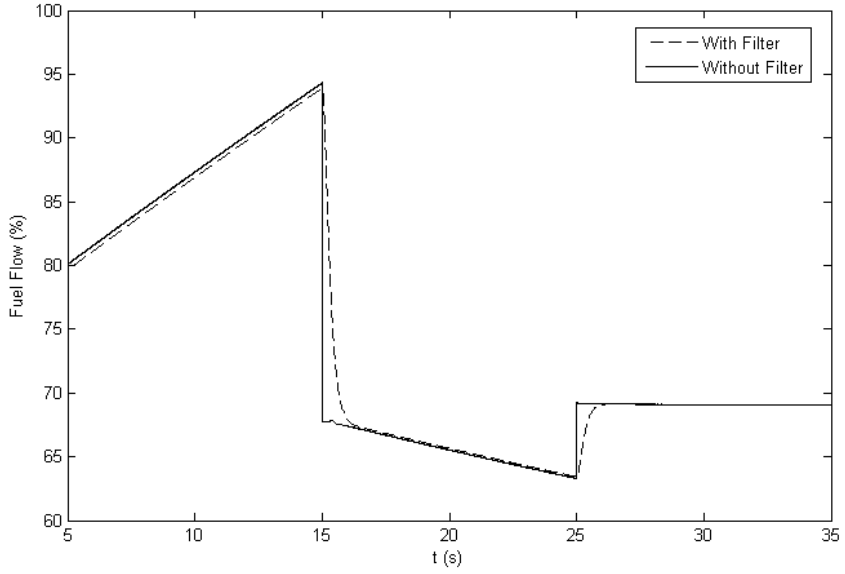
Fuel Flow (%)
t (s)
With Filter
Without Filter
100
95
90
85
80
75
70
65
60
5
10
15
20
25
30
35

(b)

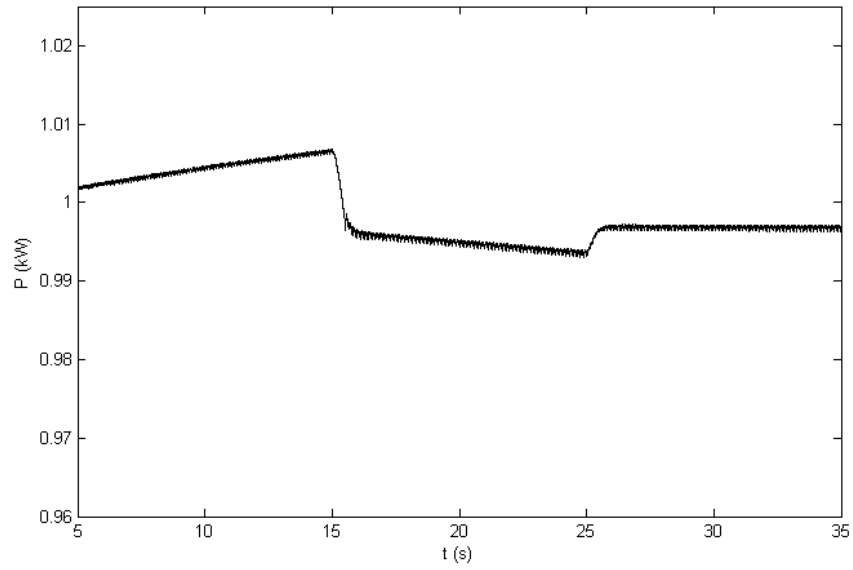

(c)

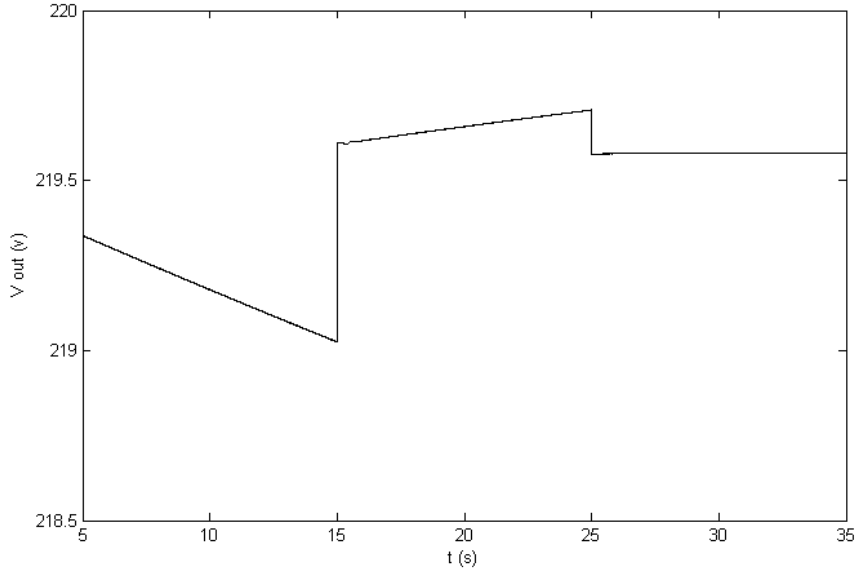

(d)

Figure 10. System performance under variable load resistance condition,
a) Step changes applied to load resistance, b) Variations of DMFC input fuel flow,
c) FC output power, d) Battery voltage

Modern Applied Science

www.ccsenet.org/journal.html

Vol. 3, No. 8

August 2009

Reduction Emissions from Transport Sector

——EU Action against Climate Change

Shuying Li

SAIC-GM-Wuling Automobile Co., Ltd.

No.18 Hexi Road, Liuzhou, Guangxi, 545007, China

Tel: 86-772-3750-956 E-mail: shuying.li@sgmw.com.cn

Abstract

There is a consensus among the majority of the world's scientists that our planet is experiencing man-made climate change, which will bring great social, economic and environmental threats to human being (Europa, 2008). The increase amount of atmospheric CO_2 concentration impacts climate changes has become a major concern to the public. Transportation is accounted for 26% of global CO_2 emissions and is one of the few industrial sectors where emissions are still growing (Chapman, 2007). In the European Union (EU), the road transport sector is one of the main sources of CO_2 emissions. Therefore, reducing CO_2 emissions and fuel consumption from road transportation is an important strategy for EU to implement the Kyoto Protocol and to develop a sustainable transport system (Fontaras and Samaras, 2007). This paper explores and discusses the initiation and development of the EU's policies and strategies against climate change and the share experiences in the EU transport sector to reduce CO_2 emission. Basing on the research, it can be concluded that the EU has acted as a front-runner in the battle of combat against climate change.

Keywords: European Union (EU), Transport sector, Reduction emissions

1. Introduction

There is a consensus among the majority of the world's scientists that our planet is experiencing climate change. The warming trend can be observed from the increasing global temperatures, the widespread melting ice, and the rising global ocean level (IPCC, 2007). According to IPCC (2007)'s report, since 1850, the average surface temperature of the Earth has risen 0.76° C. It is predicted that the global average surface temperature is likely to rise a further 1.8-4.0°C this century if no further action taken to decrease greenhouse gas emissions.

Although human-induced climate change is still questioned in US, the majority of UK senior scientists believe that man-made climate change is a significant threat and that action should not be delayed (Leaf, Verolme et al. 2003). IPCC (2007) claims that most of the warming observed over the last 50 years is caused by human activities such as burning of fossil fuels, deforestation and desertification, which lead to CO_2 emissions, the most important greenhouse gas emissions responsible for climate change. In order to halt the warming trend, CO_2 emissions must be reduced significantly.

According to IEA (2000), transportation is accounted for 26% of global CO_2 emissions and is one of the few industrial sectors where emissions are still growing(Chapman, 2007). In the European Union, transport emits 21% of the EU's greenhouse gas emissions. More severely, there is a 22% rising in emissions between 1990 and 2002(ECCP, 2007). Therefore, reducing CO_2 emissions and fuel consumption from road transportation is an important strategy for the European Union to fight against climate change(Fontaras and Samaras, 2007).

This paper attempts to review the EU's main policies and strategies against climate change, which include the United Nations Framework Convention on Climate Change (UNFCCC), the Kyoto Protocol, the European Climate Change Programme (ECCP) and the European Union Emissions Trading Scheme (EU ETS). The paper also explores the share experiences in the EU transport sector to reduce CO_2 emission, which include reducing CO_2 from new cars (Zachariadis, 2006); dieselization (Zachariadis, 2006; Zervas, 2006; Zervas, Poulopoulos et al., 2006; Fontaras and Samaras, 2007) and technology improvement such as reducing vehicle mass, enhancing engine efficiency(Zachariadis, 2006) and development of alternative fuel(Chapman, 2007).

2. Methodologies

Through plenty of researches on the policies and strategies issued on European Union official portal site: the Europa, this report chronologicaly discusses the initiation and development of the EU's main policies and strategies against climate change, which include UNFCCC, Kyoto Protocol, ECCP and ETS. On the other hand, through the exploration to many academic journals report on the EU and Member State's experiences on cutting CO_2, this report qualitatively analyses and summarizes the successful experiences and reasonable recommendation to reduce CO_2 in the EU's transport sector. Since the sample size of journals reports is not sufficient and some of the journal reports have different perspectives, the methodology used in this report may have some limitation and may be further developed.

3. EU Policies and Strategies against Climate Change

3.1 The EU's Role on Climate Change

Christiansen and Wettestad (2003) argue that basing on empirical evidence, the EU's position on climate change has a remarkable change. The EU has change from the role of "a sceptic to become a frontrunner". Similarly, Leaf et al (2003) state that the EU has been acting in many aspects as a key player in the global efforts to reduce greenhouse gases emissions. As one of the largest emitters, the EU owed about 25% of emissions of greenhouse gases in the group of "Annex I countries" addressed in Kyoto Protocol. Moreover, the EU is generally recognised to have played an significant strategic role in the climate negotiations under the UNFCCC, those policies and strategies adopted at the EU level are important not only for emissions eliminating in its Member States, but also for the evolution of the international climate regime. To give an example, EU's emission standards have been adopted by China.

3.2 The United Nations Framework Convention on Climate Change

Marmo (2008) claims that the EU has greatly contributed to the shaping of the UNFCCC. In 1990, when the UN Intergovernmental Panel on Climate Change (IPCC) sent out the warning that greenhouse gases emissions have caused increasing global temperatures in its first assessment report, the EU committed itself at the same year to keep its CO_2 emissions at the 1990 level by 2000(EUROPA, 2008). In 1991, the European Commission issued the first Community strategy to improve energy efficiency and limit CO_2 emissions (Marmo, 2008). In 1992, the EU signed the UNFCCC with an ultimate objective "to prevent dangerous anthropogenic interference with the climate system" (Marmo 2008). Since that, the EU has smoothly strengthened and progressed its actions to reduce CO_2 emissions, as well as other greenhouse gases. These efforts were further emphasized after the Kyoto Protocol was agreed.

3.3 The Kyoto Protocol

It is no doubt that the Kyoto Protocol is a remarkable step for the European Community in its efforts to address climate change. The Kyoto Protocol is a treaty made under the UNFCCC with the aim of reducing greenhouse gases. The Protocol was agreed on December 11th, 1997 when UNFCCC members met in Kyoto. It then entered into force on February 16th, 2005. According to the Kyoto Protocol, developed countries listed in "Annex I countries" must reduce a integrative average 5% of their greenhouse gas emissions by 2008-2012 compare to 1990 level (Wikipedia, 2008).

Under the Kyoto Protocol, the EU committed to achieve a combined reduction of 8% in CO_2 emissions. As for the 15 Member States, under the so-called "burden-sharing mechanism" principle, have been contributed specific percentages of reduction of CO_2 (Council Decision 2002/358/CE). These percentages vary largely from one Member State to the other. For example while Greece and Portugal are allowed to increase 25% and 27%, Denmark and Germany have committed themselves to a reduction of 21%. At the same time, the European Community is also a unit that signed the Kyoto Protocol to the UNFCCC, which means that it must demonstrate itself that it is able to achieve the 8% reduction target as an entity. Thus, it is important to set policies at the community level to help in achieving this objective and to support the more ambitious goal set by the European Council of the global annual mean surface temperature should not exceed 2 °C above pre-industrial levels (European Council, 2005).

3.4 the European Climate Change Programme (ECCP)

Although many "climate-related initiatives" have been undertaken by the European Commission since 1991(Marmo 2008), in order to achieved the 8% target by 2008-2012, it is vital that both the European Community and Member States need to reinforce their actions. Consequently, in 2000 the European Commission launched the first ECCP (ECCP I), whose goal was "to identify and develop the EU level's most environmentally and cost-effective policies and measure to implement the Kyoto Protocol "(ECCP, 2007). ECCP I was developed on comprehensive teamwork that has involved the European Community, the Member State and other stakeholders such as industries and national experts. ECCP Ⅱ was launched in October 2005 through considerable stakeholders discussions to explore further cost-effective options for cutting greenhouse gases emissions. Subsequent working groups covering "impact and adaption, carbon capture and geological storage, CO_2 emissions from aviation and light-duty vehicles" were set up for specific issues (ECCP, 2007). Under the ECCP programme to date, some 40 cross-cutting and sectoral policies and measures have been identified, most of which are already being implemented. They include the "ground-breaking" European Union

Emissions Trading Scheme (EU ETS).

3.5 EU ETS (Emission Trading Scheme)

The EU ETS, launched in January 2005, is the world's biggest company level 'cap-and-trade' system for trading in emissions of CO_2(Egenhofer 2007). Its establishment was through binding legislation put forward by the European Commission and approved by the EU Member States and the European Parliament. Since its implementation, global carbon market has expanded rapidly. This is mostly because that the EU ETS enable companies to utilize credits from the Kyoto Protocol's "project-based mechanisms - the CDM and JI" - to support them to meet their obligations within the system (ETS, 2005). This means the EU ETS not only provide "cost-effective means" for EU-based industries to reduce their emissions. But is also channelling considerable business trading emissions to cut costs and reduce emissions worldwide investment into "emission-reduction projects" in developing countries such as India and China and economies in transition. Through this particular trading, the EU ETS promotes the transfer of advanced, environmentally sound technologies to these countries to support them to achieve sustainable development (ETS, 2005).

3.6 Future Development

According to the European Commission's annual report released on, 27 November 2007(EC Press, 2007), the latest projections from Member States indicate that it is predicted that EU-15 emissions will be able to cut CO_2 to 7.4% of 1990 in 2010, which just short distance of 8% reduction target of 2012. Through measures already taken and additional initiatives adopted and implemented swiftly, the EU is moving closer and closer to achieving its Kyoto Protocol targets.

However, in order to limit global annual mean surface temperature should not rise exceed 2 °C, ambitious action is needed to succeed the Kyoto Protocal after 2012 when the Kyoto Protocal will expire. Since early of 2007, the European Commission has launched several meetings to discuss "the way ahead for 2020 and beyond" and has proposed to reduce its overall emissions to at least 20% below 1990 levels by 2020(Figure 1). On 23 January 2008, in their proposal "Climate action and renewable energy package", the European Commission even committed that the EU is ready to reduce 30% if other developed countries make comparable efforts (Europa, 2008).

4. Reduction CO_2 Emission from Transport Sector

4.1 CO_2 Emissions in Transport Sector

The transport sector is a main source of CO_2 in many countries. According to IEA (2000) reports, the transport sector accounts for 26% of global CO_2 emissions, of which about two-thirds generates in the wealthier 10% of countries(Chapman 2007). Transport was one of the key sectors highlighted to be tackled by the Kyoto Protocol with an aim to reduce worldwide greenhouse gas emissions by 5.2% of 1990 levels by year 2012(Chapman 2007). Therefore, since 1997, the 38 developed countries who signed the agreement have heavily added transport in their political agendas. In the European Union, transport was responsible for 21% of the EU's greenhouse gas emissions, with a 22% increase during the period of 1990 to 2002 (ECCP, 2007). Meanwhile, road transport is the greatest resource of greenhouse gases in the transport sector, reducing CO_2 emissions and fuel consumption from road transportation has become an important strategy for the European Union to against climate change(Fontaras and Samaras, 2007). Experiences and recommendations of reducing CO_2 from road transportation adopted by EU and Member State include reducing CO_2 emission from new cars (Europa, 2006), dieselization and technology improvement etc.

4.2 Reducing CO_2 Emissions from New Cars

Reducing CO_2 emissions from new cars is a key priority of EU climate change policy (EUROPA, 2006). The ultimate aim is to limit average CO_2 emissions from new cars sold in the EU to 120g/km by 2012. To achieve this, "three-pronged" strategy is undertaken by the EU and Member States.

Firstly, car producers' commitment to the European Commission to limit average CO_2 emissions from new cars is up to date the most important initiative to limit CO_2 emissions originated by transport and especially emissions from road transportation (Fontaras and Samaras, 2007). In 1999, driven by the trend of increasing CO_2 in the transportation sector, the European Automobile Manufactures Association (ACEA) signed a voluntary commitment with the European Commission on reducing the average CO_2 emissions from new cars (EC, 1999). One year later, the Japanese and Korean manufacturers signed the similar agreement with the European Commission. In the agreement, it was agreed that the target emission for the average ACEA vehicle should not exceed 140 g CO_2/km in 2008. This represents a reduction of around 25% compared with the mid-1990s. By implementing this voluntary agreement, since 1995, fuel economy measured in the official driving cycle has improved considerably. According to progress reports published by the EC and ACEA each year, from 1995 to 2002, European new cars CO_2 emissions of per kilometre dropped by 12% with a 1.7% annual improvement. In year 2006, carmakers were almost half-way towards meeting this target(Zachariadis 2006).

Secondly, enable consumers to choose the most fuel-efficient cars is another effective way to reduce CO_2 emission from new cars. To help consumers identify the most fuel-efficient models in a range of products, EU legislation requires that

car makers should demonstrate mandatory labelling and provision of consumer information at the sale point about each car's fuel economy and CO_2 emissions (Europa, 2006)

The third element of the strategy is fiscal support. The Commission has proposed legislation that would require Member States levying car registration taxes and/or circulation taxes to relate at least 50% of the tax to the level of a vehicle's CO_2 emissions (Europa, 2006).

4.3 Reducing CO_2 Emissions by Dieselization

The increase in the passenger cars (PCs) fleet is a main reason to the increase CO_2 emissions in the EU transport sector(Zervas 2006). Replacement of gasoline passenger cars by diesel passenger cars, also called dieselization, to decrease CO_2 emissions has achieved more awareness among EU experts(Zachariadis, 2006; Zervas, 2006; Zervas, Poulopoulos et al., 2006; Fontaras and Samaras, 2007). Zervas (2006) argued that from technical aspect, diesel passenger cars have greater thermodynamic efficiency, which provides improved fuel economy and emits less CO_2. Moreover, the study on the benefit on CO_2 emitted from new passenger cars in the case of an increased diesel penetration in Ireland(Zervas, 2006) and Greece(Zervas, Poulopoulos et al., 2006) shows the result as table 2.

The results show that with increasing diesel penetration, CO_2 emission reduction increases dramaticaly. From the experimental study, experts suggest that future total CO_2 emissions from new PCs can be partially controlled by the introduction of diesel passenger cars.

However, other experts argue that continuous increase of the diesel share in passenger cars is still a controversial practice for reducing fuel consumption (Jensen, 2003; Hugrel and Joumard, 2001). More specifically, Kavalov and Peteves (2004) and Jensen (2003) express concern for its impact. They argue that continuous dieselization has been shown can affect "the whole fuel chain and result in increased overall CO_2 emissions due to fuel production, refining and economical factors". Similarly, (Zachariadis 2006) maintains that since diesel vehicles have a lower power/mass ratio, dieselization will cause increases in engine size and vehicle mass. The European Commission indicated that dieselization is an acceptable first measure but states that "the associations would not meet the 140 g/km by a simple increase in the diesel share only, dieselization should also combine with other strategy" (EC, 2004b).

4.4 Reducing CO_2 Emissions by Technology Improvement

Technological improvement will play an increasing role in the reduction of CO_2 from transport (Chapman, 2007). A car manufactured today emits less CO_2 and pollutants than a decade ago (DfT, 2004a). This is because cars are being designed and manufactured differently today. Recently, cars are being designed much lighter, which can reduce power requirements. As Zachariadis (2006) and Zervas and Lazarou (2008) suggest that increase in weight of future EU new passenger cars would have a negative effect on CO_2 emissions. Therefore, there should be an "upper limit" to the weight of passenger cars. If each new passenger car's weight does not exceed an upper limit, a significant CO_2 benefit can be achieved, especially when this limit is low. The benefit obtained by limitations of weight is also higher than the benefit obtained from the decreased future fuel consumption. To give another example, engine efficiency is enhancing to enable cars to consume less fuel than the past. Today, "improved engines with up to 4 valves per cylinder, better combustion properties and less friction losses, enhanced automatic and manual transmission systems, tyres with lower rolling resistance and lighter automotive bodies with lower aerodynamic resistance" are now commonplace in automobiles, and continue improvements are undertaking in car makers (Zachariadis, 2006). Besides benefit from reducing weight and enhancing engine efficiency, further energy can be saved by "ecological driving", which includes measures such as "avoiding harsh acceleration and braking, using higher gears, observing speed limits and keeping the car regularly serviced with the correct tyre pressures" (SDC, 2006).

Ultimately, the most challenge for technological improvement is the development of alternative fuel such as bio fuels, natural gas, hydrogen and electric motors to replace petroleum fuels which contribute to greenhouse gas emissions(Chapman 2007). Alternative fuel, along with their advantages and disadvantages, however, governments should increasingly fund research and development of alternative fuels whilst using taxation policies to enable the switch to fuels with a low carbon content viable (DfT, 2006). Indeed, without new technologies, such emission reduction targets may be considered impossible to meet in a long term (Sandan and Azar, 2005). Fortunately, the EU realized the importance of alternative fuel development. The EU has set itself an indicative target of achieving a 5.75% share for bio fuels in the petrol and diesel market by 2010. Consequently, most Member States have introduced fuel tax exemptions in favour of bio fuels. The market share of bio fuels grew from 0.2% in 2000 to 0.8% in 2004 (Europa, 2006).

5. Conclusions

This report reviews EU's most important policies and strategies against climate change. These policies and strategies include two major treaties and two big programmes. The two main treaties are the UNFCCC, which the EU helps its shaping, and the Kyoto Protocol, a significant step taken by the European Community in its efforts to address climate change. The two big programmes undertaken by EU to reduce its own greenhouse gas emissions are the European

Climate Change Programme (ECCP) and the EU Emissions Trading Scheme (EU ETS). ECCP has helped the EU establish series of environmental and cost effective policies and measure. While EU ETS is the world's biggest company level 'cap-and-trade' system for trading in emissions of CO_2. The most worth mentioning is that, to achieve the ultimate target of limit global warming to 2°C, the EU has set up new commitment of reduce 20% greenhouse gas emission by 2020 to succeed the Kyoto Protocol.

In order to implement the Kyoto Protocol and to develop a sustainable transport system, reduction CO_2 from transport sector is the key. This report also reviews some share experiences and recommendations in the EU transport sector to reduce CO_2 emissions. Among these experiences, reducing CO_2 from new cars is a key priority of EU climate change policy. Along with the three-pronged strategy, ACEA's commitment to the European Commission to limit average CO_2 emissions from new cars is up to now the most important initiative to limit CO_2 emissions originated by transport. Although dieselzation can significantly reduce CO_2 emissions, it is still a controversial practice that needs further consideration. Technological improvement will play an increasing role in the reduction of CO_2 from transport.

However, climate change and global warming is not only one country or one community's business, it is a global issue. At the same time, it is also a moral issue. Human beings should defend the planet together. We should defend it state-by-state, city-by-city, family-by-family and person-by-person. Reducing emissions is one of the ways. Governments can reduce most emissions by legislations and establishment of strict policies. Industries can contribute by strict implementation of Code of Conduct. For every individual can contribute by using a bicycle instead of a car or even by saving water and electricity in daily life. Fortunately, there were growing public awareness of global warming and energy efficiency issues recently. More and more countries and communities have shown their concerns and have started regulated their policies. Among these countries and communities, it is no doubt that the EU is a front-runner. If all of the other countries make comparable efforts, it can believed that human being would have the capability to conquer the climate change crises as we have conquered other crises in the past.

References

Chapman, L. (2007). "Transport and climate change: a review." *Journal of Transport Geography* 15(5): 354-367. Full text [online].Available at: SeienceDirect (Accessed: 17th February 2008)

Christiansen, A. C. and J. Wettestad (2003). "The EU as a frontrunner on greenhouse gas emissions trading: how did it happen and will the EU succeed?" *Climate Policy* ***3***(1): 3-18. Full text [online].Available at: SeienceDirect (Accessed: 17th February 2008)

Council Decision 2002/358/EC of 25 April 2002 concerning the approval, on behalf of the European Community, of the Kyoto Protocol to the United Nations Framework Convention on Climate Change and the joint fulfilment of commitments thereunder (OJ L 130, 15/5/2002).

DfT (2004a)."The Future of Transport, A Network For 2030". UK Department for Transport, Crown Copyright 2004, 140pp.

DfT (2006). "Visioning and Backcasting for UK Transport Policy" (VIBAT). Stage 3 Report: Policy Packaging and Pathways. Department for Transport, Crown Copyright 2006, 75pp.

ECCP(2008), "The European Climate Change Programme", [online], Available from European Union Official Portal Site: http://ec.europa.eu/environment/climat/pdf/eu_climate_change_progr.pdf(Accessed: 17th February 2008)

ETS, "EU emissions trading: an global EU an open system promoting global innovation", [online], Available from European Union Official Portal Site:

http://ec.europa.eu/environment/climat/pdf/bali/eu_action.pdf (Accessed: 17th February 2008)

Egenhofer, C. (2007). "The Making of the EU Emissions Trading Scheme: Status, Prospects and Implications for Business." *European Management Journal* **25**(6): 453-463. Full text [online].Available at: SeienceDirect (Accessed: 15th February 2008)

Europa (2006) " Reducing Emmission from the Energy and Thansport Sectors", [online], Available from European Union Official Portal Site:

<http://ec.europa.eu/environment/climat/pdf/reducing_emissions_energy_transport.pdf>(Accessed: 15th February 2008)

Europa (2008) "Climate Change", [online], Available from European Union Official Portal Site:<http://ec.europa.eu/environment/climat/home_en.htm>, (Accessed: 17th February 2008)

European Commission (1999), "Recommendation of 5 February 1999 on the reduction of CO_2 emissions from passenger cars" (notified under document number C (1999) 107), Available from European Union Official Portal Site: <http://ec.europa.eu/environment/CO_2/99125/en.pdf>(Accessed: 17th February 2008)

European Commission (2004a), "Catching up with the Community's KYOTO Target", COM(2004) 818 final, Brussels, 20.12.2004, [online], Available from European Union Official Portal Site:

<http://europa.eu.int/eurlex/lex/LexUriServ/site/en/com/2004/com2004_0818en01.pdf>(Accessed: 17th February 2008)

European Commission (2004b) "Communication from the Commission to the Council and the European Parliament: Implementing the Community Strategy to Reduce CO_2 Emissions from Cars: Fourth Annual Report on the Effectiveness of the Strategy" (Reporting Year 2002), COM(2004) 78 final & SEC(2004) 140, Brussels, 2004, available from: <http://europa.eu.int/eur-lex/en/com/cnc/2004/com2004_0078en01.pdf> (Accessed: 17th February 2008)

European Commission (2007), "Climate change: EU on track towards Kyoto target but efforts must be maintained, projections show", Brussels, 27 November 2007, Available from European Union Official Portal Site:

<http://europa.eu/rapid/pressReleasesAction.do?reference=IP/07/1774&format=HTML&aged=0&language=EN&guiLanguage=en> (Accessed: 19th February 2008)

European Council(2005) "Presidency Conclusions of the European Council", 22–23 March 2005 Available from European Union Official Portal Site: < http://ec.europa.eu/environment/climat/pdf/spring_2005.pdf>(Accessed: 17th February 2008)

Fontaras, G. and Z. Samaras (2007). "A quantitative analysis of the European Automakers' voluntary commitment to reduce CO_2 emissions from new passenger cars based on independent experimental data." *Energy Policy* **35**(4): 2239-2248. Full text [online].Available at: SeienceDirect (Accessed: 15th February 2008)

IEA (2000). International Energy Agency. "CO_2 Emissions From Fuel Combustions 1971–1998". 2000 Edition. OECD, Paris.

Hugrel, C., Joumard, R. (2001) "Passenger cars contribution to the greenhouse effect influence of the air-conditioning and ACEA's commitment (JAMA and KAMA included) on the CO_2 emissions". In: Proceedings of the 10th International Symposium on Transport and Air Pollution, September 17–19, 2001, Boulder, CO, USA. Full text [online].Available at: SeienceDirect (Accessed: 15th February 2008)

Jensen, P. (2003) "Potential limitations of voluntary commitments on CO_2 emission". *Joint Research Center—IPTS Report*, Issue 70. Full text [online].Available at: SeienceDirect (Accessed: 15th February 2008)

Kavalov, B., Peteves, S.D. (2004) "Impacts of the increasing automotive diesel consumption in the EU, Mission of the Institute for Energy". *Joint Research Center*, ISBN 92-894-6088-1, 2004. Full text [online].Available at: SeienceDirect (Accessed: 15th February 2008)

Leaf, D., H. J. H. Verolme, et al. (2003). "Overview of regulatory/policy/economic issues related to carbon dioxide." *Environment International* 29(2-3): 303-310. Full text [online].Available at: SeienceDirect (Accessed: 15th February 2008)

Marmo, L. (2008). "EU strategies and policies on soil and waste management to offset greenhouse gas emissions." *Waste Management* 28(4): 685-689. Full text [online].Available at: SeienceDirect (Accessed: 19th February 2008)

Sandan,B.A. and Azar, C.(2005), "Near-term technology policies for long-term climate targets economy wide versus technology specific approaches", *Energy Policy* **33** (2005), pp. 1557–1576. Full text [online].Available at: SeienceDirect (Accessed: 15th February 2008)

SDC (2006). Sustainable Development Commission: "Eco-Safe Driving", available from: <http://www.sd-commission.org.uk/communitiessummit/show_case_study.php/00135.html> (accessed: 21February2008).

Wikipedia (2008) 'Kyoto Protocal', [online], Available from World Wide Web:

< http://en.wikipedia.org/wiki/Kyoto_Protocol>, (Accessed: 17th February 2008)

Zachariadis, T. (2006). "On the baseline evolution of automobile fuel economy in Europe." *Energy Policy* **34**(14): 1773-1785. Full text [online].Available at: SeienceDirect (Accessed: 20th February 2008)

Zervas, E. (2006). "CO_2 benefit from the increasing percentage of diesel passenger cars. Case of Ireland." *Energy Policy* **34**(17): 2848-2857. Full text [online].Available at: SeienceDirect (Accessed: 16th February 2008)

Zervas, E. and C. Lazarou (2008). "Influence of European passenger cars weight to exhaust CO_2 emissions." *Energy Policy* **36**(1): 248-257. Full text [online].Available at: SeienceDirect (Accessed: 18th February 2008)

Zervas, E., S. Poulopoulos, et al. (2006). "CO_2 emissions change from the introduction of diesel passenger cars: Case of Greece." *Energy* **31**(14): 2915-2925. Full text [online].Available at: SeienceDirect (Accessed: 15th February 2008)

Table 1. Diesel penetration and CO_2 benefit in Ireland and Greece

Percentage of Diesel PC		Diesel Penetration	CO_2 Benefit	
Ireland	Greece		Ireland	Greece
<17%	<1%	30%	>2.9%	>5.4%
		50%	>7.4%	>10.2%

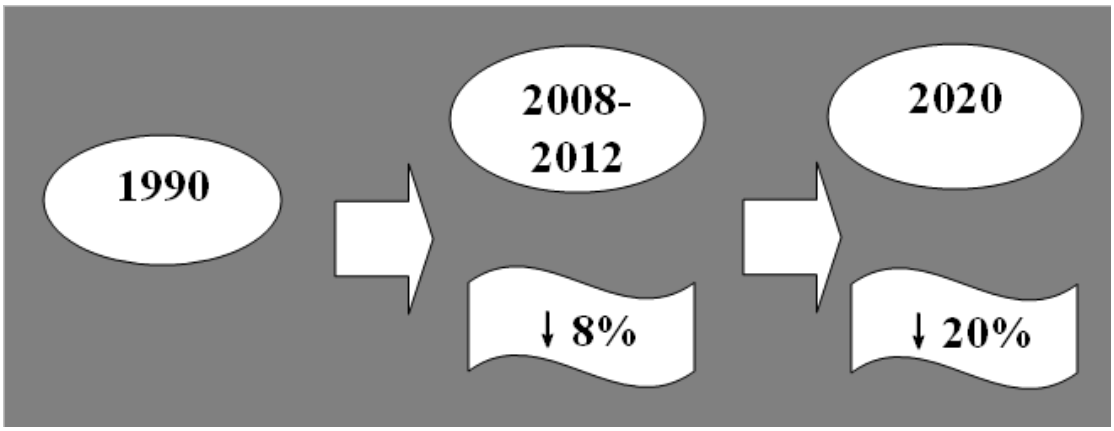

Figure 1. the EU's CO_2 Reduction Target

Modern Applied Science

www.ccsenet.org/journal.html

Vol. 3, No. 8

August 2009

Gear Ratios Strategy of PROTON Waja CNG-DI Vehicle for Improved Performance

B. B. Sahari (Coresponding Author)
Institute of Advanced Technology
Universiti Putra Malaysia
43400 UPM Serdang, Malaysia
Tel: 60-3-8948-7533 E-mail: barkawi@eng.upm.edu.my

Hamzah Adlan,
Perusahaan Otomobil Nasional Berhad (Proton)
P.O. Box 7100, 40918 Shah Alam, Selangor, Malaysia

S. V. Wong
Department of Mechanical and Manufacturing Engineering
Universiti Putra Malaysia
43400 UPM Serdang, Malaysia
Tel: 60-3-8948-7533 E-mail: wongsv@eng.upm.edu.my

A. M. Hamouda
Mechanical and Industrial Engineering Department
College of Engineering, Qatar University
P.O. Box 2713 –DOHA
Tel: 97-4-483-5125 E-mail: hamouda@qu.edu.qa

Abstract

A 1597cc gasoline CamPro engine was modified to adapt a Direct Injection (DI) technology that uses Compressed Natural Gas (CNG) as a fuel to form Compressed Natural Gas Direct Injection (CNGDI) engine. The modification includes increasing the compression ratio, redesigning the piston crown and cylinder head and a new engine control systems. These changes resulted in engine performance characteristics which is very different from its gasoline origin. This CNGDI engine is to be used with PROTON Waja vehicle body. Due to this change in the characteristics, the transmission systems utilizing an existing gear ratio combination, appears to be unsuitable, particularly for use in automatic transmission. Therefore, new gearbox with appropriate transmission matching needs to be developed. A computer based algorithm was developed for the purpose of predicting the PROTON Waja's vehicle dynamic performance when CNGDI engine is used. The parameters being considered are maximum speed, acceleration, and elapsed time and these were optimized depending on the engine characteristics such as power, torque, gear ratios, and vehicle design parameters. The results recommended that the gear ratios of 3.58, 1.95, 1.34, 0.98, 0.8 and 4.33 for first, second, third, fourth, fifth and Final Drive (FD) respectively were the most suitable.

Keywords: Gear Ratio, Compressed Natural Gas Vehicle, Transmission matching, Vehicle performance

1. Introduction

Natural Gas is cheap and abundant source of energy and suitable for automotive use. However, not many vehicles were designed specially to cater for natural gas. Most natural gas vehicles are converted from gasoline or diesel engine by fitting natural gas equipment such as gas tank and regulators (Das, A. and Watson, H. C., 1997). These vehicles are actually "gasoline or diesel vehicle runs on natural gas". Therefore, they are not dedicated to run on natural gas. Natural Gas can be used as a vehicle fuel in two forms; Compressed Natural Gas (CNG) and Liquefied Natural Gas (LNG). CNG is pressurized gas that is stored in cylindrical tank at pressure up to 250 bar (or 3600 psi) whereas LNG is cooled to a temperature of about –167ºC (-260°F) at atmospheric pressure where it turned into liquid and stored in cylindrical container. CNG is increasingly seen as effective alternative to petrol or diesel fuel in many internal combustion engines (Rousseau, S. Lemoult, B. Tazerout, M., 1999). One of the major benefits of CNG as an engine fuel is that the exhaust emission can be reduced compared to petrol or diesel. NGV has less emission level as set out by the EURO 3 and EURO 4 requirements. Table 1 shows the results of test on two types of fuel compared to the standards requirement (Middleton, A., Neumann, B., 2005). It can be seen that NGV comply all the requirements of the standards. Hence, natural gas vehicle are becoming important and acceptable.

The main disadvantage of standard petrol engine converted to natural gas is the low power output (Rousseau, S. Lemoult, B. Tazerout, M., 1999). Petrol engine combustion chamber was designed to cater for 9:1 to 10:1 compression ratio while CNG prefer ratios of around 14:1 to 18:1 to provide same performance as the equivalent capacity of petrol engine. Hence major modification on petrol engine components needs to be done before it can be used to run on CNG. The major modification may include cylinder head redesign, cam shaft or even cam timing adjustment, revision on cooling and lubrication, and inlet and exhaust tuning. Engine Management System (EMS) re-mapping has to be reconsidered to optimize the performance.

In the present work, a new direct injection common fuel rail technology was developed that will inject fuel at 20 bar pressure to the newly designed combustion chamber to achieve stoichiometric burn engine. Compression ratio used was in the range 13:1 to 15:1. It was designed to create high tumble inlet configuration that resulted in high flame speed and combustion rate with smaller minimum advance for best torque (MBT) spark ignition. This new configuration generates different Torque-speed and Power-speed characteristics. Because of this, new transmission systems need to be developed to cater for this change in torque and power characteristics. There are a number of transmission systems being researched on, and this include gear drives (Litvin, F.L., et. al., 2001), (Keiji Nemoto, Toshiharu Kumagai, Tasushi Ohnuma, 2002), continuous variable transmission systems (Mucino, V.H. et. al., 2001), (Jungmin Seo, Seung Jong Yi, 2005), hydro-mechanical (Dukhwan Sung, Sungho Hwang, Hyunsoo Kim, 2005), and gears with synchronizer (Keiji Nemoto, et. al. 2002). Different techniques were also being used in their analysis which includes simulation and modeling (Kim, J., et. al. 2005), (Jo, H.S., et. al., 2000, Bartlett, H., Whalley, R., 1998). Hence, transmission system is important in improving the vehicle performance. For the present work on CNGDI engine, new gear ratios are needed especially for automatic transmission systems. The objective of the present work was to predict the performance of PROTON Waja vehicle, as shown in Figure 1(a), when fitted with Direct Injection engine using Compressed Natural Gas as a fuel, as shown in Figure 1(b), via selection of different gear ratio and final drive. The running conditions such as 0-400 meter traveled time, 0-100 km/h acceleration time, and gear shifting point were used as performance criteria for different ratios. Computer algorithms have been developed specifically to predict the performances of the vehicle. With these algorithms, vehicle parameters such as coefficient of drag, coefficient of rolling resistance, tire rolling radius and effective mass were optimized.

2. Theoretical background

The power from the engine, P, was calculated using the following equation:-

$$P = \frac{P_{eff} V_d N_r}{1000n} \tag{1}$$

Where P_{eff} is the brake mean effective pressure, bmep, in kPa, V_d is the cylinder volume, N_r is the speed in revolutions per second and n is the revolutions per cycle.

The Traction Effort (T_E) is the force developed at the driving wheels and is the sum of wind resistance force, rolling resistance and gravitational resistance. Taking into account all these components of forces, the expression for T_E was defined by:

$$T_E = K_1 W \cos\phi + K_2 V^2 A + W \sin\phi \tag{2}$$

Where K_1 is the road surface co-efficient, K_2 is the coefficient of vehicle frontal area, V is the vehicle speed in km/h, W is the vehicle weight, A is the vehicle frontal area and Φ is the road gradient.

The selection of engine speed to the vehicle speed ratio, N_v, is given as:

$$N_V = \frac{N_e}{V} = \frac{2660 R_a R_t}{R_r} \tag{3}$$

Where N_e is the engine speed in rpm, R_a is the axle ratio, R_t is the transmission ratio and R_r is the average effective rolling tire radius.

In most design, the first gear is always chosen to be the lowest denoted by R_{T1}. The highest gear ratio R_{TN} is usually selected by the designer. Hence, when R_{T1} and R_{TN} have been defined, the numbers of forward gear, N and the intermediate gear ratios factor K are determined by using the following expression:

$$K = \left(\frac{R_{TN}}{R_{T1}} \right)^{1/(N-1)} \tag{4}$$

Having determined the value of K, the intermediate gear ratio (that is i^{th} gear ratio), R_{Tg}, is then determined from the general geometric progression expression given by:-

$$R_{Tg} = KR_{Tg-1} \tag{5}$$

Where R_{Tg-1} is the $(i-1)^{th}$ gear ratio.

Equations (1) to (5) were necessary to determine the appropriate gear ratios for the optimum vehicle driving performance. At each stage of the calculation, the power at the wheel has to be matched against the power and torque characteristics of the engine. Although CNGDI engine is derived from the gasoline engine, its characteristics differ from the gasoline base. Therefore, there is a need to reassess and determine the appropriate gear ratios.

3. Methodology

A computer algorithm was developed based on Equations (1) to (5) and was capable of calculating gear ratio and final drive for pre-determined parameters. This enables the optimized parameters for different transmission setup condition to be obtained. Table 2 shows the sets of transmission ratio that were calculated and will be used in the present study. The ratios were then obtained from the algorithms developed for a number of cases and for different conditions. Two different sets of gear ratio together with the three different set of final drive ratio at fixed vehicle parameters were used. Two sets of gear ratio are being used; namely Set 1, Set 2 and Set 3. Set 1 is the current production in-vehicle ratio and is used as a benchmark gear set. Set 2 and Set 3 are the new sets to be studied. Design parameters used are coefficient of drag, coefficient of rolling, rolling radius, effective mass and engine displacement. The weight of the vehicle was set to be a total of 1415 kg. The vehicle weight includes 1 driver and 2 adult passengers. The evaluations on the vehicle performance were based on the time taken to cover 0-100 km/h and time taken to cover 0-400 meter, 0-1000 meter traveled. In addition to that, other parameters such as maximum speed, vehicle speed, N_V ratio, engine power and total resistance could be extracted for the different running condition.

4. Results and Discussions

The variation of power and torque with engine speed for the CNG-DI CamPro engine is shown in Figure 2. It is based on the results of tests on Single Cylinder Research Engine. From Figure 2, it can be seen that the maximum torque achievable is 148 Nm at 4000 revolution per minute (rpm) whereas the power is 85 kW at 6000 rpm. The minimum torque at idling speed is 108 Nm, which is similar to a gasoline CamPro engine. The torque curve is not flat without torque dip. This torque profile is common for engine equipped with Dual Overhead Camshaft (DOHC) without variable valve timing (VVT). From 4000 rpm to 6000 rpm, the torque is relatively stable until it reaches 7000 rpm which the electronic engine cut off switch is activated. It is seen that the torque decreases from 142 Nm to 125 Nm from 6000 rpm to 7000 rpm which indicated a decrease in induction air volumetric efficiency. As for the power curve, Figure 2 indicated that the power increases almost linearly until 5000 rpm and after that the curves started to flatten and reaches its peak at about 6500 rpm. Theoretically, the maximum power output of 85 kW was achieved which is equivalent to a specific power output of 53.1 kW per liter.

The variation of flywheel power with vehicle speeds at different road gradients is shown in Figure 3 for PROTON Waja car equipped with CNG-DI CamPro engine. It can be seen that, at maximum power of 85 kW, on a flat terrain of (gradient = 0%), the car is capable to reach a top speed of 164 km/h. However, the top speed reached is reduced to 160 km/h as the slope is increased to 7 percent. A further drop to 149 km/h is apparent as the car climbs a 25 percent gradient terrain. This is considered to be an acceptable achievement since the speed limit in most expressways is 110 km/h.

The relationship between flywheel power and vehicle speeds depends on the gear ratio used and are shown in Figure 4 for Set 1, Figure 5 for Set 2 and Figure 6 for Set 3. From Figure 4, it can be seen that the intercept point from the first to the second gear occurred at 51 km/h. The intercept for second to third gear occurred at 92 km/h, third to fourth at 130 km/h, fourth to fifth at 170 km/h before reaching the top speed of 190 km/h. These intercept points indicated the maximum speed for gear change for optimum performance, particularly for automatic transmission. However, for manual transmission, gear change could be carried out at a lower than the speeds at intercept. Hence, the intercept provide useful guides for gear change strategy. For Set 2, the relation between the power and vehicle speeds is shown in Figure 5. The gear change intercept are 48 km/h, 82 km/h, 120 km/h and 160 km/h and attained maximum speed of approximately 180 km/h. These values are slightly different from that of Set 1. For Set 3, the relation is shown in Figure

6, and the intercepts occurs at 46 km/h, 66 km/h, 96 and 140 km/h and maximum speed also at 180 km/h. These values are given in Table 3 for ease of comparison. There are two conclusions that can be drawn from the above results. Firstly, a good driver can achieve the timing 0 to 100 km/h closer to the fourth gear. This shows that for Set 3 the car is faster by using a bigger final gear ratio but utilize more fuel because of higher engine rotation being used compared to Set 1 or Set 2. Secondly, one can conclude that the fifth gear is finally utilized before the maximum speed is achieved in zero gradient terrain.

Figure 7 shows the relationship between the speed attained and time taken. This is important as it shows how fast the car sprint from 0 to 100 km/h. As expected, from the shifting points for three different final gear ratios, it is clear that the bigger the final gear ratio the faster the car sprints to the 100 km/h mark. It can be seen from the curve that Set 2 is better from starting from the beginning of acceleration. Thus to achieve performance and hence fuel savings and emission control with natural gas, Set 2 is recommended to be used.

Vehicle performance for all Sets 1, 2 and 3 at different performance evaluation is shown in Figure 8. For 0 to 1000 m, Set 1 achieved 33 sec to complete while Set 2 achieved 32.9 sec and Set 3 achieved 33.2 sec. Set 2 has the fastest completion time because of bigger final drive ratio and suitable gear combination compared to Set 1 and Set 3. This is due to more torque to be delivered to the driveline as a result of faster acceleration time. The setback for the bigger final drive ratio is higher engine revolution that will give an impact on fuel consumption. Performance and fuel consumption have to be balanced depending on where (which country) to market the car, topography, demography and fuel price. Set 2 also has the best 0 to 400 meter completion time and 0 to 100 km/h sprint time.

5. Conclusion

From the results obtained, it can be concluded that Set 2 gear ratio combination for 1^{st}, 2^{nd}, 3^{rd}, 4^{th}, 5^{th}, and Final Drive of 3.583, 1.947, 1.343, 0.976, 0.804 and 4.334 respectively was found to be suitable for best performance output of PROTON Waja CNG-DI vehicle in terms of gear shifting point, acceleration and drivability. Although the overall performance difference is small, Set 2 has shown a driver friendly set of gear combination.

References

Bartlett, H., Whalley, R., (1998). "Power Transmission Systems Modeling", Proc IMechE, Part D, Journal of Automobile Engineering, Vol. 212, No. 6, pp 497-505.

Das, A., Watson, H. C., (1997). "Development Of Natural Gas Spark Ignition Engine For Optimum Performance", Proc IMechE, Part D, Journal of Automobile Engineering, Vol. 211, No. 5, pp 361-378.

Dukhwan Sung, Sungho Hwang, Hyunsoo Kim, (2005). "Design Of Hydromechanical Transmission Using Network Analysis", Proc IMechE, Part D, Journal of Automobile Engineering, Vol. 219, No. 1, pp 53-63.

Jo, H.S., Jang, W.J., Lim, W.S., Lee, J.M., Park, Y.I., (2000). "Development Of A General Purpose Program Based On The Concept of Subsystem Assembly For The Analysis of Dynamic Characteristics Of Power Transmission System", Proc IMechE, Part D, Journal of Automobile Engineering, Vol. 214, No. 5, pp 545-560.

Jungmin Seo, Seung Jong Yi, (2005). "Design Of Automatic Transmission System Having Arbritary Power Flow Using The Automatic Power Flow Generation Algorithm", Proc IMechE, Part D, Journal of Automobile Engineering, Vol. 219, No. 9, pp 1085-1097.

Keiji Nemoto, Toshiharu Kumagai, Tasushi Ohnuma, (2002). "Development Of A New Manual Transmission", JSAE Review 23, pp 513-518

Kenichi Satoh, Masanori Shinitani, Setsukazu Akai, Kazuyoshi Hiraiwa , (2003). "Development Of A New Synchronizer With The Lever Mechanism", JSAE Review 24, pp 93-97

Kim, J., Park, S., Seok, C., Song, H., Sung, D., Lim, C., Kim, J., Kim, H., (2005). "Simulation Of Shift Force For A Manual Transmission", Proc IMechE, Part D, Journal of Automobile Engineering, Vol. 217, No. 7, pp 573-581.

Litvin, F.L., Fuentes, A., Demenego, A., Vecchiato, D., Fan, Q., (2001). "New Developments In The Design And Generation Of Gear Drives", Proc IMechE, Part D, Journal of Automobile Engineering, Vol. 215, No. 7, pp 747-757.

Middleton, A., Neumann, B., (2005). "CNG Engine Technology For Fleets – Performance, Emissions And Cost Effectiveness", Paper 9, Proceedings, ANGVA 2005, 1^{st} Conference & Exhibition, Kuala Lumpur.

Mucino, V.H. Lu, Z., Smith, E., Kimcikiewicz, M., Cowan, B., (2001). "Design Of Continuously Variable Power Split Transmission Systems For Automotive Applications", Proc IMechE, Part D, Journal of Automobile Engineering, Vol. 215, No. 4, pp 469-478.

Rousseau, S. Lemoult, B. Tazerout, M., (1999). "Combustion Characterization Of Natural Gas In Lean Burn Spark Ignition Engine", Proc IMechE, Part D, Journal of Automobile Engineering, Vol. 213, No. 5, pp 481-489.

Table 1. Comparisons of emission level for different standards. (Middleton, A., Neumann, B., 2005). (Units: grams/kilowatt hour)

	CO	NMHC	CH4	NO_X	PM
EURO 3 limit	5.45	0.78	1.6	5.0	0.16
EURO 4.1 limit	4.0	0.55	1.1	3.5	0.03
NGV test results G20 gas	0.131	0.011	0.156	3.09	0.006
NGV test results G25 gas	0.134	0.020	0.459	2.88	0.007

Table 2. Simulation transmission options

	Gear ratios					
Combination	First	Second	Third	Fourth	Fifth	Final Drive
Set 1	3.583	1.947	1.343	0.976	0.804	4.052
Set 2	3.583	1.947	1.343	0.976	0.804	4.334
Set 3	3.545	2.447	1.688	1.165	0.804	4.410

Table 3. Intercept speeds for gear change.

Combination	Speeds in km/h				
	First to second	Second to third	Third to fourth	Fourth to fifth	Maximum speed
Set 1	51	92	130	170	190
Set 2	48	82	120	160	180
Set 3	46	66	96	140	180

Table Caption

Table 1. Comparison of emission level against standard (Middleton, A., Neumann, B., 2005). (Units: grams/kilowatt hour)

Table 2. Simulation transmission option

Table 3. Intercept speeds for gear change

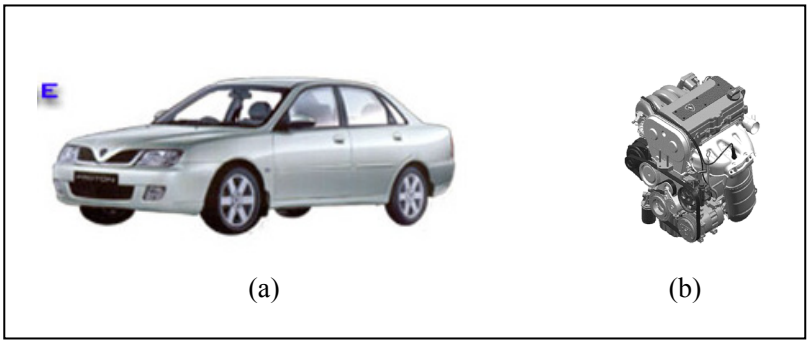

Figure 1. (a) PROTON Waja and (b) CamPro CNG-DI engine

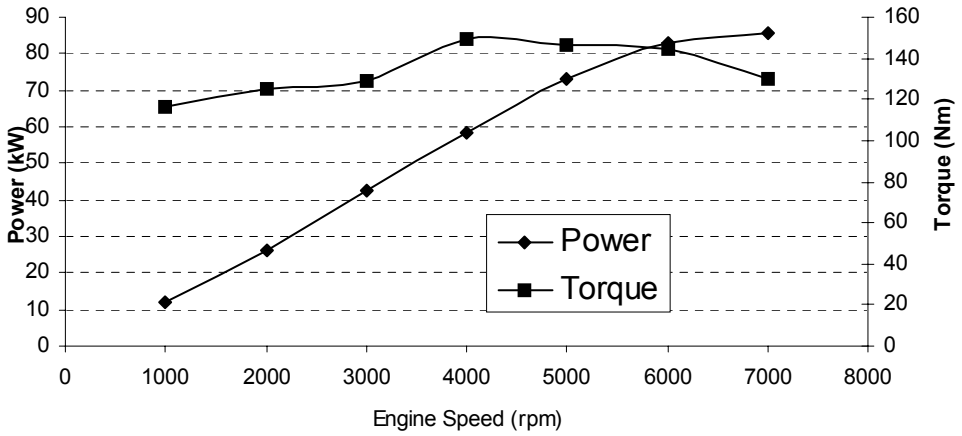

Figure 2. CNGDI Engine performance

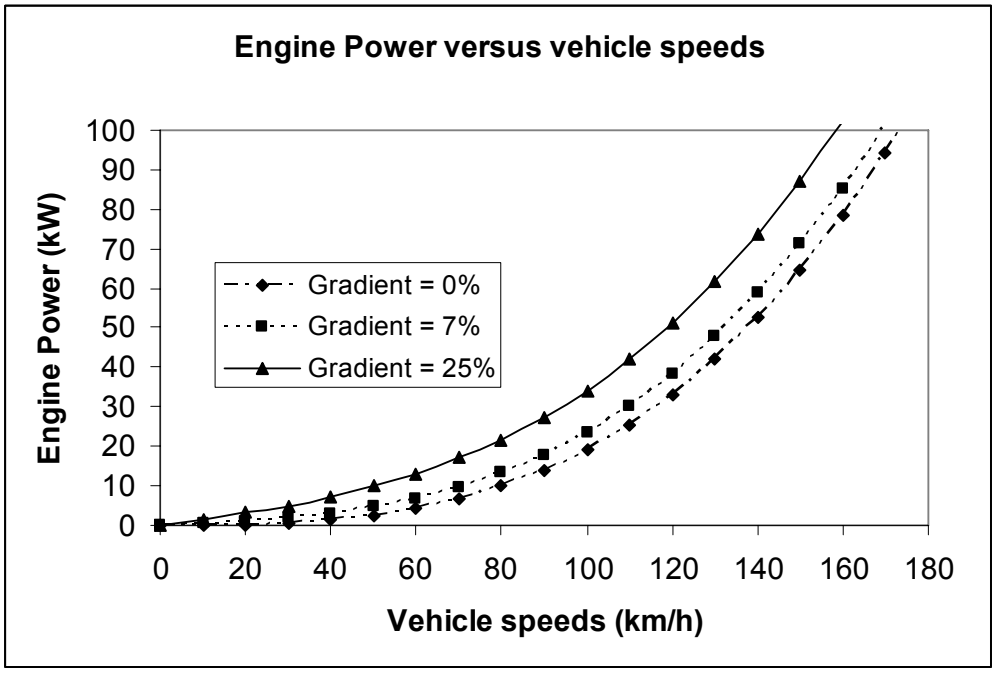

Figure 3. Power versus vehicle speed at different road gradient

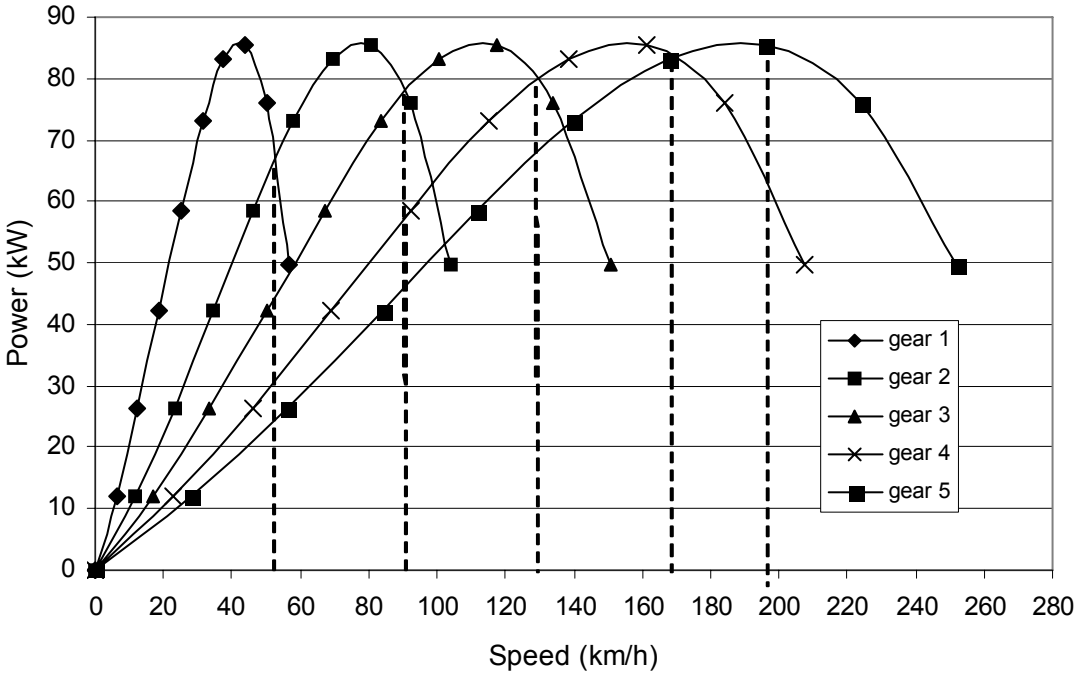

Figure 4. Power versus speed for Set 1

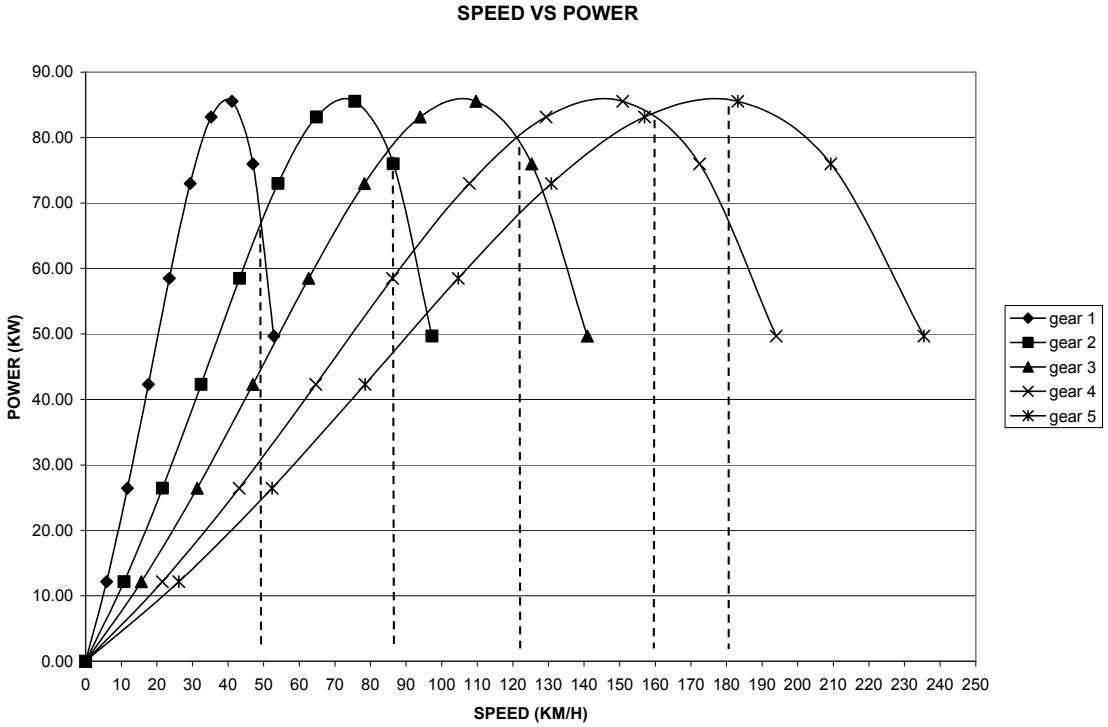

Figure 5. Power versus vehicle speed for Set 2

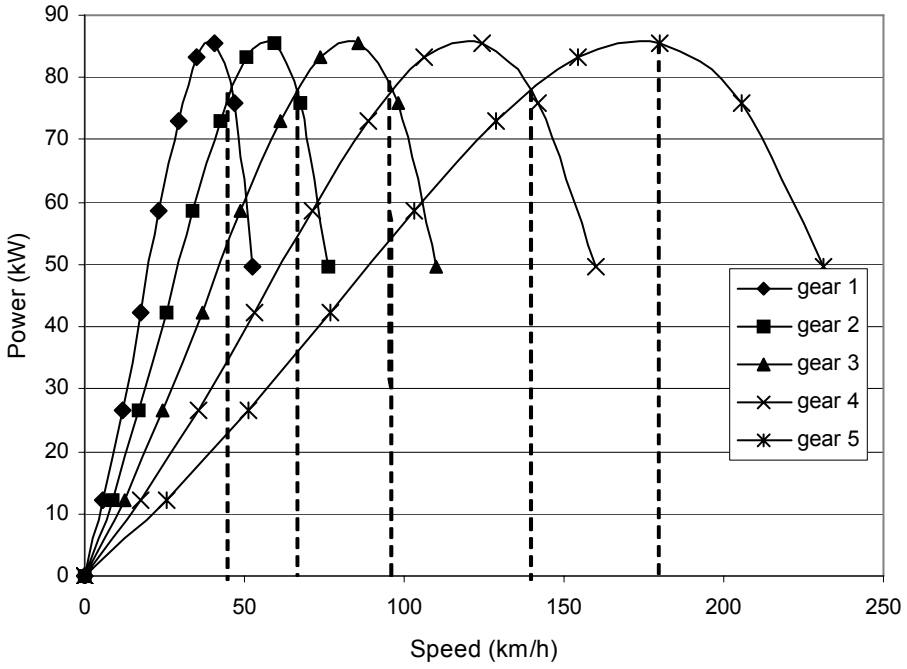

Figure 6. Power versus vehicle speed for Set 3

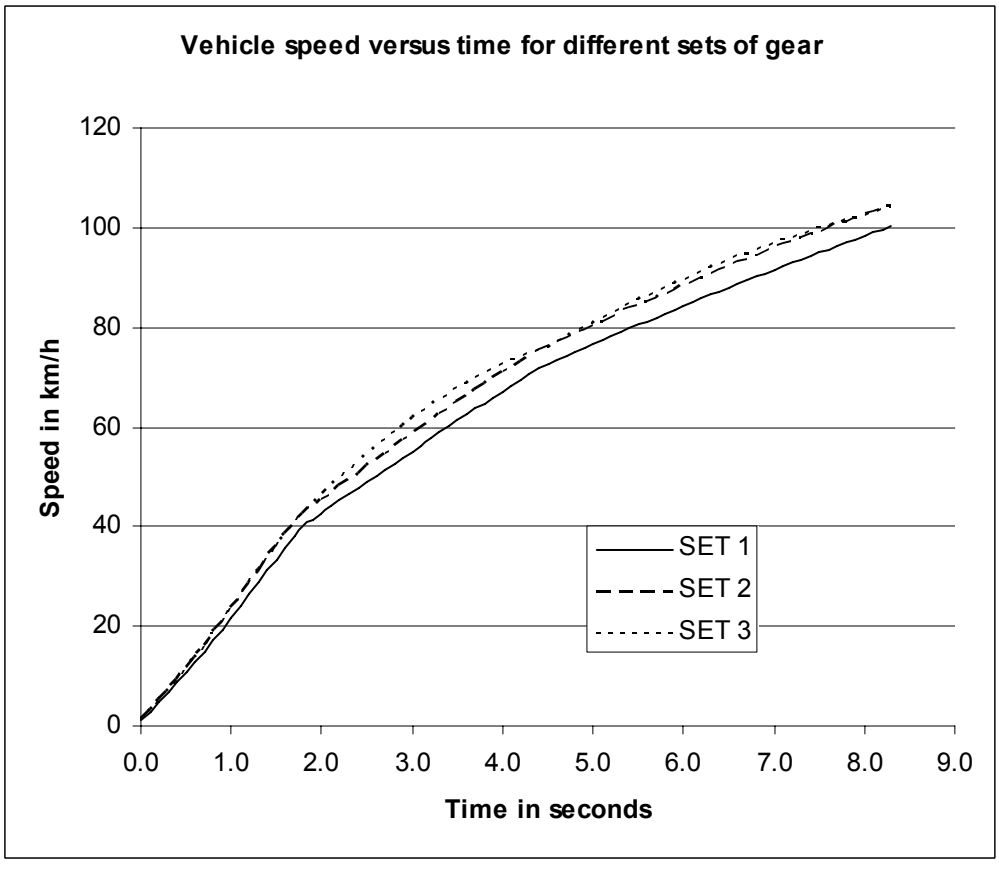

Figure 7. Speed versus time for gear set 1, 2 and 3

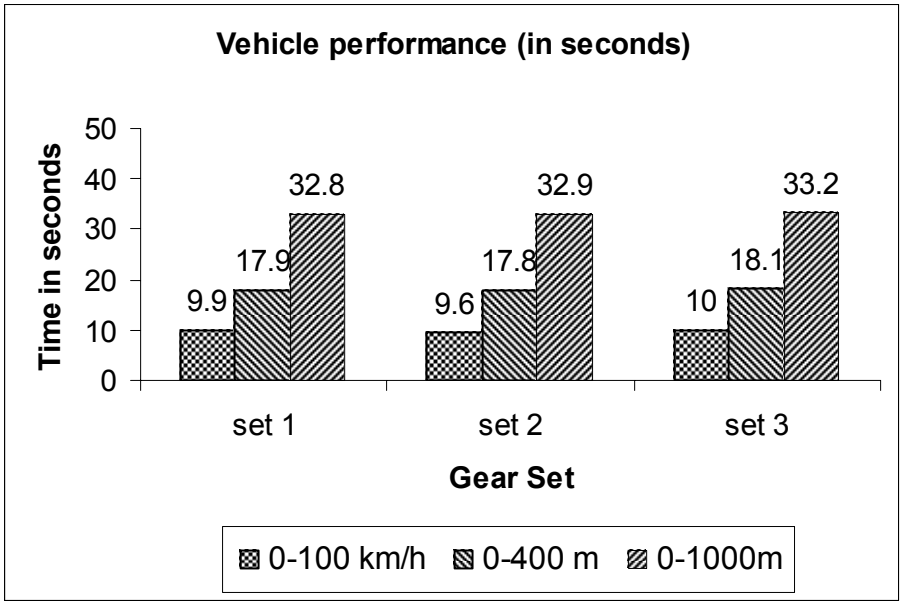

Figure 8. Vehicle performance (in sec) for different sets of gears

Figure Caption

Figure 1. (a) PROTON Waja and (b) CamPro CNG-DI engine

Figure 2. CNGDI Engine performance

Figure 3. Power versus vehicle speed at different road gradient

Figure 4. Power versus speed for Set 1

Figure 5. Power versus vehicle speed for Set 2

Figure 6. Power versus vehicle speed for Set 3

Modern Applied Science

www.ccsenet.org/journal.html

Vol. 3, No. 8

August 2009

The Precise Forming of Automobile Start Gear Shaft

Lingxian Meng, Zhongming Liu, Yuanguo Zhang, Zhihong Zhang & Heping Zhang

Zhengzhou Research Institute of Mechanical Engineering

No.81, Songshan South Rd., Zhengzhou 450052, China

Tel: 86-371-6771-0790 E-mail: mlx4857@163.com

Abstract

The start gear shaft is the key part of automobile starter, it is involute small module internal gear with addendum modification. It is step shaft with H/D>6 in the outline. Because of the concentric degree demand of the internal gear and the outline step shaft is higher, length of below shaft is large and diameter is small, So plastic forming of the shaft is very difficult. Meeting the needs of markets and improving comprehensive function of automobiles, the high efficient precision forming technology method of single-step chipless-forming for internal gear tooth surface and external step shaft is put forward based on analysis, study and repeated test. In the same time, a set of high accuracy die with simple novel structure and long service life is designed and manufactured. The advantages of the method have been verified that utilization ratio of material and production efficiency is high. For this reason, the method is profitable reference for producing the same type of complex shape gear shaft.

Keywords: Chipless-forming, Start gear shaft, Precise forming

1. Introduction

With speedy development of car industry in China, traditional processing technology cannot meet market needs of car start gear shaft. The start gear shaft is the key part of automobile starter, it is studied in the paper. Because it is involute small module internal gear with addendum modification, it is step shaft with H/D>6 in the outline, the coaxiality of the internal gear and the outline step shaft is higher, length of below shaft is large and diameter is small, So plastic forming of the shaft is very difficult. Meeting the needs of batch process and markets, improving comprehensive function of automobiles, the high efficiency precision forming technology method of single-step chipless-forming for internal gear tooth surface and external step shaft is put forward based on analysis, study and repeated test. The method can adapt at present efficiently, low consumption, superior quality of product demand. The economic benefit of the method is also notable.

2. Technology analyses

The key part of automobile starter-the start gear shaft is studied in the paper. Fig 1 shows the diagram of a light car starter gear shaft. It is involute small module internal gear at one end, it is step shaft with H/D>6 in the outline, and the coaxiality of the internal gear and the step shaft is higher. The originally manufacturing process of the shaft is: blanking—machining—shaped tooth, the process is not only low efficient, but also the size accuracy and coaxiality are low, in the same time ,utilization ratio of material for the process is low, it can't satisfy the demand of rapidly developing of car industry. Improving the production efficiency and the utilization ratio of material, and obtaining chipless-foming of internal gear and less or no cutting of outline step shaft, based on analysis, we think that precise plastic forming can replace originally manufacturing process. Because end diameter is large, step shaft is thin and long, plastic deformation goes beyond the plastic deformation limit, so it is difficult to fill material into internal gear tooth. Therefore according to the structure characteristics of the part, we use the process: cutting material--annealing--lubricating--making blank--extrusion forming--produce.

3. The design and machining of the die

3.1 The calculation of extrusion force

The extrusion force is the foundation which designs a die, it also is an important basis for choosing material of die and equipment of extrusion. According to ABAS, the extrusion force (p) of the start gear shaft is about 5000 kN, this is approximate as a result with the empirical formula $p=c*p*f$.

3.2 The design and machining of the die

Because the accuracy of the cold extrusion parts is greatly depended on the accuracy of the extrusion die, when the die is designed, it is considered according to the cold extrusion technology project, the request of concentric precision of the parts and machining process etc. So the die design is brief, easy to machining process. For this, we define the parameter of cold extrusion, and design a set of the cave and convex molding tool that is simple in structure, and opposite side fixed position and split combined cave die so as to form the starter gear once. The diagram 2 shows the extrusion molding tool of the starter gear shaft. According to the structure characteristics of the extrusion parts, we adopt a bring shape object to push out the extrusion parts directly; For the convenience of the changing molding tool and machining accuracy , the cave mold is designed to be divided and sectional body, so as to become easy that the gear's mold is machined and skived etc.

We overcome many disadvantageous factors in the manufacturing process of the molding tool, Such as, the accuracy of EDM, the asymmetry error of the inside chamber of molding tool after combining etc. We adopt many valid measures to give reasonable compensation; When we programme the line cut, we should design with special care to calculate compensated magnitudes. The line is wanted not only to design carefully when line incised a plait a distance, and but is wanted to control the discharge clearance and speed of the idler pulley and to decrease the roughness of the part surface possibly so as to obtain even and consistent size of the molding tool, insure the tolerance in the permission scope for the runout of base tangent.

3.3 The heatment process of molding tool

To satisfy the high accuracy of extrusion piece in large batch quantity, the material of molding tool for precise forming should be chosen correctly, it must be resistant wear, small deformation and long life. After variable factors are considered, a new molding tool material LD(7Cr7M02V2Si) steel is chosen, the scope of quench temperature of LD is wide: 1100 ℃--1180 ℃, the scope of temper temperature is also wide: 510 ℃-- 620 ℃. But we want to obtain the advantages of the high strength, high tenacity of LD steel, the reasonable heatment process has to be chosen. The hardness of the LD steel, grain size , remaining austenite and machining function depend on the temperature of quench and temper. The technology test and experience summary are as following, for the molding tool material LD steel of the start gear shaft extrusion , heatment process is quench 1100 ℃--1150 ℃, temper 550 ℃.thus, the comprehensive function of the LD steel is better, the molding tool life is longer.

4. The technology test and batch production

4.1 The blank softening

For lowering transform resistance of the blank, raising plastic deformation of the metal, the blank should be softened to improve the internal organization before cold extrusion. If annealing technology to soften is not appropriate, it will make the blank anticipate of the degree of hardness is high and low and different, and it will lead to increase pressure or the molding tool wear, the service life of the equipments and molding tool and the surface smooth of the piece are directly effected. The softening technology of the starter gear shaft blank is temperature to 840℃--880℃, remaining 6h--10h, cooling to 350℃, out furnace. Random sampling, the hardness is between 130 HRB--150 HRB , it feat in cold extrusion to transform.

4.2 The blank making

According to size, shape and the constant principle of the metals physical volume of product parts, cutting material of blank is determined. After reducing diameter and upsetting, the blank is shown in fig.3.

4.3 The blank lubricating

The lubrication processing of cold extrusion blank surface is an important process,surface quality of cold extrusion piece and molding tool life are greatly influenced by lubricating. For cold extrusion of black metals, for long time, traditional processing method of bonderizing and saponification is used, but defect of the method is following: it takes up the large work place, the cost is high, the environment is polluted, and the control of quality is difficulty. Therefore, we have adopted a kind of hydro-high polymer lubricant to lubricate. This lubricant uses convenience in brief: Put directly the blank after cleaning oxidize skin into the lubricant to immerse , then nature dry or oven dry, make the lubricant adhere to anticipate surface of blank , become a layer of black gray lubrication film. When extrusion forming, friction resistance can be greatly reduced, and surface of the pieces is smooth and bright, the request of application is satisfied.

4.4 The technology experiment and batch quantity production

During the experiment, the molding tool should be carefully fixed to promise size accuracy of piece. Based on experiment, it has been verified that molding tool design is reasonable, technology project is right, the internal gear tooth of the piece is filled with good, there is not any crack in internal surface, machining of internal surface and gear tooth is not needed. Through the customer detection and application, the customer think that the quality of the start gear

shaft is good, the accuracy is high, the function is superior and the request is satisfied completely.

5. Economic benefits

The start gear shaft is manufactured by using the precision forming technology, its material structure is dense, fibre structure is not damaged, the wear-resistant ability, size accuracy and concentric degree is high. So the service life of the start gear shaft is long. In the same time, it can short manufacturing cycle, save material, lower cost, So its economic benefit and social benefit is good.

6. Conclusions

Precision forming technology is the key technology which raises product function and quality, not only it can short a product manufacturing cycle, lower cost, reduce weight, but also it can raise the end size accuracy of part and the coarseness degree of the surface. The safety, the credibility and life of part are raised. The comprehensive function and quality of product also are raised, and the utilization ratio of material is raised. So the advantage of the precision forming method for the type of complex gear parts has been verified that utilization ratio of material, production efficiency are high ,the accuracy is high and the service life is long. Technology method of single-step chipless-forming of internal gear surface and external step shaft is an ideal method. So the method is profitable guide and promote for producing the same type of complex shape gear shaft.

References

Hong, Shenze. (1985). *Cold Extrusion technology and molding tool design* [M] Hefei: Anhui science and technique publisher. 1985.

Meng, Lingxian, Song**,** Xuejin and Zhang, Xiechang. (1998). "Cold extrusion technology of the motorcycle surmounts gear "[C]. *The third national youth academic meeting*. 1998.11. Beijing. China machine press. P524--P527.

Yang, Changshun. (1984). *Cold Extrusion technology fulfillment* [M]. Beijing: China machine press. 1984.

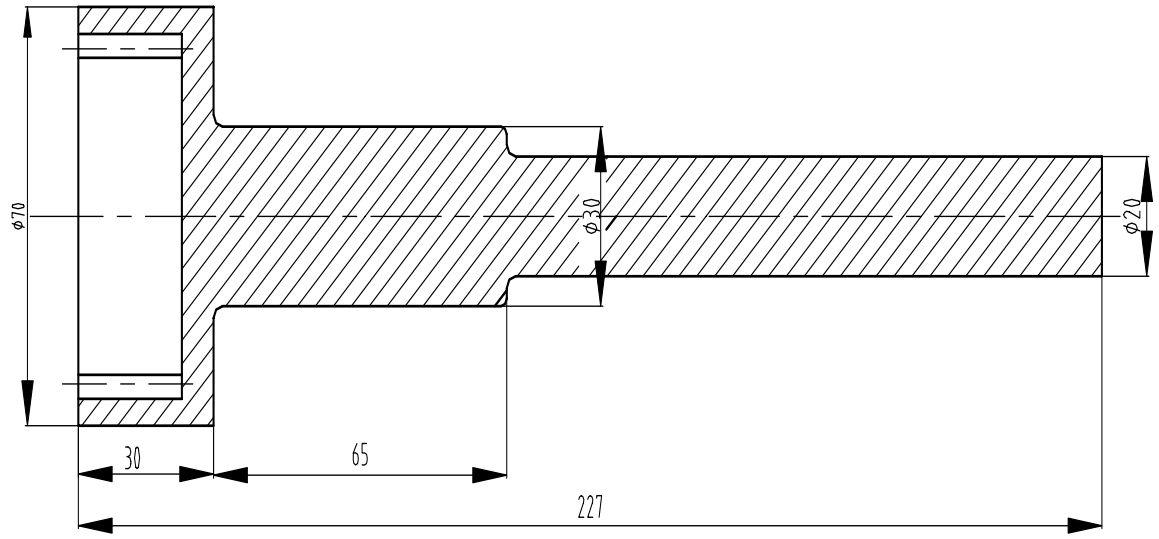

Figure 1. The diagram of the start gear shaft of a light car

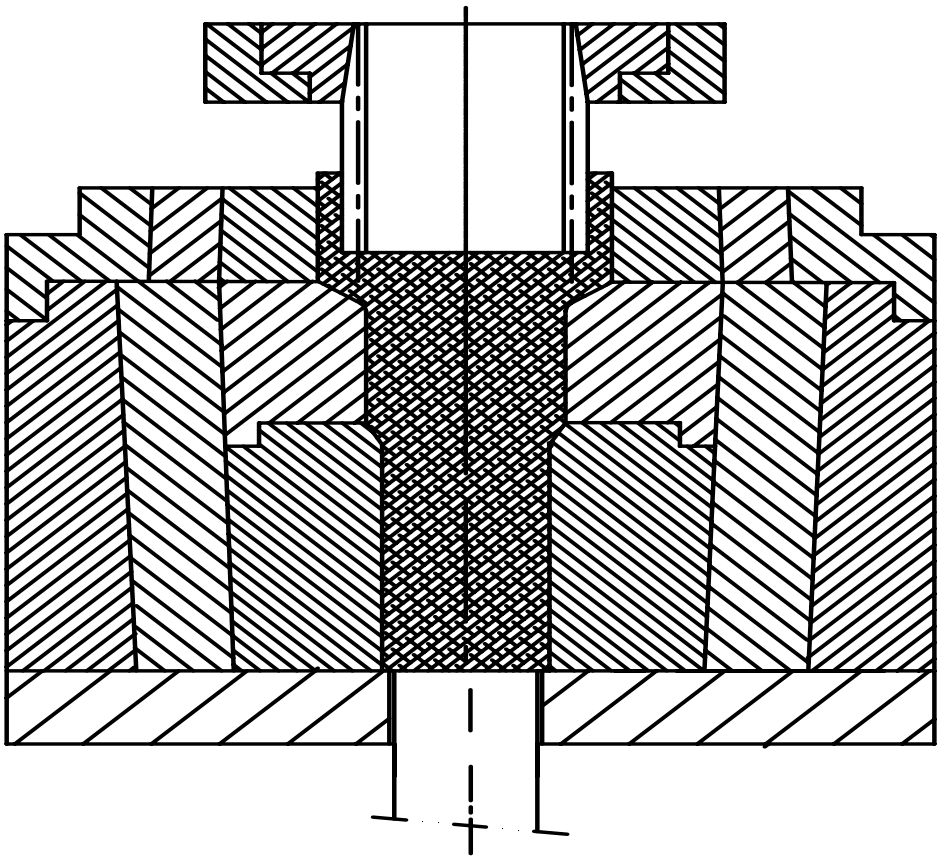

Figure 2. The diagram of chipless-forming die for the start gear shaft

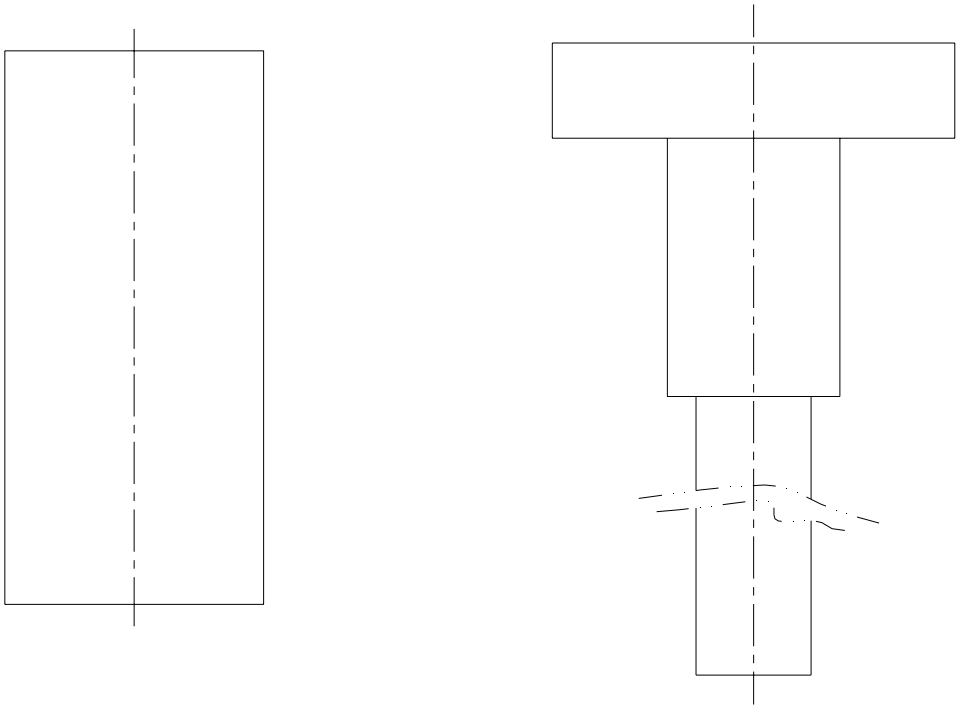

Figure 3. The diagram of the shape for the semi-finished product

Modern Applied Science

www.ccsenet.org/journal.html

Vol. 3, No. 8

August 2009

Optimal Portfolio Selection Models with Uncertain Returns

Limei Yan

Department of Mathematics, Dezhou University

Dezhou 253023, China

E-mail: yanlimei9898@163.com

Abstract

This paper provides two new models for portfolio selection in which the securities are assumed to be uncertain variables that are neither random nor fuzzy. Since there is no efficient method to solve the proposed models, the original problems are transformed into their crisp equivalents programming when the returns are chosen some special uncertain variables such as rectangular uncertain variable, triangular uncertain variable, trapezoidal uncertain variable and normal uncertain variable. Finally, its feasibility and effectiveness of the method is illustrated by numerical example.

Keywords: Uncertain variable, Portfolio selection, Mean-variance, Crisp equivalent programming

1. Introduction

Portfolio selection is concerned with an individual who is trying to allocate one's wealth among alternative securities such that the investment goal can be achieved. The problem was initialized by Markowitz (1952, p.77), and the solution of his mean-variance methodology has been serving as a basis of the development of modern financial theory. The pioneer work Markowitz combined probability and optimization theory to model the investment behavior under uncertainty. Quantifying investment return as the mean of returns of the securities, and investment risk as the variance from the mean, Markowitz formulated his models mathematically in two ways: minimizing variance for a given expected value or maximizing expected value for a given variance.

Portfolio theory has been greatly improved since Markowitz. The researches mainly focused on two directions. One direction is how to define the investment risk. In 1952, Markowitz stated that variance could be regarded as risk. Since then, mathematical analysis on portfolio management has developed greatly, and variance has become the most popular mathematical definition of risk for portfolio selection. Scholars developed a variety of models using variance to quantify risk in various situations, for example, variance models proposed by Best (2000, p.195), Chopra (1998,p.53), Gram (2003, p. 546), Deng (2005, p.278) and Huang (2007, p.396). Since in case when return distributions securities are asymmetric, the selected portfolio based on variance may have a potential danger to sacrifice too much expected return in eliminating both high return extremes and low return extremes, semi-variance was proposed as an alternative definition of risk by Markowitz (1952, p.77) and lots of models were built to minimize semi-variance in different cases, for example, Chow (1994, p.231), Grootveld (1999, p.304), Homaifar (1990, p.677), Markowitz (1993, p.307) and Rom (1994, p.431). Another alternative definition of risk is the probability of an adverse outcome Roy (1952, p.431). There are also many research works that minimize the probability of an adverse outcome such as Mao (1970, p.657) and Williams (1997, p.77). However, in reality, some people may only be sensitive to one preset disastrous loss level and regard the chance of occurring this bad case as risk, risk curse was proposed as the fourth definition of risk such as Huang (2008, p.351) and Huang (2008, p.1102). Another direction is how to choose return rate. Portfolio selection was initially handled in stochastic environments. After then, the problem was dealt with in fuzzy, random fuzzy and birandom environment. There are a variety of models in this line. Let us mention some of the representatives in recent years. For example, we have fuzzy chance-constrained model by Huang (2006, p. 500), fuzzy mean semi-variance model by Huang (2008, p.1) and random fuzzy mean-variance model by Grootveld (1999, p.304).

These studies solved the problem in different stochastic, fuzzy or random and fuzzy simultaneously environments with different risk. In practice, the real life decisions are usually made in the state of uncertainty, when the uncertainty of the return rate behaves neither randomness nor fuzziness, we need a new tool to deal with it. In such situations, the use of uncertain theory to represent unknown parameters provides an interesting help. In other words, we may employ the uncertain theory which was initialized by Liu (2009) to deal with this new type of uncertainty.

The paper is organized as follows. After recalling some definitions and results about uncertain measure and uncertain variable in section 2, the mean-variance models for portfolio selection is introduced in section 3. Then section 4 discusses its crisp equivalents when the return rates are chosen as some special uncertain variables such as rectangular uncertain

variable, triangular uncertain variable, trapezoidal uncertain variable and normal uncertain variable. In section 5, we provide a numerical example to illustrate the potential application and the effectiveness of the new models. Finally, we conclude the paper in section 6.

2. Preliminaries

Let Γ be a nonempty set, and let A be a σ-algebra over Γ. Each element $\Lambda \in \mathrm{A}$ is called an event. In order to provide an axiomatic definition of uncertain measure, it is necessary to assign to each event Λ a number $M\{\Lambda\}$ which indicates the level that Λ will occur. In order to ensure that the number $M\{\Lambda\}$ has certain mathematical properties, Liu (2009) proposed the following five axioms:

Axiom 1 (Normality) $M(\Gamma) = 1$;

Axiom 2 (Monotonicity) $M(\Lambda_1) \le M(\Lambda_2)$ whenever $\Lambda_1 \subseteq \Lambda_2$;

Axiom 3 (Self-duality) $M(\Lambda) + M(\Lambda^{\mathrm{c}}) = 1$ for every event Λ;

Axiom 4 (Countable subadditivity) For every countable sequence of events $\{\Lambda_i\}$, we have

$$M(\bigcup_{i=1}^{\infty} \Lambda_i) \le \sum_{i=1}^{\infty} M(\Lambda_i).$$

The following is the definition of uncertain measure.

Definition 1 (Liu (2009)). The set function is called an uncertain measure if it satisfies the normality, monotonicity, self-duality and countable subadditivity axioms.

Example 1 Let $\Gamma = \{\gamma_1, \gamma_2\}$. For this case, there are only 4events. Define

$$M\{\gamma_1\} = 0.4, \quad M\{\gamma_2\} = 0.6, \quad M(\phi) = 0, \quad M(\Gamma) = 1,$$

then M is an uncertain measure because it satisfies the four axioms.

Definition 2 (Liu (2009)). Let Γ be a nonempty set, A a σ-algebra over Γ, and M an uncertain measure. Then the triplet (Γ, A, M) is called an uncertain space.

The product uncertain measure is defined as follows.

Axiom 5 (Liu (2009)). Product Measure Axiom) Let Γ_k be nonempty sets on which M_k are uncertain measures, $k = 1, 2, \cdots, n$, respectively. Then the product uncertain measure on Γ is

$$M\{\Lambda\} = \begin{cases} \sup\limits_{\Lambda_1 \times \Lambda_2 \times \cdots \times \Lambda_n \subset \Lambda} \min\limits_{1 \le k \le n} M_k\{\Lambda_k\}, & \text{if } \sup\limits_{\Lambda_1 \times \Lambda_2 \times \cdots \times \Lambda_n \subset \Lambda} \min\limits_{1 \le k \le n} M_k\{\Lambda_k\} > 0.5, \\ 1 - \sup\limits_{\Lambda_1 \times \Lambda_2 \times \cdots \times \Lambda_n \subset \Lambda^c} \min\limits_{1 \le k \le n} M_k\{\Lambda_k\}, & \text{if } \sup\limits_{\Lambda_1 \times \Lambda_2 \times \cdots \times \Lambda_n \subset \Lambda^c} \min\limits_{1 \le k \le n} M_k\{\Lambda_k\} > 0.5. \end{cases}$$

For each event $\Lambda \in \mathrm{A}$, denoted by $M = M_1 \wedge M_2 \wedge \cdots \wedge M_n$.

Definition 3 (Liu (2009)). An uncertain variable is a measurable function ξ from an uncertainty space $(\Gamma, \mathrm{A}, \mathrm{M})$ to the set of real numbers, i.e., for any Borel set B of real numbers , the set

$$\{\xi \in \mathrm{B}\} = \{\gamma \in \Gamma \mid \xi(\gamma) \in \mathrm{B}\}$$

is an event.

A random variable can be characterized by a probability density function and a fuzzy variable may be described by a membership function, uncertain variable can be characterized by identification function.

Definition 4 (Liu (2009)). An uncertain variable ξ is said to have a first identification function λ if

(1) $\lambda(x)$ is a nonnegative function on R such that

$$\sup_{x \ne y} \lambda(x) + \lambda(y) = 1;$$

(2) For any set B of real numbers, we have

$$M\{\xi \in \mathrm{B}\} = \begin{cases} \sup\limits_{x \in \mathrm{B}} \lambda(x), & \text{if } \sup\limits_{x \in \mathrm{B}} \lambda(x) < 0.5, \\ 1 - \sup\limits_{x \in \mathrm{B}^C} \lambda(x), & \text{if } \sup\limits_{x \in \mathrm{B}^C} \lambda(x) \ge 0.5. \end{cases}$$

Definition 5 (Liu (2009)). The uncertainty distribution $\Phi: R \to [0,1]$ of an uncertain variable ξ is defined by

$\Phi(x) = M\{\xi \le x\}$.

Definition 6 (Liu (2009)). Let ξ be an uncertain variable. Then the expected value of ξ is defined by

$$E[\xi] = \int_0^{+\infty} M\{\xi \ge x\}\, dr - \int_{-\infty}^{0} M\{\xi \le x\} dr,$$

provided that at least one of the two integrals is finite.

Definition 7 (Liu (2009)). Let ξ be an uncertain variable with finite expected value e, then the variance of ξ is defined by $V[\xi] = E[(\xi - e)^2]$.

The detailed exposition on the uncertain theory have been recorded in the literature, the interested readers may consult it.

3. Mean-variance Model

In Markowitz models, security returns were regarded as random variables. As discussed in introduction, there does exist situations that security returns may be uncertain variable parameters. In this situation, we can use uncertain variables to describe the security returns.

Let x_i denote the investment proportion in the ith security, ξ_i represents uncertain return of the ith security, $i = 1, 2, \cdots, n$, respectively, and a the maximum risk level that the investor can tolerate. Following Markowitz's idea, we quantify investment return by the expected value of a portfolio, and risk by the variance. Then an optimal portfolio should be the one with maximal expected return for the given variance level. To express it in mathematical formula, the mean-variance model is as follows:

$$\begin{aligned} &\max\ E[x_1\xi_1 + x_2\xi_2 + \cdots + x_n\xi_n] \\ &\text{Subject to:} \\ &V[x_1\xi_1 + x_2\xi_2 + \cdots + x_n\xi_n] \le a, \\ &x_1 + x_2 + \cdots + x_n = 1, \\ &x_i \ge 0,\ i = 1, 2, \cdots, n. \end{aligned} \tag{1}$$

where E denotes the expected value operator , and V the variance operator of the uncertain total return rate, a the maximum risk level the investor can tolerate.

When the investors preset an expected return level that they feel satisfactory, and want to minimize the risk for this given level of return, the optimization model becomes

$$\begin{aligned} &\min\ V[x_1\xi_1 + x_2\xi_2 + \cdots + x_n\xi_n] \\ &\text{Subject to:} \\ &E[x_1\xi_1 + x_2\xi_2 + \cdots + x_n\xi_n] \ge b, \\ &x_1 + x_2 + \cdots + x_n = 1, \\ &x_i \ge 0,\ i = 1, 2, \cdots, n. \end{aligned} \tag{2}$$

where b denotes the minimum expected investment return that the investors can accept.

4. Deterministic Equivalents

The traditional solution methods require conversion of the objective function and the constraints to their respective deterministic equivalents. As we know, this process is usually hard to perform and only successful for some special cases. Let us consider the following forms of the uncertain return rates.

Case 1. Suppose that the return rate ξ_i of the ith security is rectangular uncertain variable $\xi_i = (a_i, b_i), i = 1, 2, \cdots, n$, then

$\sum_{i=1}^n x_i\xi_i$ is rectangular uncertain variable $(\sum_{i=1}^n x_i a_i, \sum_{i=1}^n x_i b_i)$. According to the properties of rectangular uncertain variable, we have

$$E[\sum_{i=1}^n x_i\xi_i] = (\sum_{i=1}^n x_i a_i + \sum_{i=1}^n x_i b_i)/2 = \sum_{i=1}^n x_i(a_i + b_i)/2,$$

$$V[\sum_{i=1}^n x_i\xi_i] = (\sum_{i=1}^n x_i b_i - \sum_{i=1}^n x_i a_i)^2/8 = [\sum_{i=1}^n x_i(b_i - a_i)]^2/8.$$

Since the term $[\sum_{i=1}^n x_i(b_i - a_i)]^2$ is nonnegative, $V[\sum_{i=1}^n x_i\xi_i] \le a$ is equivalent to $\sum_{i=1}^n x_i(b_i - a_i) \le 2\sqrt{2a}$. In this case, models (1) and (2) can be converted into its deterministic equivalents as follows.

$$\begin{aligned}&\max \ \textstyle\sum_{i=1}^{n} x_i(a_i+b_i)\\ &\text{Subject to:}\\ &\textstyle\sum_{i=1}^{n} x_i(b_i-a_i)\le 2\sqrt{2a},\\ &x_1+x_2+\cdots+x_n=1,\\ &x_i\ge 0,\ i=1,2,\cdots,n.\end{aligned}\tag{3}$$

and

$$\begin{aligned}&\min \ \textstyle\sum_{i=1}^{n} x_i(b_i-a_i)\\ &\text{Subject to:}\\ &\textstyle\sum_{i=1}^{n} x_i(b_i+a_i)\ge 2b,\\ &x_1+x_2+\cdots+x_n=1,\\ &x_i\ge 0,\ i=1,2,\cdots,n.\end{aligned}\tag{4}$$

Case 2. If the return rates are all trapezoidal uncertain variables, Let ξ_i be (a_i,b_i,c_i,d_i), where $a_i<b_i\le c_i<d_i, i=1,2,\cdots,n$. Then $\sum_{i=1}^{n} x_i\xi_i$ is $(\sum_{i=1}^{n} x_ia_i,\sum_{i=1}^{n} x_ib_i,\sum_{i=1}^{n} x_ic_i,\sum_{i=1}^{n} x_id_i)$. In accordance with the properties of trapezoidal uncertain variable, we have

$$E[\textstyle\sum_{i=1}^{n} x_i\xi_i]=(\sum_{i=1}^{n} x_ia_i+\sum_{i=1}^{n} x_ib_i+\sum_{i=1}^{n} x_ic_i+\sum_{i=1}^{n} x_id_i)/4=\sum_{i=1}^{n} x_i(a_i+b_i+c_i+d_i)/4,$$

$$V[\textstyle\sum_{i=1}^{n} x_i\xi_i]=\dfrac{4\alpha^2+3\alpha\beta+\beta^2+9\alpha\gamma+3\beta\gamma+6\gamma^2}{48}+\dfrac{[(\alpha-\beta-2\gamma)^+]^3}{384\alpha}$$

where

$$\alpha=(\textstyle\sum_{i=1}^{n} x_ib_i-\sum_{i=1}^{n} x_ia_i)\vee(\sum_{i=1}^{n} x_id_i-\sum_{i=1}^{n} x_ic_i),\ \beta=(\sum_{i=1}^{n} x_ib_i-\sum_{i=1}^{n} x_ia_i)\wedge(\sum_{i=1}^{n} x_id_i-\sum_{i=1}^{n} x_ic_i),$$

and $\gamma=\sum_{i=1}^{n} x_ic_i-\sum_{i=1}^{n} x_ib_i$, so the model (1) and (2) can be changed into the following formulas:

$$\begin{aligned}&\max \ \textstyle\sum_{i=1}^{n} x_i(a_i+b_i+c_i+d_i)\\ &\text{Subject to:}\\ &V[x_1\xi_1+x_2\xi_2+\cdots+x_n\xi_n]\le a,\\ &x_1+x_2+\cdots+x_n=1,\\ &x_i\ge 0,\ i=1,2,\cdots,n.\end{aligned}\tag{5}$$

and

$$\begin{aligned}&\min \ V[x_1\xi_1+x_2\xi_2+\cdots+x_n\xi_n]\\ &\text{Subject to:}\\ &\textstyle\sum_{i=1}^{n} x_i(a_i+b_i+c_i+d_i)\ge 4b,\\ &x_1+x_2+\cdots+x_n=1,\\ &x_i\ge 0,\ i=1,2,\cdots,n.\end{aligned}\tag{6}$$

In models (5) and (6), the variance $V[x_1\xi_1+x_2\xi_2+\cdots+x_n\xi_n]$ is formulated as

$$V[\textstyle\sum_{i=1}^{n} x_i\xi_i]=\dfrac{4\alpha^2+3\alpha\beta+\beta^2+9\alpha\gamma+3\beta\gamma+6\gamma^2}{48}+\dfrac{[(\alpha-\beta-2\gamma)^+]^3}{384\alpha}.$$

Case 3. An uncertain variable ξ is called normal if it has a normal uncertainty distribution

$$\Phi(x)=(1+\exp(\frac{\pi(e-x)}{\sqrt{3}\sigma}))^{-1},\ x\in R,$$

denoted by $N(e,\sigma)$ where e and σ are real number with $\sigma>0$. Suppose that the return rate of ith security is normally distributed with parameters e_i and $\sigma_i>0, i=1,2,\cdots,n$. Then we have

$$E[\textstyle\sum_{i=1}^{n} x_i\xi_i]=\sum_{i=1}^{n} x_ie_i,\quad V[\sum_{i=1}^{n} x_i\xi_i]=(\sum_{i=1}^{n} x_i\sigma_i)^2.$$

So the model (1) and (2) can be converted into the following linear equivalents:

$$\begin{aligned}&\max \ \textstyle\sum_{i=1}^{n} x_i e_i\\ &\text{Subject to:}\\ &\textstyle\sum_{i=1}^{n} x_i \sigma_i \le \sqrt{a},\\ &x_1 + x_2 + \cdots + x_n = 1, x_i \ge 0,\ i = 1, 2, \cdots, n.\end{aligned} \tag{7}$$

and

$$\begin{aligned}&\min \ \textstyle\sum_{i=1}^{n} x_i \sigma_i\\ &\text{Subject to:}\\ &\textstyle\sum_{i=1}^{n} x_i e_i \ge b,\\ &x_1 + x_2 + \cdots + x_n = 1,\\ &x_i \ge 0,\ i = 1, 2, \cdots, n.\end{aligned} \tag{8}$$

Thus we can solve the models (3)-(8) by traditional method.

5. Numerical Example

Example 2 Assume that there are 5 securities. Among them, returns of five are all normal uncertain variables $\xi_i = N(e_i, \sigma_i), i = 1, 2, 3, 4, 5$. Let the return rates be

$$\xi_1 = N(0, 1),\ \xi_2 = N(1, 2),\ \xi_3 = N(2, 3), \xi_4 = N(3, 4), \xi_5 = N(4, 5),$$

Then

$$\textstyle\sum_{i=1}^{5} x_i \xi_i = N(x_2 + 2x_3 + 3x_4 + 4x_5, x_1 + 2x_2 + 3x_3 + 4x_4 + 5x_5)$$

Thus, we have

$$\begin{aligned}&E[x_1\xi_1 + x_2\xi_2 + x_3\xi_3 + x_4\xi_5] = x_2 + 2x_3 + 3x_4 + 4x_5,\\ &V[x_1\xi_1 + x_2\xi_2 + x_3\xi_3 + x_4\xi_5] = x_1 + 2x_2 + 3x_3 + 4x_4 + 5x_5.\end{aligned}$$

Suppose that the risk is not allowed to exceed 1.5, and the minimum excepted return the investor can accept is 2, then the models (7) and (8) are as follows:

$$\begin{aligned}&\max \ x_2 + 2x_3 + 3x_4 + 4x_5\\ &\text{Subject to:}\\ &x_1 + 2x_2 + 3x_3 + 4x_4 + 5x_5 \le 1.5,\\ &x_1 + x_2 + \cdots + x_5 = 1, x_i \ge 0,\ i = 1, 2, \cdots, 5\end{aligned} \tag{9}$$

and

$$\begin{aligned}&\min \ x_1 + 2x_2 + 3x_3 + 4x_4 + 5x_5\\ &\text{Subject to:}\\ &x_2 + 2x_3 + 3x_4 + 4x_5 \ge 2,\\ &x_1 + x_2 + \cdots + x_5 = 1, x_i \ge 0,\ i = 1, 2, \cdots, 5.\end{aligned} \tag{10}$$

By use of Matlab 7.0 on PC we obtain the optimal solutions of model (9) and (10). The optimal solution of model (9) is

$$(0.6962, 0.1478, 0.1186, 0.0344, 0.0029),$$

and the value of objective function is 0.5000. This means that in order to gain maximum expected return with the risk not greater than 1.5, the investor should assign his money according to the optimal. The corresponding maximum expected return is 0.5.

The optimal solution of model (10) is

$$(0.3316, 0.0002, 0.2035, 0.2663, 0.1985),$$

and the value of objective function is 3.0000. This means that in order to minimize the risk with the expected value not less than 2, the investor should assign his money according to the optimal. The corresponding minimum risk is 3.

6. Conclusions

In this paper, uncertain variable is applied to portfolio selection problems, and two types of uncertain programming models for portfolio selection with uncertain returns are provided. In order to solve the proposed models by traditional methods we discuss the crisp equivalents when the uncertain returns are chosen to be some special uncertain variables

and give one example to explain the efficiency of the method. The paper does not include the conditions when the return rates are general uncertain variables, this can be interesting areas for future researches.

References

A.D. Roy. (1952). Safety first and the holding of assets. *Econometrics,* 20, 431-449.

B. Liu. (2009). Uncertainty theory. [Online] Available: http://orsc.edu.cn/liu.

B.M. Rom, K. W. Ferguson. (1994). Post-modern portfolio theory comes of age. *Journal of investing*, 3, 11-17.

G. Homaifar, D.B. Graddy. (1990). Variance and lower partial moment betas as alternative risk measures in cost of capital estimations: a defense of the CAPM beta. *Journal of business finance and accounting*, 17, 677-688.

H. Grootveld, W. Hallerbach. (1999). Variance vs downside risk: Is there really that much different? *European Journal of operational research*, 114, 304-319.

H. Markowitz. (1952). Portfolio selection, *Journal of finance*, 7, 77-91.

H. Markowitz. (1993). Computation of mean-semivariance efficient sets by the critical line algorithm. *Annals of operational research*, 45, 307-317.

J. C. T. Mao. (1970). Models for capital budgeting: E-V vs. E-S. *Journal of financial and quantitative analysis,* 5, 657-675.

J.O. Williams. (1997). Maximizing the probability of achieving investment goals. *Journal of portfolio management*, 46, 77-81.

K. Chow, K. C. Denning. (1994). On variance and lower partial moment betas: the equivalence of systematic risk measures. *Journal of business finance and accounting*, 21, 231-241.

M. J. Best, J. hlouskova. (2000). The efficient frontier for bounded assets. *Mathematical methods of operations research*, 52, 195-212.

V. K. Chopra, W. T. Ziembia. (1998). The effect of errors in means, variances and covariances on optimal portfolio choices. Worldwide asset and liability modeling, Cambridge university press, Cambridge , 53-61.

X. T. Deng, Z. F. Li, S. Y. Wang. (2005). A minimax portfolio selection strategy with equilibrium. *European Journal of operational research* , 166, 278-292.

Xiaoxia Huang. (2006). Fuzzy chance-constrained portfolio selection. *Applied mathematics and computation,* 177, 500-507.

Xiaoxia Huang. (2008). Mean-semivariance models for fuzzy portfolio selection. *Journal of computational and applied mathematics,* 217, 1-8.

Xiaoxia Huang. (2008). Portfolio selection with a new definition of risk. *European Journal of operational research,* 186, 351-357.

Xiaoxia Huang. (2008). Risk curve and fuzzy portfolio selection. *Computers and mathematics with applications*, 55, 1102-1112.

Xiaoxia. Huang. (2007). Two new models for portfolio selection with stochastic returns taking fuzzy information. *European Journal of operational research* , 180, 396-405.

Y. Gram, M. Schyns. (2003). Simulated annealing for complex portfolio selection problems. *European Journal of operational research* , 150, 546-571.

Modern Applied Science

www.ccsenet.org/journal.html

Vol. 3, No. 8

August 2009

Virtual Power Extraction Method of Designing Starting Control Law of Turbofan Engine

Yuchun Chen(Corresponding author), Yiming Zhang, Fu Hu, Siyuan Xu & Qiuye Tu

School of Power and Energy, Northwestern Polytechnical University

No. 127, Youyi Xilu, Xi'an 710072 Shaanxi, China

Tel: 86-29-8849-2043 E-mail: chych888@nwpu.edu.cn

The research is financed by Northwestern Polytechnical University (Key supporting project for bachelor's paper)

Abstract

Virtual power extraction method (VPEM) of designing starting control law of turbofan engine was presented, and the computer program was developed. The VPEM of designing starting control law is based on the principle of VPEM of designing acceleration control law of turbofan engine, and combined with the method of extrapolation of component maps. The starting control law of some turbofan engine at single flight state and in whole starting envelope was designed by using the program, some computing results were analyzed. Computing results showed that VPEM is accurate and effective for designing starting control law of turbofan engine.

Keywords: Turbofan engine, Virtual power extraction method (VPEM), Starting, Starting control law

1. Introduction

The starting character affects directly the use of a turbofan engine, and one effective way to improve the starting character is to design the starting control law properly. There are lots of researches on starting character simulation technology (R. K. Agrawal, 1982, pp.194-201. Y. De-You, 1983, ISABE 83-7045. TU Qiu-ye, 1999, pp.21-24. WANG Zhan-xue, 2004, pp.444-448. WU Hu, 2007, pp.2068-2072), while there were few studies on design or optimization methods of the starting control law. According to starting character of common low speed component characters, R. K. Agrawal (1982, pp.194-201) built the common computing model to evaluate the starting character with the given fuel supply law in starting process. The common computing model of starting character was generalized (Y. De-You, 1983, ISABE 83-7045. TU Qiu-ye, 1999, pp.21-24. CHEN Yu-chun, 2002, pp.568-570. XIE Guang-hua, 2003, pp.232-235), and applied to the engines with different structure in different starting conditions. Wayne R Sexton (2001, pp.4-75) established the low speed component characters simulation method which is suitable for the starting character computing of turbo engines, and researched about the starting character of turbofan engines with variable geometry. The starting character computing did not relied on the common model any more, while adopted an improved model, which is based on the component character alike the engine performance computing. The precision of starting character computing was improved to large extent with this new technology. WANG Zhan-xue (2004, pp.444-448) and WU Hu (2007, pp.2068-2072) mainly focused on the starting character and the stability of the engine in the starting process on basis of the low speed component characters prediction method of Wayne R Sexton (2001, pp.4-75). In the studies mentioned, only XIE Guang-hua (2003, pp.232-235), with the test data and the given control law, has researched on the starting control law with the engineering experience and artificial iteration. So actually up to now, the research about the design and optimization method of starting control law is nearly blank, for the lacking of theory foundation and design methods.

A new method, Virtual Power Extraction Method(VPEM) of designing the acceleration and deceleration control law of turbo engine, was presented by Chen Yu-chun(2008, pp.327-332). CHEN (2009, pp.2242-2248) developed the improved VPEMs and researched about the acceleration of some turbofan engine. With the low speed component character, there is no essential difference between starting and acceleration or deceleration process, so the VPEM(CHEN Yu-chun, 2008, pp.327-332) and the improved VPEMs(CHEN Yu-chun, 2009, pp.2242-2248) can also be applied to design the starting control law. The VPEM model of designing starting control law of turbofan engine was

presented in this paper combined with the improved VPEMs and low speed component character prediction model.

2. Model of the VPEM

CHEN(2008, pp.327-332) presented the VPEM of designing acceleration control law of turbojet engine and introduced the implementation of VPEM in detail: Based on the turbojet character computing program in existence (variable specific heat computing program based on component character), a virtual extra power extraction was introduced (the value of the power can be set optionally), and the control law of the engine was that the rotor speed was constant. When the power is larger than zero, since the power of the turbine is larger than that of the compressor, the fuel supply must be higher than the normal condition (without the power extraction), resulting in the operating point moving closer to the surge margin. On condition that the surge margin limit of the compressor, the total temperature limit of the turbine inlet and the rich oil flameout limit were not exceeded, the fuel supply, which met the power extraction as much as possible, was the fuel supply in acceleration process, in other words, the virtual power extracted was the acceleration power. To obtain the control law of accelerating, several speeds between the idle state and the maximum state were selected and computed.

To solve the inconvenience problem in using the pure VPEM presented above, three improved methods of VPEM were presented (CHEN Yu-chun, 2009, pp.2242-2248): Constant surge margin method, constant turbine inlet total temperature method and constant combustor excess air coefficient method. With the fixed value of the compressor surge margin, turbine inlet total temperature or the combustor excess air coefficient, the improved VPEMs could get directly the fuel supply of certain speed to design the control law of accelerating. The feature of the improved VPEMs are that, in the engine character computing, only the mass flow balance is needed, while the power balance between turbine and compressor need not be met (the power that the turbine power output minus the compressor power needed is the extra power extracted, namely the acceleration power). However, the improved methods are still the power extraction method in essence. The improved VPEMs can be applied to design the acceleration control law of turbojet, turbofan engines.

2.1 Concept of VPEM

VPEM, which does not depend on the transient calculating program, executes acceleration and deceleration control law design on basis of steady-state performance calculating program. It could turn the transient problem into steady-state problem to great extent. For single-spool turbojet engine, when the corrected shaft speed of the engine maintains at a certain constant, if a virtual power HPEXT (Addition to the normal power extraction) is extracted from the engine shaft, the steady-state operating point will move from the original point to a different position. Figure 1 shows that with the HPEXT increasing, steady-state operating points will move to higher points near the surge line, which is just similar to the trend in the acceleration process. When the HPEXT (which may be a negative value) decreases, steady-state operating points will move to lower points near the choke line, which is similar to the trend in the deceleration process. Based on the steady-state calculating program, the virtual power extraction HPEXT is introduced, and the acceleration and deceleration control law is designed by changing HPEXT. So this method is called virtual power extraction method (VPEM).

VPEM can ensure that the turbine steady-state operating point and the actual acceleration and deceleration process are approximately consistent, and the HPEXT is very close to the acceleration and deceleration power in actual process, so it is helpful to estimate the acceleration and deceleration time. If VPEM is applied to single-spool turbojet engine, the HPEXT is extracted directly from the engine shaft. To two-spool turbofan engine, HPEXT can also be extracted directly from the high-pressure rotor. And if it is necessary to ensure the operating points of fan, virtual power could also be extracted from low-pressure rotor at the same time.

As shown in Figure 1, HPEXT = 0 corresponds to the normal operating point A. Being HPEXT > 0, the turbine power is larger than the compressor power, and the fuel flow of the combustor exceeds that of normal state, which corresponds to the acceleration operating point B. In case of HPEXT < 0, the turbine power is lower than the compressor power, and the fuel flow of combustor is less than that of normal state, which corresponds to the deceleration operating point C. Being HPEXT $\neq$ 0, at certain number of corrected speeds between idling rating and maximum rating, certain number of points B and C which form the acceleration and deceleration line could be achieved by changing the HPEXT. The fuel supply law in the acceleration and deceleration line is just the acceleration and deceleration control law when HPEXT is cancelled, and the transient problem of the acceleration and deceleration control law is turned into steady-state problem.

2.2 Mathematical mode of VPEM

In traditional steady-state performance computing model, to describe the separate-exhaust turbofan engine, the error equations are:

$$E_1 = L_{TH} - L_{CH} = E_1(X_1, X_2, ..., X_6) \quad (1)$$

$$E_2 = L_{TL} - L_{CL} = E_2(X_1, X_2, ..., X_6) \quad (2)$$

$$E_3 = TFF_{HP} - TFF_{HPc} = E_3(X_1, X_2, ..., X_6) \quad (3)$$

$$E_4 = TFF_{LP} - TFF_{LPc} = E_4(X_1, X_2, ..., X_6) \quad (4)$$

$$E_5 = WG_{72} - WG_{72c} = E_5(X_1, X_2, ..., X_6) \quad (5)$$

$$E_6 = WG_{71} - WG_{71c} = E_6(X_1, X_2, ..., X_6) \quad (6)$$

Wherein, E_1,E_2 stand for high pressure turbine(HPT)/ high pressure compressor(HPC) power balance and low pressure turbine(LPT)/fan power balance equations, E_3,E_4 for combustor/HPT mass flow balance and HPT/LPT mass flow balance equations, E_5 for duct/ duct nozzle mass flow balance, E_6 for LPT /main nozzle mass flow balance, L_{TH} and L_{TL} for the power of HPT and LPT, L_{CH} and L_{CL} for the power of HPC and fan, TFF_{HP} for turbine flow function of HPT, TFF_{HPC} for turbine flow function of HPT calculated from the combustor exit parameters, TFF_{LP} for turbine flow function of LPT, TFF_{LPC} for turbine flow function of HPT calculated from the HPT exit parameters, WG_{72} for mass flow of bypass duct, WG_{72C} for mass flow of bypass duct calculated from duct nozzle parameters, WG_{71} for mass flow of LPT, WG_{71C} for mass flow of core calculated from main nozzle parameters. X_1-X_6 are independent variables which are related with operating points of fan, HPC, HPT and LPT. They vary with the different control law. For example, when the control law of fixed geometry turbofan engine is that the high-pressure-rotor speed is constant, X_1-X_6 are separately ratio of fan pressure ratio Z_F, ratio of HPC pressure ratio Z_C, low-pressure-rotor speed n_L, turbine entry temperature T_{t4}, turbine flow function of HPT TFF_{HP}, and turbine flow function of LPT TFF_{LPP}.

Virtual power extraction HP_{EXT1} (HPC spool) and HP_{EXT2} (FAN spool) are introduced into equations (1) and (2), and then the power balance equations become:

$$E_1 = L_{TH} - L_{CH} - HP_{EXT1} \quad (7)$$

$$E_2 = L_{TL} - L_{CL} - HP_{EXT2} \quad (8)$$

Equations (3) to (6) remain the same as the original ones, and the control law is that the high-pressure-rotor speed is constant. Using the traditional performance computing method to calculate the steady state operating points, VPEM can be implemented by changing the HP_{EXT1} and HP_{EXT2}. It is proved in follow that VPEM can achieve the optimal acceleration and deceleration process:

The power balance equations of two-spool turbofan in acceleration and deceleration model are:

$$E_1 = L_{TH} - L_{CH} - I_{PH}\omega_H d\omega_H / dt \quad (9)$$

$$E_2 = L_{TL} - L_{CL} - I_{PL}\omega_L d\omega_L / dt \quad (10)$$

Wherein, I_{PH} and I_{PL} stand for the moment of inertia of high-pressure-rotor and low-pressure-rotor separately,ω_H andω_L for angular velocity of high-pressure-rotor and low-pressure-rotor.

If the component volume inertia is ignored, the other error equations of transient model will be the same as those of the steady-state performance model.

By comparing equations (7), (9), and equations (8), (10), virtual power extraction HP_{EXT1} from high-pressure-rotor is equal to the acceleration power of high-pressure-rotor $I_{PH}\omega_H$ $d\omega_H/dt$, and virtual power extraction HP_{EXT2} from low-pressure-rotor is equal to the acceleration power of low-pressure-rotor $I_{PL}\omega_L$ $d\omega_L/dt$.

In the case of designing acceleration control law (HP_{EXT1}>0), with the increase of HP_{EXT1}, the steady-state operating points (corresponding to the transient points at the same corrected high-pressure-rotor speed) are forced to move to the surge margin (T_{t4} increasing and α decreasing at the same time). Therefore, if certain number of corrected low-pressure-rotor speeds are chosen and the surge margin limit ΔSMC of compressor, turbine inlet total temperature T_{t4} limit, and the excess air coefficient flameout limit α for combustor are satisfied, once HP_{EXT1} is increased as much as possible, the fuel flow supply of combustor at these steady states will be minimum-time control law. Because the acceleration power of high-pressure-rotor and the angular acceleration rate are maximized at any high-pressure-rotor speed, the total acceleration time is minimized. It is obviously shown in the next equation (11):

$$t_{acc} = \int_0^t dt = (\frac{\pi}{30})^2 I_{PH} \int_{n_{idle}}^{n_{max}} \frac{nh}{HP_{EXT1}} dnh \quad (11)$$

Wherein, n_{idle} stands for the idle rating speed, n_{max} for the maximum rating speed.

The design process is similar in deceleration. To the control law whose objective is the minimum of the acceleration and deceleration time, the law designed by VPEM is optimal. Complex mathematical methods based on traditional model are avoided, and this is the advantage of VPEM.

The further study shows that there are some inconveniences in the application of "pure VPEM" described above in the design of acceleration and deceleration control law. I.e. As ΔSMC, T_{t4} or α is presented in advance, the maximum HP_{EXT} should be obtained by artificial or computer's iteration, which means that the calculating process is very time-consuming. Therefore, it is necessary to improve the model. The improvement of the "pure VPEM" for turbojet

and turbofan engine is listed as follows:

For equations (1) to (6), if combustor exit gas flow is corrected directly and be assumed as the corrected mass flow of high pressure turbine inlet (set $TFF_{HP}=TFF_{HPc}$, so $E_3=0$), and if high pressure turbine exit gas flow is corrected directly and be assumed as the corrected mass flow of low pressure turbine inlet (set $TFF_{LP}=TFF_{LPc}$, so $E_4=0$), equations (1) to (6) will be simplified to four-variables nonlinear equations (E_3, TFF_{HP}, E_4, and TFF_{LP} are eliminated). Furthermore, if n_L and Z_C are known (Z_C can be calculated by a given surge margin of HPC), equations (1) to (6) will be simplified to binary nonlinear equations:

$$E_5 = E_5(T_{t4}, Z_F) \tag{12}$$

$$E_6 = E_6(T_{t4}, Z_F) \tag{13}$$

If n_L and T_{t4} are known, equations (1) to (6) will also be simplified to binary nonlinear equations:

$$E_5 = E_5(Z_C, Z_F) \tag{14}$$

$$E_6 = E_6(Z_C, Z_F) \tag{15}$$

When equations (12) to (13) or (14) and (15) were solved, the mass flow balance can be satisfied, but the power balance is not satisfied. The difference of HPT power and HPC power is the virtual power extraction HP_{EXT1}, and the difference of LPT power and fan power is the virtual power extraction HP_{EXT2}. The modified performance computing model of turbofan is still VPEM essentially, but for given n_L Z_C (according to ΔSMC) or T_{t4} or α could be restricted directly, and the control law can be designed conveniently.

As for fixed geometry single-spool turbojet, the three-variables nonlinear equations can also be simplified to a single nonlinear equation, and the acceleration and deceleration control law can be designed conveniently for given Z_C (according to ΔSMC) or T_{t4} or α .

And if the low speed component characters are obtained, the starting process does not have essential difference with the process of acceleration, so the VPEM and the improved VPEMs could also be used to design the starting control law.

2.3 VPEM model of designing starting control law

With the successful applications of the VPEM and improved VPEMs to design the acceleration control law of the turbojet and turbofan engines, this paper researched about the application of VPEM to design the starting control law of turbofan engine. It is shown that even if relatively accurate low speed component character is obtained, with the traditional simulation methods of character computing (WANG Zhan-xue, 2004, pp.444-448 and WU Hu, 2007, pp.2068-2072), it is still difficult to simulate the starting process, and more difficult to design the starting control law. The reasons are as follows:

(1)To most turbo engines, the steady operating points with the lower speed than the idle state are hard to get. Since the decrease of the speed, the efficiency of each component decreased heavily, resulting in the temperature to maintain the speed would be quite high. During the iteration, the operating points would move to or even enter the surge margin, so it is very hard for the engine character computing to be balanced;

(2)Secondly, with the decrease of the speed, the condition of combustor inlet gets worse, and the combustion efficiency decreases. So it is probably that the turbine inlet temperature could not be achieved to its requiring value, no matter how the fuel increases;

(3)Below the self-operating speed (ignite speed is normally lower than self-operating speed), the traditional engine character computing method cannot achieve the balanced computing, for if the starter power is not in consideration, the power balance would not be met. However, there is not essential relationship between designing starting control law and starter character;

(4) To design the starting control law with traditional methods, there are the same problems, the functional optimization problem (CHEN Yu-chun, 2009, pp.2242-2249) based on the dynamic character computing, as designing acceleration or deceleration control law: the optimum function relationship between the fuel supply (or some parameter related to the fuel) and the speed which suits the starting process should be computed.

Based on the four reasons above, it is hard to achieve designing starting control law and optimization with the traditional methods.

If the VPEM is applied to the starting character simulation and designing control law, the problems met in the traditional methods would be solved. The reason is that the power balance is not required in the improved VPEMs, as described in section 2.2. In the engine steady character computing process which is based on VPEM, the imbalanced power is the acceleration power (if the turbine residual power is positive value) or the minimum required starter power (if the turbine residual power is minus).

In the starting process of the engine, when combustor is ignited and starter stops working, the engine will accelerate to

idle state itself. The control law after starter stop working is very important. This paper mainly studied on the design of the starting control law at this phase. The model of VPEM of designing starting control law of the turbofan engine after ignition is followed:

(1)According to the character prediction method of low speed components (Wayne R Sexton, 2001, pp.4-75), the characters of the fan, compressor, the high pressure turbine and low pressure turbine in low speed needed of the turbofan engine are predicted, and suitable character of the combustion is adopted;

(2)Using steady performance computer program, "the steady performance" below the idle state of the engine (note: "the steady performance" is useless in fact) was calculated to get the fuel supply in the steady state. If the calculation of steady performance was divergent, check out the three parameter values, namely the compressor surge margin ΔSMC, inlet temperature of turbine T_{t4} and excess air coefficient of combustion α, whether exceeded their limitation, and reset the parameter value which exceeded firstly with its limitation value (CHEN Yu-chun, 2009, pp.2242-2249), then continue to compute "the steady performance" below the idle state. The steady fuel supply below the idle state is marked as the lower boundary of the solution space in designing starting control low. The engine with the fuel supply under the lower boundary can not start to accelerate automatically.

(3)According to the improved VPEMs (CHEN Yu-chun, 2009, pp.2242-2249), set the values of ΔSMC, or T_{t4}, or α in the starting process, the engine operating points where compressor and combustion can work stably were obtained, as well as the fuel supply, which was marked as the upper boundary of solution space in designing starting control low.

(4)According to the starting envelop of engine, as well as the selected starting control law pattern, the influence of the altitude, Mach number and atmosphere to the upper boundary of the solution space were analyzed obtain the starting control law suitable for the whole starting envelop.

3. Examples and Analysis

3.1 Characters prediction of low speed components

According to the studied characters of fan, compressor, high pressure turbine and low pressure turbine of turbofan engine in the paper, adopting the extrapolated method (Wayne R Sexton, 2001, pp.4-75), the component characters below the idle state are predicted respectively. To save the space, only the predicted results of compressor (Figure 2(a), (b)) and high pressure turbine (Figure 3(a), (b)) are shown as follows.

It should be mentioned that the character prediction method of low speed turbine in WANG Zhan-xue's paper (2007, pp.444-448) were according to the methods of Wayne R Sexton, (2001, pp.4-75), as well as other published papers in domestic (omitted). However, there is a mistake in these papers: the efficiency of turbine remains the same when corrected speed of turbine is lower than the existed lowest corrected speed. The reason for this mistake is that the prediction method of the turbine torque was not completely comprehended in these papers. It showed clearly by Wayne R Sexton (2001, pp.4-75), in the process of predicting the character of turbine below the lowest corrected speed, the exponent m of the turbine torque variation with the corrected speed should be adjusted artificially to make the torque of the actual lowest corrected speed "most close" to the torque of the lowest corrected speed, which was obtained by the torque of second lowest corrected speed varying with the exponent m. To examine the torque curve obtained with the actual toque curve whether "most overlap", the technique is applicable if any better idea unavailable.

The model of combustor character in the paper is from R. K. Agrawal (1982, pp.194-201).

3.2 Designing starting control law at single flight state

The starter worked from 0 to 35% of the high pressure rotor speed. This paper only designed the starting control law when the starter cranking was finished. According to the method shown in 2.2, the steady operating line of the fuel supply fuel below idle state of the turbofan engine was obtained in the standard atmosphere, H=0km, Ma=0.0; With the improved VPEMs, the surge margin of high compressor was set as ΔSMC=1%, then the corresponding fuel supply was obtained(the upper boundary). Adopting the pattern of starting control law $W_{fb}/P_{t3}=f(n_H)$ (the relationship between ratio of fuel supply of combustion W_{fb} to total pressure of compressor outlet P_{t3} and high pressure rotor speed n_H), the solution space of starting control law of turbofan engine was obtained , shown in Figure 4.

If one certain starting control law of engine is needed at H=0km, Ma=0.0 in standard condition, a straight line or a broken line or a curve line in the solution space in Figure 4 would be the one, in consideration of the actual condition of engine(control system and combustion character). If a minimal starting time control law is needed, the line would be the upper boundary.

It should be mentioned that, when VPEM is applied in designing starting control law of the two spool turbofan engine, the low pressure rotor speed n_L is linear to the high pressure rotor speed n_H: $n_L=n_{L,idle}\times n_H/n_{H,idle}$ (the subscript "idle" is idle state). It has been proved by CHEN Yu-chun (2009, pp.2242-2249) that the different speed of low pressure rotor would affect the fuel supply W_{fb}, while have little effect on W_{fb}/P_{t3}, namely, no effect on the designing starting control law.

3.3 Designing starting control law in the starting envelope

To design one certain starting control law which guarantees the reliable start in all conditions, the computation must be implemented in the whole starting envelope and all climate conditions. With the starting envelope and climate conditions of some turbofan engine, the influence of the flight altitude H, flight Mach number Ma and temperature TH on the upper boundary of the starting control law were computed respectively, the results showed in Figure 5-7. It is shown in the figures that the upper boundary of the low speeds increased obviously with the altitude increasing, the upper boundary of the high speeds increased with the Mach number increasing, and the influence of the TH on the upper boundary was similar to that of H. For the minimum value of the upper boundary should not be exceeded (to avoid surge and stall in the starting process), so the minimum value of the upper boundary would be obtained by accumulating the data in Figure 5-7, as shown in Figure 8.

As described in section 2.3, with the lower boundary in Figure 4 and the upper boundary in Figure 8, the starting control law solution space of some turbofan in the whole starting envelope and all climate conditions was obtained, as shown in Figure 9 (the actual starting control law was also presented).

As shown in Figure 9, the actual starting control law was just in the starting control law solution space. But the computing results showed that the control law could move upper (closer to the upper boundary) in the low speed to shorten the engine starting time.

Unlike the design of acceleration or deceleration control law (CHEN Yu-chun, 2009, pp.2242-2249), the starting control law with VPEMs was designed without consideration about the influence of Mach number and atmosphere on the "steady operating points" below the idle state. The reasons are that most "steady points" do not need fuel supply when the Mach number increases. The speeds of these points are named windmill speeds, and the research on windmill speeds has exceeded the research field of this paper. It is referred from the research that although the flight conditions and climate conditions affect the "steady points" whose speeds are below idle speed, but this does not affect the feasibility of designing starting control law. The reasons are: (1) with the increase of the flight altitude, the engine inlet total temperature decreases, which leads the fuel air ratio to maintain the steady condition decreases appreciably. But the decrease extent is little enough to be neglected; (2) with the increase of the flight Mach number, the engine inlet total temperature increases and the turbine pressure ratio increases, so the fuel air ratio to maintain the steady condition decreases to great extent. If the starting control law designed in the static condition on the ground is applied to the flight condition with some Mach number, the starting speed will increase greatly. For the compressor surge margin predicted in the starting process is not precise, it is hard to evaluate whether it will cause "hot hanging", so it is unnecessary to consider the influence of Mach number on the "steady operating points"; (3) the influence of the atmosphere temperature on the "steady points" is similar to that of the flight altitude.

4. Conclusions

Based on the VPEM of designing the acceleration control law of turbo engine, combined with the predict method of the low speed engine component character, the VPEM of designing starting control law of turbofan engine was presented. With the comparison between the solution space of the some two spool separate exhaust turbofan and the actual starting control law, it was shown that the VPEM was of better precision and could be applied to design of the starting control law of turbofan engines in both single condition and the whole starting envelope in all climate conditions. To the engines with larger starting envelope or with windmill start, the application of VPEM is need to be researched further.

References

Chen, Yuchun, Liu, Zhende, Yuan, Ning and et al. (2008). A New Method of Acceleration Control Law Design for Turbine Engines. *Acta aeronautica et astronautica sinica*, 2008, 29(2):327-332 (In Chinese)

Chen, Yuchun, Lu, Yao, Wang, Jujin and et al. (2002). Research on cartridge starting characteristics of turbofan engine. *Acta aeronautica et astronautica sinica*, 2002, 23(6):568-570 (In Chinese)

Chen, Yuchun, Xu, Siyuan Liu, Zhende and et al. (2009). Power extraction method for acceleration and deceleration control law design of turbofan engine. *Journal of Aerospace Power*, 2009, 24(4):2242-2248 (In Chinese)

R. K. Agrawal. (1982). A Generalized Mathematical Model to Estimate Gas turbine Starting Characteristics, 1982,104(1):194-201.

Tu, Qiuye and Tang Diyi. (1999). Study on startup model and startup control law of turbofan engine. *Journal of Propulsion Technology*, 1999, 20(2):21-24 (In Chinese)

Wang, Zhanxue, Qiao Weiyang and Li, Wenlan. (2004). Modeling Turbofan Engine Startup Based on Component Matching Principles. *Journal of Aerospace Power*, 2004, 19(4):444-448 (In Chinese)

Wayne R Sexton. (2001). A Method to Control Turbofan Engine Starting by Varying Compressor Surge Valve Bleed. Virginia Polytechnic Institute and State University, 2001.

Wu, Hu, Feng and Wei-lin. (2007). Numerical simulation of the start-up process of augmented turbofan engines. *Journal of Aerospace Power*, 2007, 22(12):2068-2072 (In Chinese)

Xie, Guanghua, Niu, Tianhua, Wang, Yijun and et al. (2003). Starting and acceleration control law design for a missile turbojet engine. *Journal of Propulsion Technology*, 2003, 24(3):232-235 (In Chinese)

Y. De-You and M. Zhong-Fan. (1983). A Dynamic Model of Turbojet in Starting at High Altitude. ISABE 83-7045, 1983.

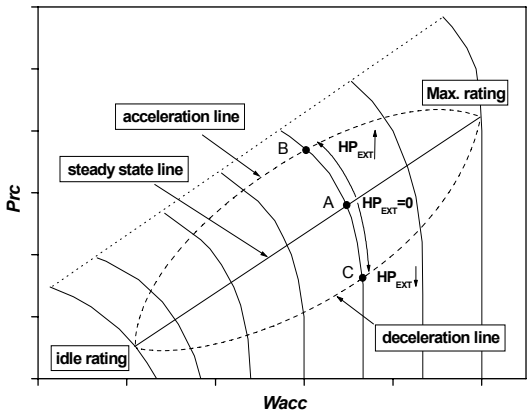

Figure 1. Influence of HPEXT on steady operating point

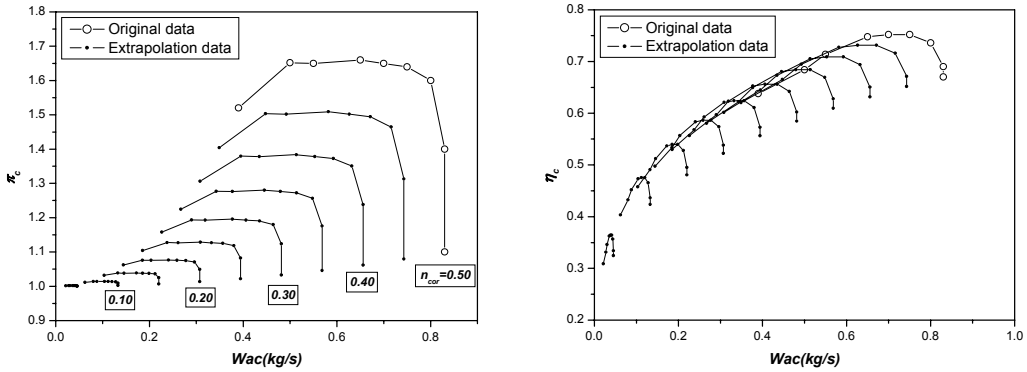

(a) (b)

Figure 2. Extrapolated data of compressor maps at low speed lines of some turbofan

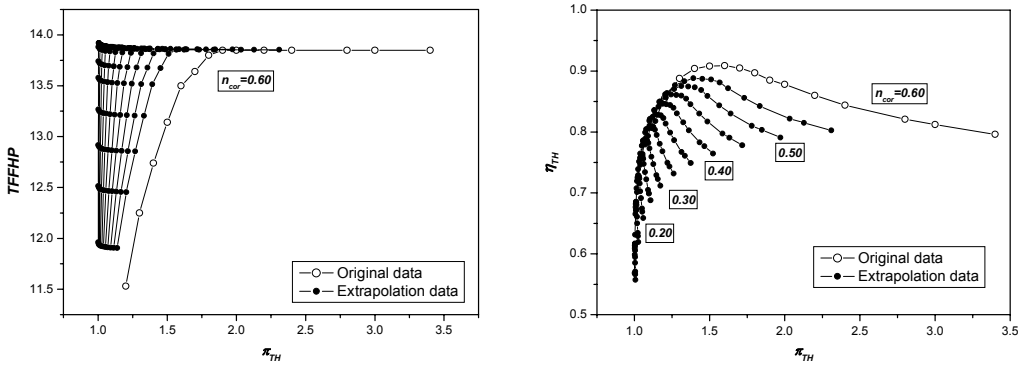

(a) (b)

Figure 3. Extrapolated data of HPT maps at low speed lines of some turbofan

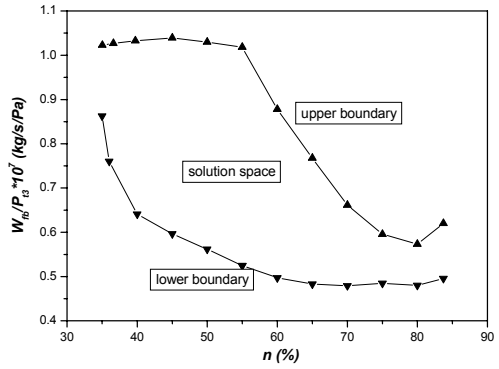

Figure 4. Solution space of designing starting control law of some turbofan

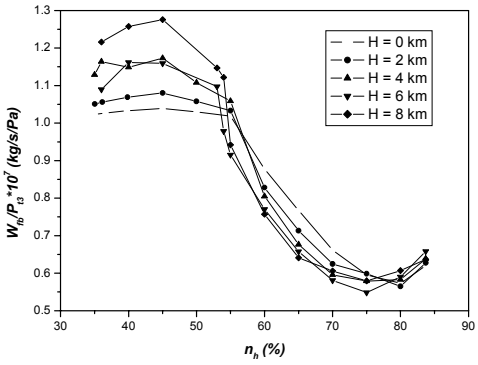

Figure 5. Influence of the flight altitude on the upper boundary

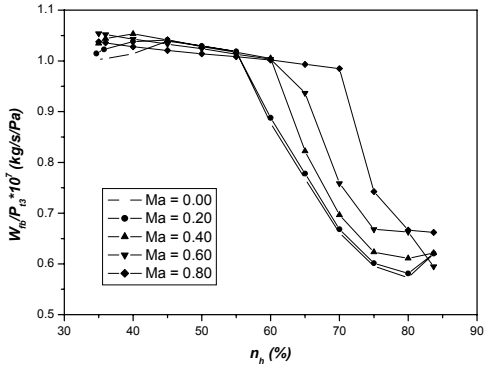

Figure 6. Influence of Mach number on the upper boundary

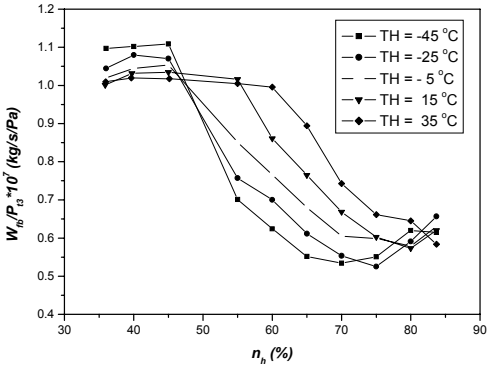

Figure 7. Influence of the temperature on the upper boundary

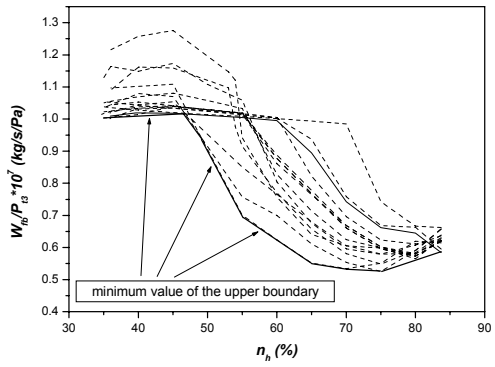

Figure 8. The starting control law upper boundary

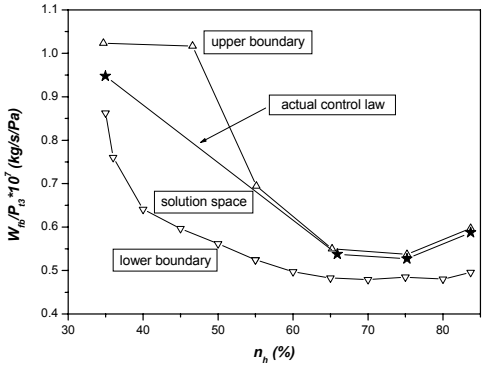

Figure 9. Solution space of designing starting control law and actual starting control law of some turbofan

Modern Applied Science

www.ccsenet.org/journal.html

Vol. 3, No. 8

August 2009

Oscillation of First-order Neutral Difference Equation

Xiaohui Gong (Corresponding author)

Department of Science, Yanshan University

438 West of He Bei Avenue, Qinhuangdao 066004, China

E-mail: gongxiaohui318@yahoo.com.cn

Xiaozhu Zhong, Jianqiang Jia, Rui Ouyang & Hongqiang Han

Department of Science, Yanshan University

438 West of He Bei Avenue, Qinhuangdao 066004, China

Abstract

The oscillation of the first order neutral difference equation

$\Delta[x(n)-px(n-\tau)]+qx(n-\sigma)=0$

is studied in this paper,where $p\in(0,1)$ and q , τ , σ are positive constants. The sufficient conditions for oscillation of the equation are obtained by suitable inequality and characteristic equation.

Keywords: Difference equation, Neutral, Oscillation

1. Introduction

Qualitative behavior of solutions of difference equations has received considerable interest recently. In [1] the oscillation of the first order nertral difference equation

$$\Delta[x(n)-px(n-\tau)]+qx(n-\sigma)=0\,, \tag{1}$$

was considered and some oscillation criteria were given, where Δ is the forward difference, i.e., $\Delta x_n=x_{n+1}-x_n$, $p\in(0,1)$,and q , τ , σ are positive constants. In this paper we assume $\tau-\sigma>1$ and $\tau-\sigma=1$ and study the oscillation for (1) in both cases and obtain further oscillatory criteria.

A solution of equation (1) is called oscillatory, if it is neither finally positive nor negative. Otherwise it is called nonoscillatory.

2. main result

Lemma 1 [2] A necessary and sufficient condition for all solutions of equation (1) to oscillate is that the characteristic equation

$$F(\lambda)=(\lambda-1)\lambda^{\sigma-\tau}(\lambda^{\tau}-p)+q=0 \tag{2}$$

has no positive real root.

Theorem 1 Assume that $0<p<1$ and $\tau-\sigma>1$, a sufficient condition for every solution of equation (1) to oscillate is that $q-\dfrac{\tau}{\tau-\sigma-1}(1-p^{\frac{1}{\tau}})>0$.

Proof: Since $F(\lambda)=(\lambda-1)\lambda^{\sigma-\tau}(\lambda^{\tau}-p)+q=0$ and $q>0$, the equation (2) possibly has roots only when $(\lambda-1)\lambda^{\sigma-\tau}(\lambda^{\tau}-p)<0$.

But $0<p<1$, when $\lambda\geq 1$ and $\lambda<p^{\frac{1}{\tau}}<1$, $(\lambda-1)\lambda^{\sigma-\tau}(\lambda^{\tau}-p)>0$ and the equation (2) has no positive

solution .Therefore the equation (2) possibly has roots only on $(p^{\frac{1}{\tau}},1)$.

Since $F(\lambda)=(\lambda-1)\lambda^{\sigma-\tau}(\lambda^{\tau}-p)+q$ continuous when $\lambda\in[p^{\frac{1}{\tau}},1]$, $F(\lambda)$ has greatest value and smallest value on interval $[p^{\frac{1}{\tau}},1]$.

Obviously, $F(1)=F(p^{\frac{1}{\tau}})=q$ is greatest value, then there is at least a point $\xi\in(p^{\frac{1}{\tau}},1)$ such that $F(\xi)$ is a smallest value.

Evidently function $F(\lambda)=(\lambda-1)\frac{1}{\lambda^{\tau-\sigma}}(\lambda^{\tau}-p)+q=0$,$(\tau-\sigma>1)$ is continuous and derivables on interval $(p^{\frac{1}{\tau}},1)$, then ξ is a minimum point also.

By Fermat's theorem we know $F'(\xi)=0$, i.e.:

$$F'(\xi)=\xi^{\sigma-\tau}(\xi^{\tau}-p)+(\sigma-\tau)(\xi-1)\xi^{\sigma-\tau-1}(\xi^{\tau}-p)+(\xi-1)\xi^{\sigma-\tau}\tau\xi^{\tau-1}=0$$

Obviously,

$$\xi^{\tau}-p=-\frac{\tau(\xi-1)\xi^{\tau}}{\xi+(\sigma-\tau)(\xi-1)}$$

$$F(\xi)=(\xi-1)\xi^{\sigma-\tau}(\xi^{\tau}-p)+q=(\xi-1)\xi^{\sigma-\tau}\left[-\frac{\tau(\xi-1)\xi^{\tau}}{\xi+(\sigma-\tau)(\xi-1)}\right]+q=q-\frac{\tau(\xi-1)^2\xi^{\sigma}}{\xi+(\sigma-\tau)(\xi-1)}.$$

Let $\xi=1-s,(0<s<1)$,

$$F(\xi)=q-\frac{\tau^2(1-s)^{\sigma}}{1-s-(\sigma-\tau)s}=q-\frac{\tau^2(1-s)^{\sigma}}{1+(\tau-\sigma-1)s}$$

From $\tau-\sigma>1$ we have $\tau-\sigma-1>0$, then

$$F(\xi)>q-\frac{\tau^2(1-s)^{\sigma}}{(\tau-\sigma-1)s}=q-\frac{\tau(1-s)^{\sigma}}{\tau-\sigma-1}=q-\frac{\tau(1-\xi)\xi^{\sigma}}{\tau-\sigma-1}>q-\frac{\tau(1-p^{\frac{1}{\tau}})}{\tau-\sigma-1}>0$$

Because ξ is a smallest point, the equation(2) has no real root on interval $(p^{\frac{1}{\tau}},1)$. Therefore all solutions of equation (1) are oscillatory.

Theorem 2 Assume that $0<p<1$, $\tau-\sigma=1$ and $\tau>\frac{1}{2}$, a sufficient condition for every solution of equation (1) to oscillate is that $\sqrt{pq(2\tau-1)}(\frac{2\tau}{2\tau-1})^{\tau}>\frac{1}{2}$.

Proof: Obviously, the equation (2) has no real root when $\lambda\geq 1$,so if $F(\lambda)=0$ has real roots, it must be on $(0,1)$.

Let $u=\frac{1}{\lambda}$, then $h(u)=\frac{\mathrm{F}(\frac{1}{u})u^{\tau}}{u-1}=pu^{\tau}-1+\frac{qu^{\tau}}{u-1}\geq 2u^{\tau}\sqrt{\frac{pq}{u-1}}-1$.

We will prove that $h(u)$ has no zero point:

Let $h_1(u)=2u^{\tau}\sqrt{\frac{pq}{u-1}}-1$, then $h_1(u)$ has minimum value $2\sqrt{pq(2\tau-1)}(\frac{2\tau}{2\tau-1})^{\tau}-1$ at $u=1+\frac{1}{2\tau-1}$.

However $2\sqrt{pq(2\tau-1)}(\frac{2\tau}{2\tau-1})^{\tau}-1>0$, so $h(u)$ has no zero point and the equation(2) has no real root on interval $(0,1)$ .Therefore all solutions of equation (1) are oscillatory.

Theorem 3 Assume that $0<p<1$ and $\tau-\sigma=1$, a sufficient condition for every solution of equation (1) to oscillate is that $q-\tau\left(p^{\frac{1}{\tau}}-1\right)^2>0$.

Proof: We know that there is at least a point $\xi \in (p^{\frac{1}{\tau}},1)$, by theorem 1,such that $F(\xi)$ is a minimum value and $F'(\xi)=0$,then $F(\lambda)==q-\dfrac{\tau(\xi-1)^2\xi^{\sigma}}{\xi+(\sigma-\tau)(\xi-1)}$

From $\tau-\sigma=1$ we have $F(\lambda)=q-\tau(\xi-1)^2\xi^{\sigma}$,

Since $\xi\in\left(p^{\frac{1}{\tau}},1\right), F(\lambda)=q-\tau(\xi-1)^2\xi^{\sigma}>q-\tau\left(p^{\frac{1}{\tau}}-1\right)^2>0$.

Because ξ is a smallest point, the equation (2) has no real root on interval ($p^{\frac{1}{\tau}}$,1). Therefore all solutions of equation (1) are oscillatory.

3. Examples

Example 1. Consider difference equation $\Delta\left(x(n)-\dfrac{1}{4}x(n-2)\right)+3x(n-\dfrac{1}{2})=0$ where $p=\dfrac{1}{4},\tau=2$,

$\sigma=\dfrac{1}{2}, q=3$. Then $\tau-\sigma=\dfrac{3}{2}>1, q-\dfrac{\tau}{\tau-\sigma-1}(1-p^{\frac{1}{\tau}})=1>0$

so the conditions in theorem 1 are satisfied and the characteristic equation is

$$F(\lambda)=(\lambda-1)\lambda^{-\frac{3}{2}}\left(\lambda^2-\frac{1}{4}\right)+3=0 \tag{3}$$

From the figure 1 we can see the equation (2) has no real root. Therefore all solutions of equation (1) are oscillatory.

Example 2. Consider difference equation $\Delta\left(x(n)-\dfrac{1}{10}x(n-2)\right)+10x(n-1)=0$ where $p=\dfrac{1}{10},\tau=2$,

$\sigma=1, q=10$. Then $\tau-\sigma=1$ and $\sqrt{pq(2\tau-1)}(\dfrac{2\tau}{2\tau-1})^{\tau}=\dfrac{16\sqrt{3}}{9}>\dfrac{1}{2}$,

so the conditions in theorem 2 are satisfied and the characteristic equation is

$$F(\lambda)=(\lambda-1)\lambda^{-1}\left(\lambda^2-\frac{1}{10}\right)+10=0 \tag{4}$$

From the figure 2 we can see the equation (2) has no real root. Therefore all solutions of equation (1) are oscillatory.

Example 3. Consider difference equation $\Delta\left(x(n)-\dfrac{1}{4}x(n-2)\right)+3x(n-1)=0$, where $p=\dfrac{1}{4},\tau=2$,

$\sigma=1$, $q=3$ .Then $\tau-\sigma=1$ and $q-\tau\left(p^{\frac{1}{\tau}}-1\right)^2=\dfrac{5}{2}>0$

so the conditions in theorem 1 are satisfied and the characteristic equation is

$$F(\lambda)=(\lambda-1)\lambda^{-1}\left(\lambda^2-\frac{1}{4}\right)+3=0 \tag{5}$$

From the figure 3 we can see the equation (2) has no real root. Therefore all solutions of equation (1) are oscillatory.

4. Conclusion

In this paper, the conditions for oscillation of difference equation [1] were studied through their characteristic equation and some new oscillatory criteria were given. But these criteria are conditions only of sufficient and not of necessary. The sufficient and necessary conditions of the equation are needed to study further.

References

He, Xinguang, Luo, Zhiguo, & Li, hua. (2003). Oscillation of neutrul difference equations with positive and nagative coefficients. *Journal of Mathematical Study.* 36[4]:388-393.

Li, Qiaoluan, Liu, Zhaoshuang, & Bai, Jingshan. (2004). Oscillation of First-order Neutral Difference Equation. *Journal of Hebei Normal University*. 28(6): 569-570.

Li, Yumei, Wang, Youbin, & Fan, Yehua. (2007). Qscillation of First-order Neutral Difference Equation. *Math in*

practice and theory. 27(31), 188-191.

PARHIN, & TRIPATHY A K. (2003). Oscillation of a class of nonlinear neutral difference equation of higher order. *J. Math.Anal Appl*. 28(4): 756-774.

SABER N E. (1995). *.An Introduction to Difference Equation*. New York: Spring-verlag.

Zhou, Yinggao, & Tang, Xianhua. (2002). Oscillation of First-order Nonlinear Delay Difference Equations. *Acta mathematical Applicatae sinica.* 15(3):132-135

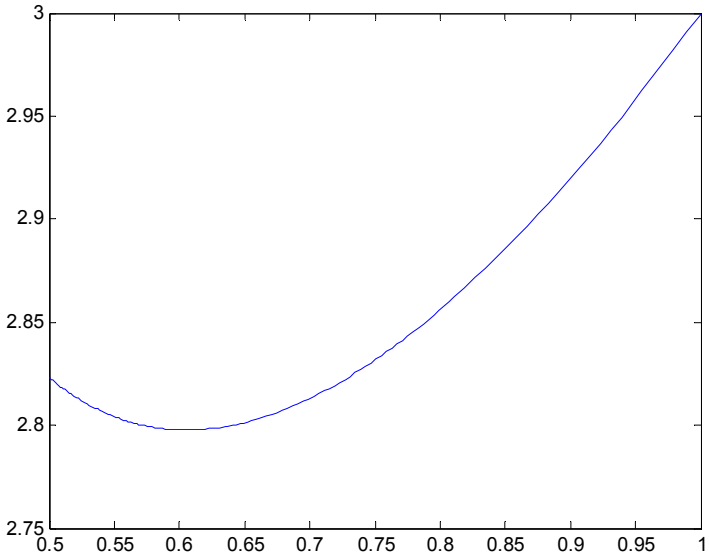

Figure 1. The figure of (3) on interval （ $(\frac{1}{4})^{\frac{1}{2}}$,1)

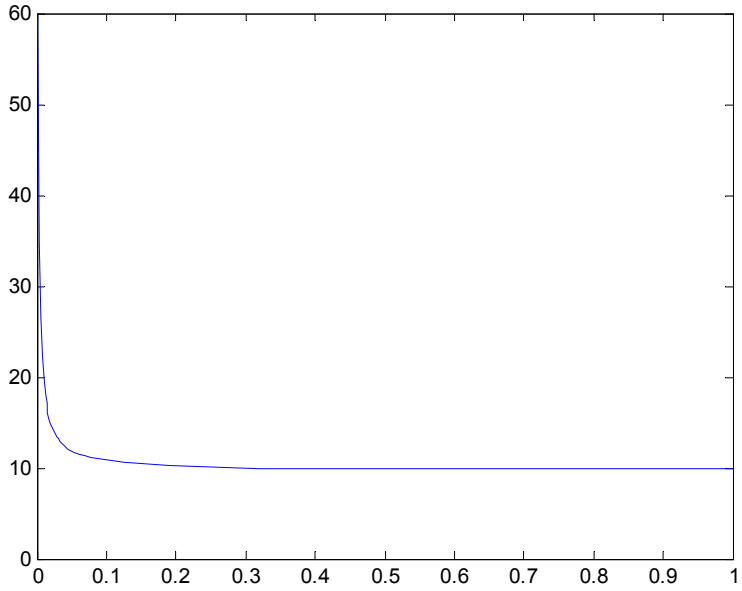

Figure 2. The figure of (4) on interval (0,1)

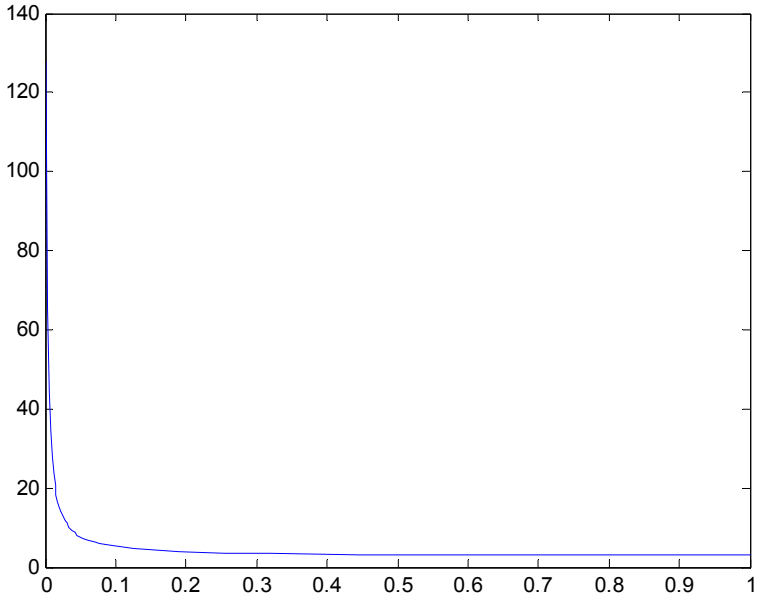

Figure 3. The figure of (5) on interval (0,1)

Modern Applied Science

www.ccsenet.org/journal.html

Vol. 3, No. 8

August 2009

Study on the Technology of the Coal Mining Safety Monitoring System

Zhi Chang, Zhangeng Sun & Junbao Gu

School of Mechanical and Electronic Engineering, Tianjin Polytechnic University

Tianjin 300160, China

E-mail: changzhi2007.cool@163.com

Abstract

New development and application of the wireless radio frequency make the application of the RFID (Radio Frequency Identification) technology become more and more extensively, and combining the characteristics of RFID technology with the mine, we established an underground safety monitoring system with integrality, real-time and flexibility, which could automatically alarm when dangers happen and enhance the search and rescue efficiency. The system could manage the harm-gas concentration, planning arrangement of workers, access control for the works passing in and out laneway, distribution of laneway personnel and workers' data, realize the informationization and visualization of the underground management, and enhance the mining production management level and the work safety level of the mine.

Keywords: RFID, Safety monitoring system, E-tag, Reader-writer

Mining accidents often happened in China in recent years, and except for mine owners' weak safety and legal consciousness, the lagged safety establishments and the imperfect managements of the mining personnel and equipments were the important causes. Through analyzing several extra serious accidents in the near period, following common problems generally existed (Qiu, 2007, P.28-29), (1) the information communication between the ground personnel and the underground was not timely, (2) ground personnel could not dynamically grasp the underground personnel's distribution and operation situation, and could not exactly position underground personnel, (3) once the mine accident happened, the efficiency of rescue was low, and the effect was worse. Therefore, it is very important and urgent to exactly and quickly carry out the coal mining safety monitoring function (Liu, 2004, P.22-25 & Guo, 2005), effectively manage the miners, and ensure the high-efficiency operation of the rescue.

The coal mining personnel and vehicle safety monitoring system proposed in the article can track, monitor and position the harmful gases, personnel and vehicles in the mine real time, and offer dynamic information about the mine laneway network, personal position, vehicle position, dangerous region and corresponding clews for ground personnel. If the accident happens, the system also can inquire about the personnel distribution, the personnel quantity, the personnel withdrawal line to offer scientific references for the accident rescue from the monitoring computer. At the same time, the mangers can utilize the daily attendance function in the system to implement attendance management for miners.

1. Introduction of the RFID technology

RFID (Zhou, 2006 & Nadeem Raza, 1999) is a sort of non-contact automatic identification technology, and it can automatically identify the objective by the radio frequency signals, quickly track the goods and exchange data. The identification work needs not human operation, and can work under various severe environments. RFID technology can identify high-speed objects and identify multiple tags simultaneously, and the operation is quick and simple. RFID technology was generated in the Second World War, and it is the successor of the traditional code technology, and its major core part is the E-tag, and the identification system could read the information stored in the E-tag through the radio waves emitted by the reader-writer from a few centimeters to a few meters, and identify the identity of the goods, people and objects represented by the E-tag.

1.1 Composing of RFID system

RFID system (seen in Figure 1) is generally composed by E-tag, reader-writer and computer communication network (Simson Garfinekel, 2005).

1.1.1 E-tag

E-tag stores correlative information of the identified objects, and it is usually put on the identified objects, and the

information stored by it can be read and written by the radio frequency reader-writer through the non-contact mode.

1.1.2 Reader-writer

The reader-writer is the equipment which can be used to read and write the information of the E-tag by the radio frequency technology. The tag information read by the reader-writer can be managed and transmitted by the computer network system.

1.1.3 Computer communication network

In the RFID system, the computer communication network is generally used to manage the data and complete the function of communication transmission. The reader-writer can connect with the computer communication network by the standard interface to realize the communication and data transmission.

1.2 Work principle of RFID system

RFID technology is a sort of non-contact information transfer mode realized by the radio frequency signals through space coupling (alternating magnetic field or electromagnetic field), and it identifies the objective through the transferred information. Its work principle can be described as follows (Klaus Finkenzeller, 2003): reader-writer emits energy in one region, form the electromagnetic field, and the size of the region is decided by the work frequency and antenna size, and when the E-tag passes this region, the system checks the signal of the reader-writer and stores the electromagnetic wave energies emitted by the reader-writer to be the electric energy needed by the tag, and the tag transmits the interior information to the reader-writer by the form of the radio wave, and the reader-writer accepts the data of the E-tag, encodes and implement fault check to judge the validity of the data, and transfers the data to the computer communication network for the data processing.

1.3 Technical characteristics of RFID

1.3.1 Data read and write

RFID reader can read the data to the database without contact, and process multiple tags once, and write the logistic processing state into the tag for the logistic processing in the next stage.

1.3.2 Miniaturized and diverse form

RFID will not be limited by the size or form when it reads data, so it needs not to use the paper with fixed size or print quality to fit for the precision. In addition, E-tag of RFID can be applied in different products by small size, so we can more flexibly control the production of the products, especially the application on the production line.

1.3.3 Anti-pollution

RFID possesses strong anti-pollution nature for water, oil or drugs. And in the dark or polluted environment, RFID also can read data.

1.3.4 Repetitive use

Because RFID is electric data which can be written repetitively, so the tag can be used repetitively.

1.3.5 Penetrability

If RFID is covered by the paper, wood, plastics or non-metal or non-transparent materials, it can communicate through these materials except for the irons or other metals.

1.3.6 Big memory capacity of data

The data capacity will be extended with the development of the memory scale, and the quality of the material carried by the goods is larger, the requirement of the capacity for the volume label also increase, and RDID will not be restrained.

1.3.7 System safety

The system stores the data from the central computer to the work piece which will largely enhance the safety of the system.

1.3.8 Data safety

The checkout method or the cycle redundancy checkout method will be used to ensure the data veracity stored in the radio frequency tag.

2. Total design and work principle of the monitoring system

2.1 System design

Except for fulfilling the function requirements, the design project should fully consider the stability, reliability, anti-jamming ability, fault-tolerance ability and abnormity protection, so the total design of the system should be embodied in following aspects.

(1) The design could effectively identify and monitor underground personnel, and realize the humanization, informationization and automatization.

(2) The design could effectively offer personnel's passing in and out, attendance and monitoring and relative management information, and once the accident happens, the design could ensure the normal implementation of the rescue.

(3) The design of the system could possess the natures of safety, maintenance and expansion.

(4) The design could effectively test the concentration of harmful gases and quickly react.

2.2 System work principle

The underground station equipment emits the encrypted information to the exterior by the antenna and forms certain signal emission region. The RFID cards carried by the workers will be activated when they enter into the emission region, and the information carried with the encrypted objective identification are emitted by the emission module, and the substation equipment will receive these signals and abstract the objective identification code, and transmit the code to the ground computer system to complete the function of the system. When the concentration of the harmful gases achieves certain value, the gas sensor of the substation equipment transmits the information to the A/D converter, and after the information are converted, they are transmitted to the monitoring network to realize the test and monitoring.

3. Composing and structure of the system

The safety monitoring system includes the ground part and the underground part (seen in Figure 2).

The products in the system adopt the sap hanging design (Tan, 2007) to ensure the normally and continually running of the system in the severe environment and offer power supply for 1~3 hours after power-down.

The underground part and the ground part adopt the RS-485 serial interface standard communication and the RS-232 standard serial interaction to connect with the transmission network. The data conversion interface is mainly composed by the power supply board, signal conversion board and safety bolt, and it is placed on the mouth of the mine, and it is mainly used to ensure the information exchange between the underground monitoring points and the ground monitoring center, so the system needs not the RFID and A/D converter. Figure 3 is the exchange of the communication signals between the ground and the underground.

3.1 Underground part

The underground part is the core part of the monitoring system, and it includes the fieldbus and a series of substations which are used to monitor and control the personnel. The fieldbus is the network which connects the substation and transmits information. Some substations are used to position the underground workers and equipments real time. The positioning mode of the personnel and equipments is the signal strength monitoring method, and when the E-tag carried by one worker is near certain positioning station, the signals acquired by the station are strong, so we can judge the position of the tag, and when the E-tag is in the superposition region of two stations, the signal strengths of two station will be different, and we can judge the position of the tag by comparing the strengths of the signals. Other substations are mainly composed by sensor, A/D converter, micro-controller and RFID module, and they can monitor the harmful gases real time and acquire the transmission of the information, and when the concentration of the harmful gases exceeds the safety value, the ground work platform and the underground fixed monitor point emit the alarm simultaneously. The substation in the underground part adopts the wire communication, the serial interface and the RS-232 serial data interface standard, and the bus transmission and the serial interface are used for the future expansion of the system function.

3.2 Ground part

The ground part mainly includes the management operation system, and it is the base of the whole safety monitoring system, and its main functions are to complete the information acquirement, real-time processing and storage of the check point. The information from the underground include not only the concentration of the harmful gases, but the information about the underground personnel and equipment, and these large-size data are all stored in the database through compression as the base of the monitoring and controlling.

4. Conclusions

In this article, we applied the RFID technology in the coal mining management, and established an underground safety monitoring system with integrality, real-time and flexibility, which could automatically alarm when dangers happened and enhanced the search and rescue efficiency. The system could manage the harm-gas concentration, planning arrangement of workers, access control for the works passing in and out laneway, distribution of laneway personnel and workers' data, realize the informationization and visualization of the underground management, and largely enhance the mining production management level and the work safety level of the mine.

The safety monitoring system is based on the safe production of the mine, and the module of RFID is the major

equipment, and the wire communication network is the ligament, and the monitoring central PC computer is the central computer management system. The system could improve the safety mechanism for the miners and reduce the cost of the management, and the technology will be the new trend of the mining safe production monitoring.

References

Guo, Yanli. (2005). Mine Application Example of South Africa Mining Industry. *Automatic Identification Technology & Application.* No. 5.

Klaus Finkenzeller. (2003). *RFID Handbook: Fundamentals and Applications in Contactless Smart Cards and Identification (second Edition).* John wiley & Sons, 2003.

Liu, Lili & Yao, Meng. (2004). Coal Mine Security Intelligent Control System Based on RFID. *Global Electronics China.* No.9. P.22-25.

Nadeem Raza, Viv Bradshaw, Matthew Hague, et al. (1999). Application of Technology. The Institution of Electrical Engineer, 1999.

Qiu, Like. (2007). The Principle of Staff Positioning System for Those Working in Underground Coalmine and Its Application in Xinglongzhuang Coalmine. *Coal Mine Modernization.* No.1. P.28-29.

Simson Garfinekel, Beth Rosenberg. (2005). RFID, Applications, Security and Privacy. Addison-wesley, 2005.

Tan, Min & Liu, Yu. (2007). *RFID Technical System Engineering and Application Directory.* Beijing: China Machine Press. April of 2007.

Zhou, Xiaoguang & Wang, Xiaohua. (2006). *Technical Principle and Application Example of RFID.* Beijing: Posts & Telecom Press. Dec. of 2006.

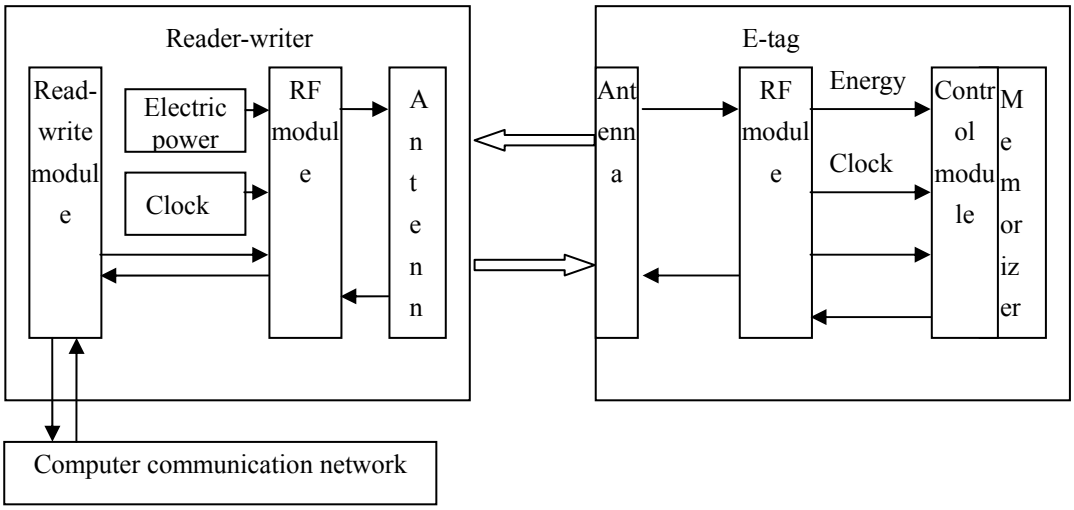

Figure 1. Structure of RIDF System

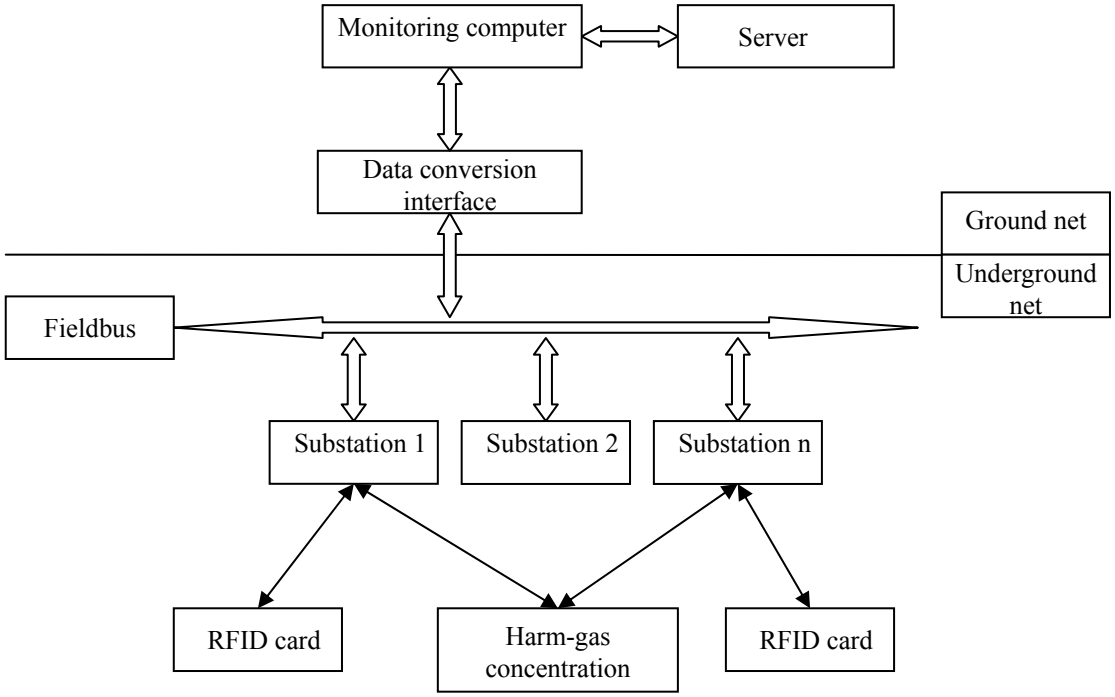

Figure 2. Structure of Safety Monitoring System

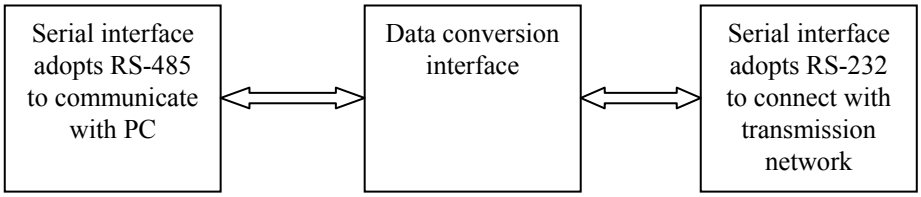

Figure 3. Communication Singles Exchange between Ground and Underground

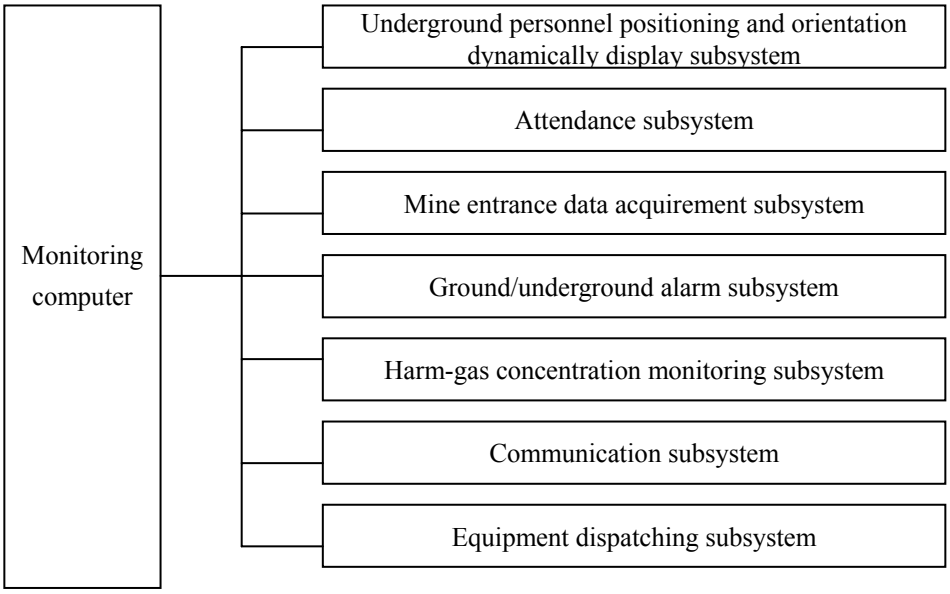

Figure 4. PC Management System

Modern Applied Science

www.ccsenet.org/journal.html

Vol. 3, No. 8

August 2009

Data Mining Based on Fuzzy Rough Set Theory and Its Application in the Glass Identification

Ruying Sun

College of Information, Linyi Normal University, Linyi 276005, China

E-mail: srysd@163.com

Abstract

To overcome the disadvantage of determining artificially the class number, fuzzy C means clustering is introduced to fuzzify the continual attribute, and the best minute class number is obtained by cluster validity analysis. The relationship of glass composition and its application is excavated using data mining method in this paper.

Keywords: Data mining, Fuzzy clustering, Fuzzy rough Set, Glass identification

1. INTRODUCTION

Data Mining is defined as a large number of incomplete, noisy, fuzzy and random data extracted implicit in which people do not know in advance, but potentially useful information and knowledge, such as concepts, knowledge rules, restrictions, laws and so on. Rough set theory has been successfully applied to relational database data mining, such as A Fuzzy Search Method for Rough Sets in Data Mining, Mining Stock Price using Fuzzy Rough Set System and so on (Osei Adjei and LiChen , 2001, 980).

The continuous attributes must be discrete before extracting the rules using rough set theory. This process will result in some degree of information loss because discrete attribute values will not be retained in property values in the actual existence of numerical differences. French scholar D.Dubios and H.Prad presented the definition of fuzzy rough set combined rough set and fuzzy set to solve the problem of information loss in the course of attribute discrete based on rough set. Using the fuzzy rough set theory to deal with data sets can retain more original data set contains information.

However, the current attribute fuzzification method need to artificially divide into several classes, almost not considering the specific characteristics of attribute values. Methods are often too subjective, unreasonable and poor operability.

2. FUZZY CLUSTERING ANALYSIS

2.1Fuzzy C-means Clustering Method (FCM)

$X = \{x_1, x_2, \cdots x_n\} \subset R^p$ is a limited data set in the feature space, n is the number of data items , c is the number of clusters with $2 \le c \le n$, $R^{c \times n}$ is all the real matrix collection, $V = \{v_1, v_2, \cdots v_c\} \subset R^p$ is the vector collection in the feature space R^p, has c cluster center vector. $\mu_i(x_j)$ simply recorded as μ_{ij}, is the membership which is No. samples j belongs to No. centers i. The objective function of fuzzy C-mean clustering analysis is defined as follows.

$$\min J_m(U,V;X) = \sum_{i=1}^{c}\sum_{j=1}^{n} \mu_{ij}{}^m \parallel x_j - v_i \parallel_A^2$$

1) $\mu_{ij} \in [0,1], 1 \le i \le c, 1 \le j \le n$;

2) $\sum_{i=1}^{c} \mu_{ij} = 1, 1 \le j \le n$;

3) $0 < \sum_{j=1}^{n} \mu_{ij} < n, 1 \le i \le c$.

where

$$v_i = \frac{\sum_{j=1}^{n} u_{ij}{}^m x_j}{\sum_{j=1}^{n} u_{ij}{}^m}, 1 \le i \le c \tag{1}$$

$$\mu_{ij} = \frac{1}{\sum_{k=1}^{c} \left(\frac{d_{ij}}{d_{kj}} \right)^{1/m-1}} \tag{2}$$

$d_{ij} = \| x_j - v_i \|_A^2$, $1 \le i \le c, 1 \le j \le n$, is a distance measure between object x_j and cluster centre v_i, m is a weighting exponent on each fuzzy membership. A solution of the object function can be obtained via a process of iterating (1) and (2). The result is an optimal fuzzy division of x, $U^* = [\mu_{ij}{}^*]$.

2.2 Cluster Validity Analysis

Formula (3) defines the function of clustering validity.

$$FP(U;c) = \frac{1}{n} \sum_{j=1}^{n} \left(\sum_{i=1}^{c} \mu_{ij}^2 / \sum_{i=1}^{c} \mu_{ij} \right) - \frac{1}{c} \sum_{i=1}^{c} \left(\sum_{j=1}^{n} \mu_{ij}^2 / \sum_{j=1}^{n} \mu_{ij} \right) \tag{3}$$

Where c is the number of clusters, U is the membership matrix. If there is (U^*, c^*) to meet $FP(U^*, c^*) = \min_{c} \{ \min_{\Omega_c} FP(U;c) \}$, then (U^*, c^*) is the optimal effective clustering, c^* is the number of the best classification.(GAO Xinbo, 2004, 59).

3. Data Mining Based on Fuzzy Rough Set

3.1 Attribute fuzzy-dependent analysis

Each equivalence class is fuzzy in the fuzzy-rough set, its lower and upper approximation is as follows. (Hongli Liang, Huaguang Zhang and Derong Liu, 2004, 584)

$$\begin{aligned} \mu_{\underline{X}}(F_i) &= \inf_x \max\{1 - \mu_{F_i}(x), \mu_X(x)\}, \forall i \\ \mu_{\overline{X}}(F_i) &= \sup_x \min\{\mu_{F_i}(x), \mu_X(x)\}, \forall i \end{aligned} \tag{4}$$

Where, F_i is a fuzzy equivalence class, $\mu_X(x)$ is the membership which x belongs to arbitrary fuzzy set X in the domain U.

Formula (5) defines the fuzzy domain of F_i.

$$\mu_{POS_C}(F_i) = \sup_{X \in U|D} \mu_{\underline{X}}(F_i) \tag{5}$$

Where $F_i \in U \mid C$, X is one fuzzy equivalence class of decision attribute D.

$\mu_{POS_C}(x)$ is the degree of x ($x \in U$) belonging to the fuzzy domain.

$$\mu_{POS_C}(x) = \sup_{F_i \in U|C} \min\{\mu_{F_i}(x), \mu_{POS_C}(F_i)\} \tag{6}$$

According to the definition of fuzzy domain, the degree of decision attribute set D dependence on condition attribute set C can be obtained based on the fuzzy-rough set.

$$\gamma_C(D) = \frac{| \mu_{POS_C}(x) |}{| U |} = \frac{\sum_{x \in U} \mu_{POS_C}(x)}{| U |} \tag{7}$$

3.2 Attribute Reduction Algorithm

Attribute reduction is defined as deleting redundant attribute in the premise of maintaining the classification of decision table or decision-making ability. It can be expressed as the following definition (Richard Jensen and Qiang Shen, 2002,

30).

Definition1: If there is $C' \in C$ to meet

1) $\gamma_C(D) = \gamma_{C'}(D)$;

2) $\gamma_{C'-\{a\}}(D) < \gamma_{C'}(D), \forall a \in C'$

then C' is a reduction C compared to D. Where C is the condition attribute set and D is decision attribute set.

In order to reduce computational complexity, attribute reduction algorithm which attribute gradually reduced is used in this article. This method does not require verifying the conditions of each subset of attributes. Attributes that will not result in the loss of information of decision table system are gradually reduced from condition attributes set. Algorithm is as follows.

1) $R \leftarrow C$;

2) do;

3) $S \leftarrow \{\}$;

4) $\forall x \in R$;

5) $if\ \gamma_{R-\{x\}}(D) = \gamma_R(D)$;

6) $S \leftarrow S \cup \{x\}$;

7) $if\ \ s = \{\}$;

8) return R ;

9) $\gamma_\circ \leftarrow \gamma_C(D); T \leftarrow \{\}$;

10) $\forall x \in S$;

11) $if\ \gamma_x(D) < \gamma_\circ$;

12) $T \leftarrow \{x\}$;

13) $\gamma_\circ \leftarrow \gamma_x(D)$;

14) $R \leftarrow R - T$.

3.3 Data Mining Based on Fuzzy Rough Set Theory

The steps extracting rules from database are as follows.

First. Pretreatment. Complete loss of data, and delete the duplicate object, then structure the decision table.

Second. Data Reduction. Eliminate redundant attributes used attribute reduction algorithm based on fuzzy rough set and structure new decision table, and then eliminate redundant attribute value of the new decision table. Thus minimum reduction of decision table is obtained.

Third. Extract rules. Extract valuable rules according to the minimum reduction getting ahead.

4. EXAMPLES ANALYSIS

Example 1

A simple data set of weather information.

First. Pretreatment.

Structure the decision table such as table 1.

The decision table contains a conditions attribute set C and a decision attribute d .where C={a1, a2, a3, a4}, a1 is the sunny index , a2 is the temperature index,a3 is the humidity index and a4 is the wind conditions index. Decision

attribute d contains two values, d=0 indicates that he did not go out to play, d=1 play out.

Second. Data Reduction.

The fuzzy partitions matrix U of the four attributes are obtained by Fuzzy C-means clustering respectively. The results of clustering validity analysis are shown in table 2. From Table2 we can see, it is the most effective that a1, a2 are divided into 3 categories and a3, a4 2ategories. At the same time the partition of domain based on attributes are obtained as follows.

U/a1={{1,2,8,9,11},{4,5,6,10,14},{3,7,12,13}}

U/a2={{1,2,3,5,13},{6,7,9},{4,8,10,11,12,14}}

U/a3={{1,2,3,4,8,10,12,14},{5,6,7,9,11,13}}

U/a4={{2,4,6,7,9,10,11,12,14},{1,3,5,8,13}}

Attribute a3 can be reduced by the attribute reduction algorithm in this article. Eliminate redundant attribute value of the new decision table, then obtain a minimum reduction of decision table which show in table 3.

Third. Extract Rules.

The valuable decision rules are extracted as follows.

1) if $0.75 \le a1 \le 0.95$ and $0.85 \le a2 \le 0.95$ then d=0;

2) if $0.45 \le a1 \le 0.6$ then d=1;

3) if $0.45 \le a2 \le 0.7$ and $0.4 \le a4 \le 0.65$ then d=1;

4) if $0.1 \le a1 \le 0.25$ and $0.4 \le a4 \le 0.65$ then d=0;

5) if $0.75 \le a1 \le 0.95$ and $0 \le a4 \le 0.3$ then d=0;

6) if $0.75 \le a1 \le 0.95$ and $0.2 \le a2 \le 0.4$ then d=1.

The results showed that the practical significance and a smaller set of rule can be explored by the algorithm used in this paper.

Example 2

Glass Identification Database (http://ftp.ics.uci.edu/pub/machine-learning-databases/glass).

Glass Identification Database contains 214 instances, each instance include 9 attributes and a decision attribute. C={c1,c2,…c9}={RI, Na, Mg, Al, Si, K, Ca, Ba, Fe}, all attributes are continuously valued. where, c1(RI) is refractive index, unit measurement of c2 to c9 is weight percent in corresponding oxide. Decision attribute d is the type of glass, it has 7 discrete values.

1--building_windows_float_processed;

2--building_windows_non_float_processed;

3--vehicle_windows_float_processed;

4--vehicle_windows_non_float_processed ;

5--containers;

6--tableware;

7--headlamps.

Attribute c1, c3, c6, c9 can be reduced by the attribute reduction algorithm in this article. Eliminate redundant attribute value of the new decision table, then obtain a minimum reduction of decision table, and 31 valuable decision rules are extracted.

The results showed that 31 useful decision rules are excavated from the original 214 information indicates used the proposed data mining algorithm, the 183 redundant information indicates are deleted, simplifying the basis for judging. And the 31 rules show the relationship between glass compositions and their application. As long as the weight percent of Na, Al, Si, Ca, Ba in its corresponding oxide can be judged that the use of glass is confirmed. In other words, for an unknown glass, as long as the content of Na, Al, Si, Ca, Ba in its corresponding oxide is detected, the source of glass can be determined, thus the identification methods for glass is simplified.

5. CONCLUSIONS

Data mining based on fuzzy rough set provides an effective way to resolve the continuous attributes database mining. Limited useful information can be excavated from massive data by this method. It has great significance of saving the data storage and reducing the explosion possibility of information systems. Also it has important practical significance

in the production and related projects.

REFERENCES

Gao, Xinbo. (2004). *Fuzzy Cluster Analysis and its Application*, Xidian University Press (chapter5).

Hongli, Liang, Huaguang, Zhang, and Derong, Liu. (2004). Roughness of Fuzzy Sets Based on Two New Operators. *0-7803-8353-2/04©2004 IEEE*, 583-586.

http://ftp.ics.uci.edu/pub/machine-learning-databases/glass.

Osei, Adjei and LiChen. (2001). A Fuzzy Search Method for Rough Sets in Data Mining. *0-7803-7078-3/01©2001 IEEE*, 980-985.

Richard Jensen and Qiang, Shen. (2002). Fuzzy-Rough Sets for Descriptive Dimensionality Reduction. *0-7803-7280-8/02©2002 IEEE*, 29-34.

Table 1. Decision table of weather information

No	a1	a2	a3	a4	d
1	0.8	0.9	0.9	0.3	0
2	0.75	0.85	0.88	0.5	0
3	0.5	0.95	0.75	0.2	1
4	0.2	0.6	0.8	0.4	1
5	0.15	0.95	0.5	0	0
6	0.25	0.3	0.55	0.6	0
7	0.45	0.2	0.55	0.65	1
8	0.78	0.7	0.85	0.1	0
9	0.9	0.4	0.45	0.4	1
10	0.2	0.65	0.9	0.45	1
11	0.95	0.55	0.6	0.55	1
12	0.5	0.55	0.8	0.6	1
13	0.6	0.9	0.6	0.2	1
14	0.1	0.45	0.85	0.5	0

Experimental steps are as follows.

Table 2. The results of clustering validity analysis for weather information

Class Number	FP(U; c)			
	a1	a2	a3	a4
2	0.0358	0.0974	-0.0034	-0.0369
3	-0.0069	0.0334	0.0084	-0.0241
4	0.0156	0.0434	0.0028	0.0356
5	0.0073	0.0663	0.0052	-0.0182

Table 3. A minimum reduction of decision table

No	a1	a2	a4	d
1	1	1	×	0
2	3	×	×	1
3	×	3	1	1
4	2	×	1	0
5	1	×	2	0
6	1	2	×	1

Modern Applied Science

www.ccsenet.org/journal.html

Vol. 3, No. 8

August 2009

Design and Implementation of Speech Recognition System Based on Field Programmable Gate Array

Haitao Zhou

Information and Communication Department

Tianjin Polytechnic University

Tianjin 300160, China

E-mail: zhouanni@126.com

Xiaojun Han

Information and Communication Department

Tianjin Polytechnic University

Tianjin 300160, China

The research is financed by Applied Program of Basic Research of Tianjin (08JCYBJC14700)

Abstract

In this paper, a Hidden Markov Model (HMM) speech recognition system which is based on Field Programmable Gate Array (FPGA) is designed. It introduces the principle of speech recognition algorithm and deduces the hardware frameworks accordingly. In terms of HMM recognition module, the conventional Viterbi algorithm has been improved and recognition speed has been increased. The core part of the hardware is EP2S60F1020C3 FPGA chip. The experimental result of this system shows that the speech recognition accuracy reaches 94% when ten numbers are being recognized, and the average recognition time is 0.669s.

Keywords: Field Programmable Gate Array, Hidden Markov Model, Speech Recognition, Viterbi Algorithm

1. Introduction

As a new convenient means of human-machine interaction, speech recognition is widely applied to many portable embed speech products. The ultimate aim of speech recognition is to make machine understand natural language. It is of great significance not only in practical application but scientific research. The research on speech recognition technology mainly concentrates on two aspects. One is the software running on computer, the other is embedded systems. The advantages of Embedded systems are high-performance, convenience, cheap and they have huge potential for development.

FPGA has advantages of short development cycle, low-cost design and low-risk. In recent years, FPGA has become the key components in high-performance digital signal processing systems in digital communication, network, video and image fields. In this paper, the design was implemented on an EP2S60F1020C3 FPGA, sitting on stratix II development board.

2. Speech Recognition Basics

Fig.1 shows the speech recognition algorithm flow. A typical speech recognition system starts with the Mel Frequency Cepstrum Coefficient (MFCC) feature analysis stage, which is composed of the following items: 1) Pre-emphasis. 2) Divide the speech signal into frames. 3) Apply the hamming window. 4) Compute the MFCC feature. The second stage is vector quantization stage. In this stage, codebook is used to quantize the MFCC feature and get MFCC feature vector. The codebook is generated on compute via LBG arithmetic, and is downloaded to ROM. The last stage is recognition, which is performed by using a set of statistical models i.e. hidden Markov models (HMM). In this stage, the probability

of MFCC feature vector has been generated by each model and the result is the model which generated the largest probability.

2.1 MFCC Feature analysis

Figure 2 shows the process of creating MFCC features. The first step is to be taken the Discrete Fourier Transform (DFT) of each frame. Certain amount of 0s are added to the end of Time-domain signal $s(n)$ of each frame, in order to form the sequence of N-length. And then the DFT of each frame is taken to get the linear spectrum $X(k)$. In the second step, linear spectrum $X(k)$ is multiplied by the Mel frequency filter banks and converted to Mel spectrum. Mel frequency filter banks are several band pass filters $H_m(k)$, and each band pass filter is defined as follows:

$$H_m(k)=\begin{cases}0 & (k<f(m-1))\\ \dfrac{k-f(m-1)}{f(m)-f(m-1)} & (f(m-1)\le k\le f(m))\\ \dfrac{f(m+1)-k}{f(m+1)-f(m)} & (f(m)\le k\le f(m\_1))\\ 0 & (k>f(m+1))\end{cases} \quad (0\le m<M) \tag{1}$$

Where $0\le m<M$, M is the number of the band pass filters, and $f(m)$ is the central frequency.

The third step is to be taken the logarithm of Mel spectrum to get logarithmic spectrum $S(m)$. Thus, the transfer function from linear spectrum $X(k)$ to logarithmic spectrum $S(m)$ is

$$S(m)=\ln\left(\sum_{k=0}^{N-1}\left|X(k)\right|^2 H_m(k)\right) \quad (0\le m<M) \tag{2}$$

In the last step, logarithmic spectrum $S(m)$ is transformed into cepstrum frequency by Discrete cosine Transform (DCT)in order to yield MFCC feature.

2.2 Vector Quantization

In this paper, due to the discrete hidden markov model is used, it is necessary to transform continuous MFCC feature which has been yielded into discrete MFCC feature.

Vector quantization is to map one K dimensional vector $X\in\widetilde{X}\subset R^K$ to another K dimensional quantize vector $Y\in\widetilde{Y}_N=\{Y_1,Y_2,\cdots Y_N\,|\,Y_i\in R^K\}$, in where X is input vector, Y is quantize vector or codeword, $\widetilde{X}$ is source space, $\widetilde{Y}_N$ is output space, N is the size of codebook, and R^K is K dimensional Euclidean space.

The process of quantizing vector X is to search a codeword which is the nearest one from the vector X in codebook $\widetilde{Y}_N$. In this paper, square distortion measure is applied to calculate distortion, which is defined as

$$d(X,Y)=\|X-Y\|^2 \tag{3}$$

2.3 HMM Recognition

The role of HMM Recognition is to find out the maximum probability of the HMM which has generated the feature vector, according to the given feature vector. In this paper, viterbi algorithm is used to solve the problem, and an improved algorithm is proposed based on the original algorithm.

The given HMM parameters $\lambda=\{\pi,A,B\}$ $(\pi=\{\pi_i\},A=\{a_{ij}\},B=\{b_{jk}\})$, and the observation sequence $O=O_1,O_2,\cdots,O_T$, in where N is the number of HMM states, $\delta_t(j)$ is the highest probability along with a single path, at time t, which accounts for the first observations and ends in state j, $\varphi_t(j)$ is the HMM state at time t. The detailed algorithm is defined as follow:

1) Initialization

$$\begin{aligned}\delta_1(j)&=\pi_j b_j(O_1)\\ \varphi_1(j)&=0\end{aligned} \quad (1\le i\le N) \tag{4}$$

2) Recursion

$$\delta_t(j)=[\max_i\{\delta_{t-1}(i)a_{ij}\}]b_j(O_{t+1}) \quad (1\le i\le N)$$

$$\varphi_t(j)=\arg\max_i\{\delta_{t-1}(i)a_{ij}\} \quad (1\le j\le N) \tag{5}$$

3) Termination

$$P = \max_j[\delta_T(j)] \qquad (1 \le j \le N)$$

$$q_t = \arg\max_j[\delta_T(j)] \tag{6}$$

4) Path backtracking

$$q_t = \varphi_{t+1}(q_{t+1}) \quad (1 \le t \le T-1) \tag{7}$$

5) Algorithm improving

In practice, π, A and B are decimal fractions between 0 and 1. It is not conducive for FPGA to implement decimal fraction operation, because decimal fraction multiplication may cause the problem of gross underflow when T is larger than a threshold. So it is important to take the logarithm of π, A and B before operation. When π, A and B are transformed to logarithmic probability π', A' and B', floating point numbers multiply operation is transformed to integer addition operation. In addition, considering taking out the sign bit before operation, (4) and (5) should be changed to

$$\begin{aligned}\delta_1(j) &= \pi'_j b'_j(O_1) \\ \varphi_1(j) &= 0\end{aligned} \quad (1 \le i \le N) \tag{8}$$

$$\delta_t(j) = [\min_i\{\delta_{t-1}(i) + a'_{ij}\}] + b'_j(O_{t+1}) \qquad (1 \le i \le N)$$

$$\varphi_t(j) = \arg\min_i\{\delta_{t-1}(i) + a'_{ij}\} \qquad (1 \le j \le N) \tag{9}$$

Thus (8) and (9) are improved algorithm expression.

3. Design of Speech recognition hardware

3.1 Design of MFCC module hardware

As shown in Fig.3, MFCC module is consisted of DFT module, Mel filter banks, endpoint detection module, logarithm operation module, DCT module, output control module and control module.

Speech signal is sampled at a sample rate of 8 k. Each speech frame is composed of 256 24-bit sample points. Data will be sent to the Mel filter bank under the control of the control element, and the result after calculation will be told to control element. The output of the Mel filter bank will be exported to logarithm computation unit and DCT module to calculate the MFCC parameter. Meanwhile, the point detection will be executed: control element determine whether put out the MFCC parameter according to the output of speech endpoint module. Data get through the module in a pipeline mode, which enhance the system processing speed.

3.2 Design of Vector quantization module hardware

Vector quantization module hardware is designed as Fig.4. The order number is stored in counter1. The index of codebook is stored in counter2. The index of the nearest codebook is stored in register2. The value of the distance between ROM (codebook) and RAM (MFCC) is stored in address module.

The work flow is shown as follows:

1) Under the control of the controller, counter1 starts counting. The MFCC of each frame and codebook are read, subtracted, and send to accumulator.

2) To compare the value of register2 and the output of accumulator: if the output of accumulator is larger than the value of register2, the controller stops the compute of current codebook and tends to next codebook. Counter1 and accumulator are cleared. The value of counter2 plus 1.

3) If the output of accumulator is less than the value of register2 when the value of counter 1 is 12. The output of accumulator is stored in counter 2. The current value of counter 2 is stored in register 1. The index of the nearest codebook and the index of codebook are renewed. Counter1 and accumulator are cleared. The value of counter2 plus 1.

4) To repeat above process, until the value of counter 2 is 256. Then the vector quantization of a speech frame is accomplished.

3.3 Design of HMM recognition module hardware

A 4 state left-to-right HMM without skipping is adopted in this paper.

The design of HMM recognition module hardware is shown in Fig.5. FSM is the controller of state machine. The observation sequence is stored in RAM O. The value of initial probability is stored in RAM Pi. State transition probability A is stored in RAM A. Output probability B is stored in RAM B. The address of RAM A and REM B are generated from GENaddrA and GENaddrB respectively. CurrentMin is used for preserving the smallest probability of the recognition model until the current model, CounterIndex is used for saving the model label of the smallest

probability,

The key point of the Viterbi algorithm is seeking $\delta_t(j)$ via type (9), as a result, the PE unit has been designed for calculating $\delta_t(j)$ in this paper. As shown in Figure 6, PE unit is consisted of three adders and two data selectors. First, to calculate the value of $\delta_{t-1}(j-1)+a'_{j-1,j}$ and $\delta_{t-1}(j)+a'_{j,j}$. Second, to choose the smallest value through data selector, and add a value of $b'_j(O_t)$ on it to get $\delta_t(j)$. In the initial state, if j=1, it only needs to compare the value of $\delta_{t-1}(j)+a'_{j,j}$ and π'_j, and to take the smaller value as the smallest value.

4. Implementation and Results

It was achieved the entire voice training and the recognition process by using Stratix II EP2S60 DSP development board as the hardware platform of Voice processing module. Fig.7 is the RTL view.

Acquire the voice signal through the microphones and PC-in tape recorder. The sample rate was 11025KHz, and the sample precision was 16bits. Gain 50 samples for each mandarin digit from 1 to 10 as the experiment subjects.

The experimental results were shown in table 1. The average recognition accuracy of speaker-independent mandarin digits reaches 94% and the average recognition time is 0.669s in this system, which achieves the recognition rate and real-time requirements.

5. Conclusions

In this paper, a FPGA-based Hidden Markov Model speech recognition system was designed. It completes the acquisition of voice by microphone and PC-in tape recorder and the generation of code book and training data. In the system, calculate the MFCC feature vector was calculated, quantized and recognized by Vertibi algorithms. In the HMM recognition, the traditional Viterbi algorithm was improved to enhance the recognition speed, which was able to meet the needs for real-time voice recognition systems and the requirements of the recognition accuracy.

References

Altera Corporation. (2006). *Nios II Processor Reference Handbook*, 1-1.

Altera Corporation. (2006). *Nios II Software Developer's Handbook*, 4-1.

Bok-Gue Park, Koon-shik Cho, & Jun-Dong Cho. (2002). Low power VLSI architecture of vertibi scorer for HMM-based isolated word recognition. *International Symposium on Quality Electronic Design*, 235-39.

Elmisery, F, A, Khalil, A, H, Salama, A, E, & Hammed, H, E. (2003). A FPGA-Based HMM for a discrete Arabic speech recognition system. Proceedings of the 15th International Conference on 9-10 Dec, 322-325

Lawrence, R, Rabiner. (1989). A Tutorial on Hidden Markov Models and Selected Applications in Speech Recognition. *Proceedings of the IEEE,* VOL.77, NO 2, February.

Lawrence, Rabiner, & Biing-Hwang, Juang. (1999). *Fundamentals of speech recognition*. Beijing: Prentice-Hall International, Inc.

Melnikoff, S, J, Quigley, S, F, & Russell, M, J. (2002). Implementing a simple continuous speech recognition system on an FPGA. *Field-Programmable Custom Computing Machines, Proceedings*.10th annual IEEE Symposium, 275-276

Nedevschi, S, Patra, R, K, & Brewer, E, A. (2005) Hardware speech recognition for user interfaces in low cost, low power devices.Design, Automation Conference. Proceedings. 42nd13-17 June, 684-689.

Yoshizawa, S, Miynamaga, Y, & Wada, N. (2002). A low-power VLSI design of an HMM based speech recognition system. *Circuit sand Systems*. Midwest Symposium on Volume 2, II-489-II-49292.

Table 1. Experiment result

Number	1	2	3	4	5	6	7	8	9	10
Correct rate (%)	96	94	94	92	96	92	94	92	96	94
Time (μs)	0.67	0.69	0.65	0.70	0.66	0.65	0.68	0.65	0.64	0.70

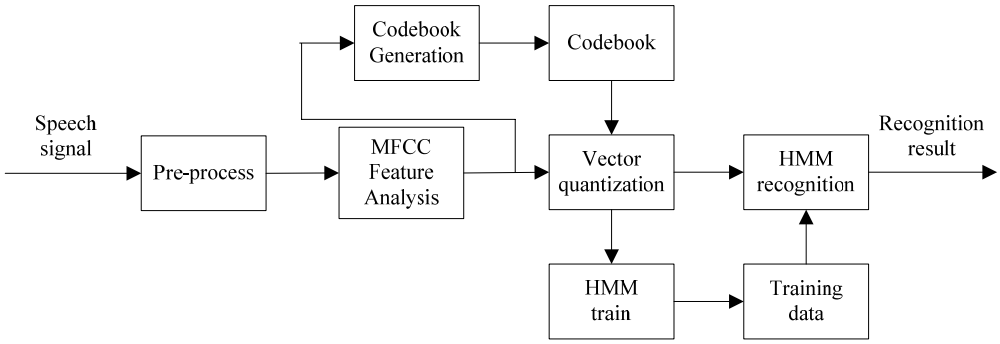

Figure 1. Speech recognition algorithm flow

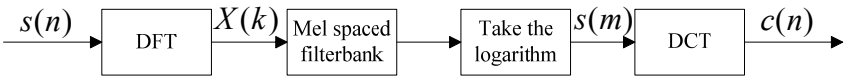

Figure 2. MFCC Feature analysis algorithm flow

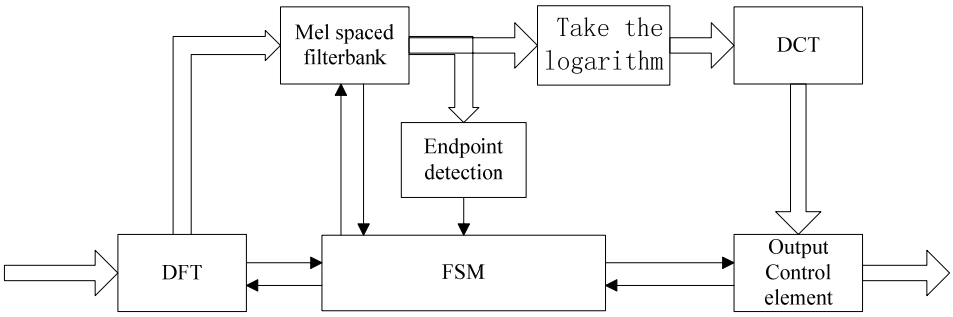

Figure 3. MFCC feature analysis hardware structure

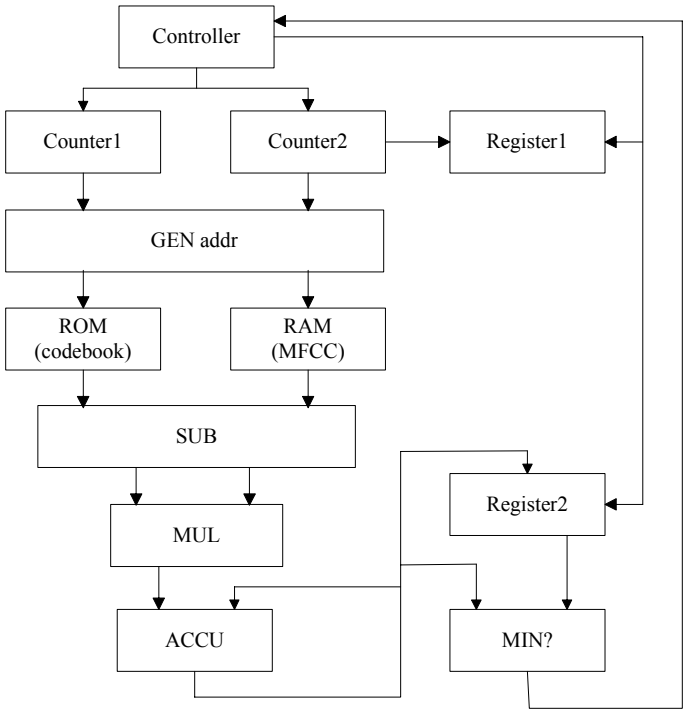

Figure 4. Vector quantization hardware structure

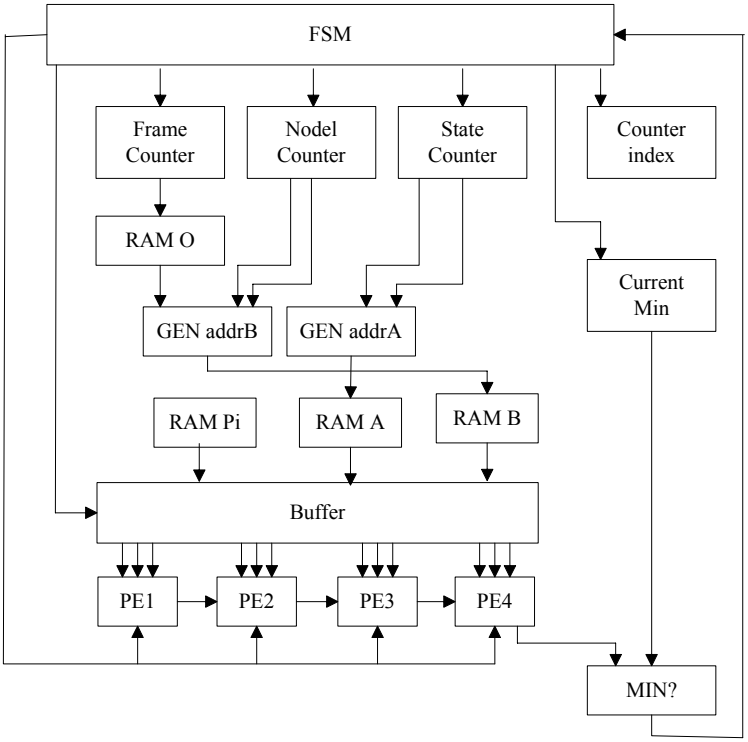

Figure 5. HMM recognition hardware structure

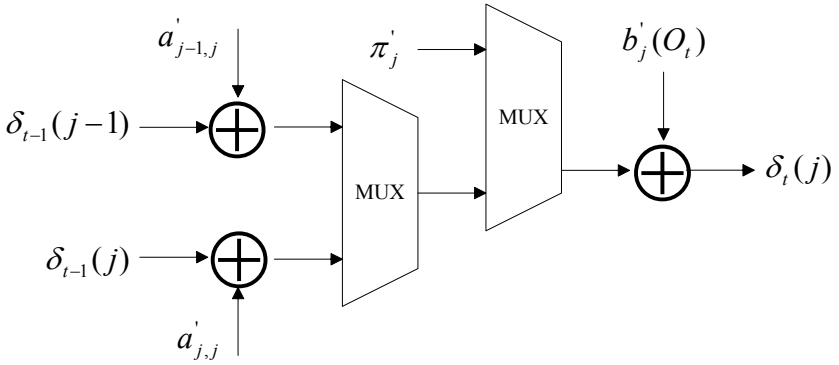

Figure 6. processing element

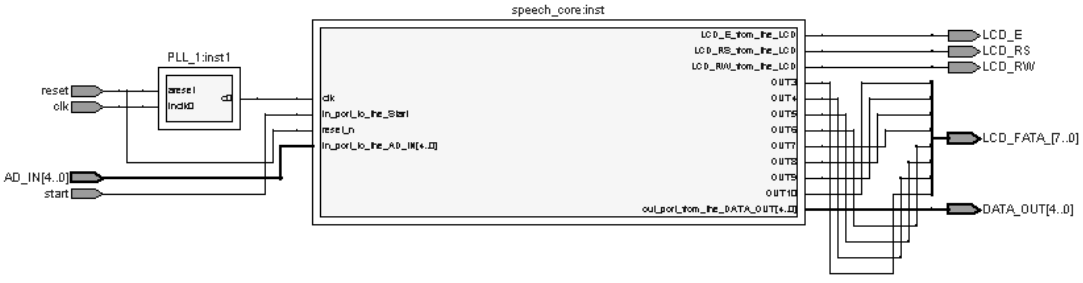

Figure 7. RTL view

Modern Applied Science

www.ccsenet.org/journal.html

Vol. 3, No. 8

August 2009

The Research of the Marketing Channel Conflict Based on the Analysis of the Game Theory

Ying Liu

School of Economic Management, ShenYang LiGong University

Abstract

In order to solve the marketing channel conflict more rationally, this thesis advances a new way by making use of game theory. It connects the game theory and the conflict of marketing channels together and puts up two kinds of models based on the game theory. According to the models, the thesis analyzes channel member's behavior. And then it finds the reasons of marketing channel conflicts by game theories.

Keywords: Marketing channel, Channel conflict, Game theory model

1. Introduction

The marketing channel conflict means that a channel member considered another member preventing or disturbing his goal. With the constant development of the socialist market economy of our country, the furious market competition comes along with the marketing channel conflict, some of which has already affected enterprises' performance. More and more analysis of the marketing channel conflict have been put into handling so as to get a better understanding to manage it. When analyzing the marketing channel conflict, it's always thought to be a member of social system, the subjective factors such as emotion and knowledge are taken into consideration. But from the research angle of economics, this thesis below supposes channel members to be rational decision maker who maximize their own profits when faced with a given condition, in spite of the subjective characteristics. It constructs two kinds of game models with retailers and manufacturers so as to carry out a detailed analysis of the conflict in marketing channels.

2. The Hypothesis of Building A Model

In order to facilitate the study, several hypotheses of building a model are introduced at first:

(1) For facilitating the analysis, the marketing channel of product M (M below) is made up of producer and the only retailer, however, it's more complex than this in reality.

(2) The demand of the M is uncertain for the not fully competitive market it's faced with. Supposes the demand for the product to be a linear function of $q=a-bp$, in which b stands for the uncertainty of marketing demand, defined as continuous random variable$(0, \infty)$,and F as its distribution function, and the final price of product M is composed of two parts - wholesale w and retail increase business r, that is $p=w+r$.

(3) Manufacturers and retailers are both rational decision makers, that is, both of them maximize profits for their own decision-making. Additionally, the risk that may be faced with is neutral, which means that the decision-makers are aim to maximize mean profits (or profit expectations) with the condition of the uncertainty of marketing demands.

(4) The cost of production and distribution of M is fixed, and also generally sets as zero, whose simplification will not affect the conduct of members of the channel analysis.

According to 4 hypotheses above, the profit for the function of manufacturers and retailers can be partly showed as:

$$\Pi=w\times q=w[a-b(w+r)] \quad (1)$$

$$\pi=r\times q=r[a-b(w+r)] \quad (2)$$

3. The Decision-Making Model of Manufacturers and Retailers at the Same Time

There're three kinds of situations below, all of which are game models in decision-making at the same time, that is, static games, involved in manufacturers and retailers.

3.1 Decision-makers Both Know the Specific Function of the Demand - Cournot Model

In this case, manufacturers and retailers are both know the exact product demand. At this point, based on the different b, manufactures will be choose w to maximize their own profits, and the profit maximization of the first order conditions are as follows:

$$\frac{d\Pi}{dw} = a - 2bw - br = 0 \tag{3}$$

According to this, it has a response function: $w = \frac{a - br}{2b}$; similarly, retailers' maximize profit for the first-order conditions:

$$\frac{d\pi}{dr} = a - bw - 2br = 0 \tag{4}$$

Its response function: $r = \frac{a - bw}{2b}$, which means that the balance of these two conditions meet at the same time, and solve function reaction of the two available Cournot equilibriums:

$$w = r = \frac{a}{3b} \tag{5}$$

Take(5)into(l) (2)can be:

$$\Pi = \pi = \frac{a}{3b}(\frac{3ab - 2ab}{3b}) = \frac{a^2}{9b} \tag{6}$$

The type (6), in which we can get the biggest profits mean of manufacturers and retailers:

$$\mathrm{E}[\Pi]' = \mathrm{E}[\pi]' = \int \frac{a^2}{9b} dF = \frac{a^2}{9} \int \frac{1}{b} dF \tag{7}$$

3.2 Neither of Decision-makers Know the Specific Needs of Function – Cournot Model Expanding

In this case, neither of them know the specific needs of the function, just know the distribution function of the demand function. The model distinguishes the model Cournot with the decision-makers' uncompleted information. Taking the uncertainty of demands into consideration, both sides make decisions on prices based on maximizing their own profits.

For manufacturers, profit expectations as follows:

$$\mathrm{E}[\Pi] = \int w\left[a - b(w + r)\right] dF \tag{8}$$

The first order condition of profit maximization is:

$$\frac{d\mathrm{E}[\Pi]}{dw} = \int \left[a - b(w + r) + w(-b)\right] dF = 0 \tag{9}$$

Its reaction function: $w = \frac{a - \bar{b}r}{2\bar{b}}$; as for retailers, the expectation for profits:

$$\mathrm{E}[\pi] = \int r\left[a - b(w + r)\right] dF \tag{10}$$

First-order conditions for profits maximization:

$$\frac{d\mathrm{E}[\pi]}{dr} = \int \left[a - b(w + r) + r(-b)\right] dF = 0 \tag{11}$$

Its reaction function: $r = \frac{a - \bar{b}w}{2\bar{b}}$; which means that the balance of these two conditions meet at the same time, solving the response of the two functions can get:

$$w = r = \frac{a}{3\bar{b}} \tag{12}$$

Take (12) into(8)(10)can get the biggest expectation for profits of manufacturers and retailers:

$$\mathrm{E}[\Pi]^2 = \mathrm{E}[\pi]^2 = \int \frac{a}{3\bar{b}} \left(a - \frac{2ab}{3\bar{b}}\right) dF = \frac{a^2}{9\bar{b}} \tag{13}$$

3.3 Only Manufacturers Know the Specific Function of the Demand - Uncompleted Information of Static Games

In this case, assuming that only manufacturers know the specific needs of products, who is aware of the specific value of b, however, retailers just know the distribution of it, both sides make a decision at the same time. At this point, according to each specific value of b, manufacturers will set a w to maximize its profits for the first-order conditions:

$$\frac{d\Pi}{dw} = a - b(w + r) + w(-b) = 0 \tag{14}$$

According to which can get its reaction function:

$$w = \frac{a - br}{2b} \tag{15}$$

As retailers know that manufacturer decide the value of w based on the specific value of b, who also set w as the function of b, so as to determine to maximize their own profits, that is:

$$\frac{d\mathrm{E}[\pi]}{dr} = \int \left[a - b\left(w(b) + r\right) + r\left(-b\right) \right] dF = 0 \tag{16}$$

Take(15)into(16), that is: $$r = \frac{a}{3\bar{b}} \tag{17}$$

Then, take(17)into(15), getting: $$w = \frac{a}{2b} - \frac{a}{6\bar{b}} \tag{18}$$

Take(17) (18)into(10), in which we can get the expectation for profits of retailers:

$$\mathrm{E}[\pi]^3 = \int \frac{a}{3\bar{b}} \left[a - b\left(\frac{a}{2b} - \frac{a}{6\bar{b}} \right) - b\frac{a}{3\bar{b}} \right] dF = \frac{a^2}{9\bar{b}} \tag{19}$$

Take(17)(18)into(1),in which we can get producers' profits:

$$\Pi(b) = \frac{a^2}{4b} + \frac{a^2 b}{36\bar{b}^2} - \frac{a^2}{6\bar{b}} \tag{20}$$

Take the expectation value of type(20), manufacturers' average profit can be achieved:

$$\mathrm{E}[\Pi]^3 = \int \Pi(b) dF = \frac{a^2}{4} \int \frac{1}{b} dF - \frac{5a^2}{36\bar{b}} \tag{21}$$

3.4 Conclusions

Different circumstances of three models above show the balance of state channels and channel members'average profit. In order to analyze the behavior of the members, we need to compare the average profits of the three cases, in which we need to come to understand the relationship between $\int \frac{1}{b} dF$ and $\frac{1}{b}$ for the reason that $\frac{1}{b}$ is a kind of strict convex function, then we can get $\int \frac{1}{b} dF > \frac{1}{\bar{b}}$ based on an inequality of Jense, so $\int \frac{1}{b} dF - \frac{1}{\bar{b}} > 0$.

Compared with three cases above about decision-makers' average profits and mean average profits, we can draw the following conclusions:

(1) The average profits of channels and average profits of channel members in the situations that both two sides do not know the specific needs of product information are the smallest value.

(2) If only one side knows the specific circumstances, who will maximize its channel average profits and the channel members average profits, but another one just the opposite.

4. Manufacturers -Led Models

The following three cases, the assumption is made that manufacturers are in the dominant on pricing when producers make a price at first, after which retailers make their decision-making prices. For the order of the game, so the three conditions are called dynamic games.

4.1 Both of the Decision-makers Know the Function of the Specific Needs of Model-Stackelberg

It is a kind of typical completed information of dynamic games, the strategy is the choice of price rather than production. With the Stackelberg of the solution into reverse, the first order conditions of the retailer's profit maximization is:

$$\frac{d\pi}{dr} = a - b\left(w + r\right) + r\left(-b\right) = 0 \tag{22}$$

Its reaction function: $$r = \frac{a - bw}{2b} \tag{23}$$

r should be noted that it is the retailers'actual selection after the w of manufacturer of choice. Retailers also know that the producers will make a pricing decision in accordance with the above-mentioned reaction functions, then the manufacturers' issue will be the Max Π (r), the first order conditions are as follows:

$$\frac{d\Pi}{dw} = a - 2bw - b\frac{a - bw}{2b} = 0 \tag{24}$$

In which we can get: $$w = \frac{a}{2b} \tag{25}$$

In accordance with the reaction functions, retailers' increasing price will be as follows:

$$r = \frac{a - bw}{2b} = \frac{a}{4b} \tag{26}$$

Take(25) (26)into(1)(2):

$$\Pi(b) = \frac{a}{2b}\left[a - b\left(\frac{a}{2b} + \frac{a}{4b}\right)\right] = \frac{a^2}{8b} \tag{27}$$

$$\pi(b) = \frac{a}{4b}\left[a - b\left(\frac{a}{2b} + \frac{a}{4b}\right)\right] = \frac{a^2}{16b} \tag{28}$$

Take the expectation value of type(27)(28), both sides' maximizing profits can be achieved:

$$\mathrm{E}[\Pi]^4 = \int \frac{a^2}{8b} dF = \frac{a^2}{8}\int \frac{1}{b} dF \tag{29}$$

$$\mathrm{E}[\pi]^4 = \int \frac{a^2}{16b} dF = \frac{a^2}{16}\int \frac{1}{b} dF \tag{30}$$

4.2 Neither of the Decision-makers Know the Function of the Specific Needs of Model-Stackelberg Expanding

In this case, both two sides will make a decision in accordance with the distribution of b, in which the strategy game collection is no longer a certainty. Additionally, the decision-makers' goal is to maximize profit expectations. We are still considering retailers' decision-making as a starting point. At this point, the first-order conditions of retailers' maximizing profits are:

$$\frac{d\mathrm{E}[\pi]}{dr} = \int \left[a - b(w + r) + r(-b)\right] dF = 0 \tag{31}$$

Its reaction function: $$r = \frac{a - \bar{b}w}{2\bar{b}} \tag{32}$$

Retailers come to know that producers will react for the price in accordance with the reaction functions mentioned above, then the manufacturers' issue will be MaxE[Π](r), the first order conditions are as follows:

$$\frac{d\mathrm{E}[\Pi]}{dw} = \int w\left[a - \left(w + \frac{a - \bar{b}w}{2\bar{b}}\right)\right] dF = 0 \tag{33}$$

In which we can get: $$w = \frac{a}{2\bar{b}} \tag{34}$$

In accordance with the reaction functions, retailers' increasing price will be as follows:

$$r = \frac{a - \bar{b}w}{2\bar{b}} = \frac{a}{4\bar{b}} \tag{35}$$

Take(34)(35)into(8)(9) both producers'and retailers'maximizing profits can be achieved:

$$\mathrm{E}[\Pi]^5 = \int \frac{a}{2\bar{b}}\left[a - b\left(\frac{a}{2\bar{b}} + \frac{a}{4\bar{b}}\right)\right] dF = \frac{a^2}{8\bar{b}} \tag{36}$$

$$\mathrm{E}[\pi]^5 = \int \frac{a}{4\bar{b}}\left[a - b\left(\frac{a}{2\bar{b}} + \frac{a}{4\bar{b}}\right)\right] dF = \frac{a^2}{16\bar{b}} \tag{37}$$

4.3 Only Manufacturers Know the Specific Function of the Demand - Uncompleted Information of Dynamic Games

In this case, retailers' information is uncompleted. If retailers still make pricing decisions on maximizing expecting profits, whose first-order conditions of maximizing profits will be:

$$\frac{d\mathrm{E}[\pi]}{dr} = \int \left[a - b(w + r) + r(-b)\right] dF = 0 \tag{38}$$

Its reaction function: $$r = \frac{a - \bar{b}w}{2\bar{b}} \tag{39}$$

Retailers know that the producers will make decisions on price in accordance with the reaction functions mentioned

above, then the manufacturers' issue will be Max Π (r), the first order conditions are as follows:

$$\frac{d\Pi}{dw} = a - b\left(\frac{a}{2\bar{b}} - \frac{w}{2} + w\right) - \frac{1}{2}bw = 0 \tag{40}$$

In which we can get: $$w = \frac{a}{b} - \frac{a}{2\bar{b}} \tag{41}$$

In accordance with the reaction functions, retailers'increasing price will be as follows:

$$r = \frac{a - \bar{b}w}{2\bar{b}} = \frac{3a}{4\bar{b}} - \frac{a}{2b} \tag{42}$$

Take(41)(42)into(1):

$$\Pi(b) = \left(\frac{a}{b} - \frac{a}{2\bar{b}}\right)\left[a - b\left(\frac{a}{b} - \frac{a}{2\bar{b}} + \frac{3a}{4\bar{b}} - \frac{a}{2b}\right)\right] = \frac{a^2}{2b} - \frac{a^2}{2\bar{b}} + \frac{a^2 b}{8\bar{b}} \tag{43}$$

Their expected profits from manufacturers are:

$$\mathrm{E}[\Pi]^6 = \int\left(\frac{a^2}{2b} - \frac{a^2}{2\bar{b}} + \frac{a^2 b}{8\bar{b}}\right)dF = \frac{a^2}{2}\int\frac{1}{b}dF - \frac{3a^2}{8\bar{b}} \tag{44}$$

Take(41)(42)into(10),retailers'expected profits:

$$\mathrm{E}[\pi]^6 = \int\left(\frac{3a}{4\bar{b}} - \frac{a}{2b}\right)\left[a - b\left(\frac{a}{b} - \frac{a}{2\bar{b}} + \frac{3a}{4\bar{b}} - \frac{a}{2b}\right)\right]dF = \frac{5a^2}{16\bar{b}} - \frac{a^2}{4}\int\frac{1}{b}dF \tag{45}$$

4.4 Conclusions

Compared with three cases above about decision-makers'average profits and mean average profits, we can draw the following conclusions:

(1) The average profits of channels and average profits of channel members in the situations that both two sides know the information can get more value.

(2) If only one side knows the specific circumstances, the total profits of channels are the largest value.

(3) It can get larger profits from the exclusive information than the sharing information for some particular channel members.

5. Summary

Simultaneously mutual-decision-making model and manufacturer-led model distinguish as follows:

(1) Under any circumstances, the total profits (E[Π]+E[π]) are worth more value in simultaneously mutual-decision-making model than one side-led model.

(2)Two types of models show that average profits may increase on the condition that both sides know the information of products. The one side-led model, however, the first actor (such as the manufacturers) will obtain more incremental profits than simultaneously mutual-decision-making model works, while another side gets smaller.

(3)As with the simultaneously mutual-decision-making model, the one side-led model, whose exclusive information is more of the profits for members of the specific channels (such as the manufacturers), thus the exclusive information brings up more driving force.

With the marketing channels conflicts analyzed though the game model, we can see the causes of the conflicts lies in the channel members who would like to achieve the maximization of self-interest in different concerns. If some members of the channel are given priority to enjoy the first operation dueling to various of reasons, their driving force of departure from the cooperation will be more obvious, which leads into the channel conflicts with a decline in the overall operational efficiency and profits, conflicts become inevitable.

References

Liao, Chenglin and Liu, Zhongwei. (2003). Channel management companies and distributors of game analysis. *Journal of Chongqing University*.

Philip. Kotler. (2003). *Marketing Management*. China People's University Press Beijing.

Rosenbusch. Roma. (2003). *Marketing Channel Management*. Sixth Edition. China Machine Press Beijing.

Zhang, Weiying. (2004). *Game theory and information economics*. Joint Press Shanghai.

A journal archived in Library and Archives Canada
A journal indexed in CANADIANA (The National Bibliography)
A journal indexed in AMICUS
A journal indexed in Zentralblatt MATH
A journal included in the Chemical Abstracts database
A journal included in DOAJ (Directory of Open-Access Journal)
A journal included in Google Scholar
A journal included in LOCKSS
A journal included in PKP Open Archives Harvester
A journal listed in Journalseek
A journal listed in Ulrich's
A peer-reviewed journal in applied science research

Modern Applied Science

Monthly

Publisher Canadian Center of Science and Education
Address 4915 Bathurst St. Unit # 209-309, Toronto, ON. M2R 1X9
Telephone 1-416-208-4027
Fax 1-416-208-4028
E-mail mas@ccsenet.org
Website www.ccsenet.org
Printer William Printing Inc.
Price CAD.$ 20.00

ISSN 1913-1844